



Review

Carbon nanomaterials in coatings: A review focusing thin film photovoltaic solar cells



Wajahat Ahmed Khan^a, Salim Newaz Kazi^{b,*}, Zaira Zaman Chowdhury^{a,**}, Mohd Nashrul Mohd Zubir^b, Yew Hoong Wong^b, Kaleemullah Shaikh^b, Rab Nawaz^b, Samr Ul Hasnain^b

^a Nanotechnology & Catalysis Research Centre (NANOCAT), Institute for Advanced Studies, Universiti Malaya, 50603, Kuala Lumpur, Malaysia

^b Department of Mechanical Engineering, Faculty of Engineering, Universiti Malaya, 50603, Kuala Lumpur, Malaysia

ARTICLE INFO

Keywords:
Thin films
Solar cells
Carbon
Nanomaterials
Carbon nanotubes
Graphene

ABSTRACT

Surface engineering of thin films in multiple applications have gained immense attention due to advancement in nanotechnology, fabrication and synthesis of nanomaterials. Thin film solar cells are at the forefront of the renewable energy harvesting, they offer numerous benefits over traditional counterparts which have lower efficiencies and stability, rapid degradation, higher cost and reduced lifetime. Carbon nanomaterials are unique materials comprising desirable properties for the application in thin film solar cells making them potential material for photovoltaic application. This review highlights the common mechanisms used for deposition of carbon and thin film layer formation in solar cells, namely physical and chemical vapor deposition. Both at the research and industrial scales, high production yields are easier to attain through vapor deposition methods, as a result, these approaches have a clear cost benefit over solution processing. It also discusses about the carbon nanomaterials (graphene and nanotubes) applied in different solar cell configurations and their subsequent contributions in enhancement of cell performance. Carbon nanomaterials offer comparatively inexpensive and effective way for enhancing absorption of solar radiation and also the overall stability in thin film solar cell. Inexpensive synthesis of defect free engineered carbon nanomaterials based thin film solar cells provides positive outlook for the industry. More research efforts should be given to environmental considerations for both, carbon synthesis and cell fabrication methods.

1. Introduction

Application of materials are governed by their inherent properties. The advent of modern technological advancements has stretched the conventional materials to their limits, hence engineered materials are extensively investigated. Surface engineering focuses on the range of methods to optimize the chemical and physical properties of substrate's thin top surface layers where the surface phase of the solid is modified for obtaining desired properties without modifying the bulk. Surface engineering allows component surfaces to be modified to increase the required attributes such as resistance to – corrosion, wear, friction, oxidation, and sulfidation and to enhance the thermal, mechanical,

optical, and electronic properties and also to improve aesthetics characteristics, etc. Continuous research is being conducted in surface engineering involving all stages of design, formation, investigation and utilization [1], (Fig. 1). Several surface engineering technologies can be administered to the surface to improvise, design, and modify the surface properties. Depending on the treatment method techniques such as 'modification in surface metallurgy', 'modification in surface chemistry', and 'coating or addition of layers' can be adopted, and extensively discussed by Walia et al. [2].

In general, the surface modification by applying a functional layer on substrate's surface to obtain the required properties is known as coating. The substrate constitutes one phase and coating another phase of the

* Corresponding author.

** Corresponding author.

E-mail addresses: khanwajahat@outlook.com (W.A. Khan), salimnewaz@um.edu.my (S.N. Kazi), dr.zaira.chowdhury@um.edu.my (Z.Z. Chowdhury), nashrul@um.edu.my (M.N. Mohd Zubir), yhwong@um.edu.my (Y.H. Wong), engrkaleemullah05@gmail.com (K. Shaikh), rabnawazkhan2867@gmail.com (R. Nawaz), samarhasnain135@gmail.com (S.U. Hasnain).

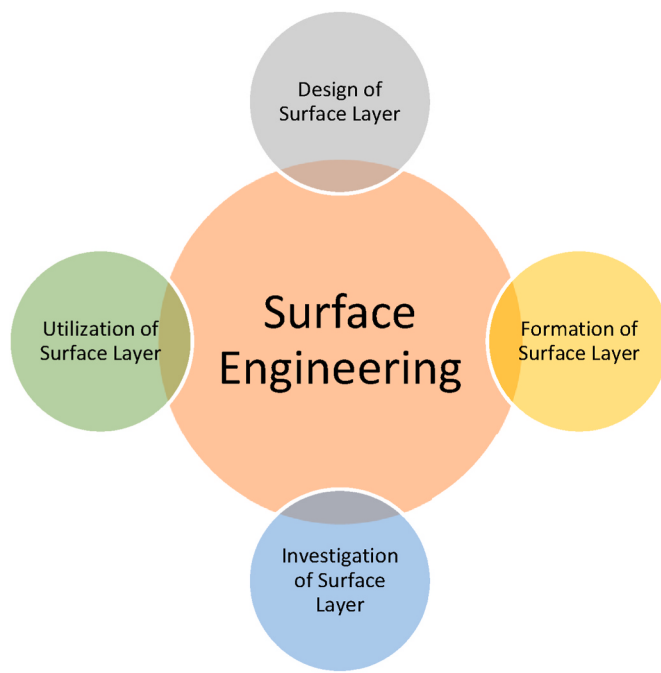


Fig. 1. Schematic representation of the area of activity of surface engineering [2].

system. The substrate is typically constructed out of a less expensive material that lacks certain necessary characteristics and is therefore subjected to surface modification. The interface between coating and substrate often aids in the film's adhesion to the substrate.

To accomplish the desired thermal, electrical, and optical properties for non-stress applications, a film is typically formed on the surface. Coatings are typically developed for wear-resistant and cladding for corrosion-resistant applications [1]. Coatings ($10\text{--}1000\ \mu\text{m}$), films ($<10\ \mu\text{m}$), and claddings ($>1000\ \mu\text{m}$) are characterized by their different thickness. Thin films can be defined as the two-dimensional layered material which are restricted in the third. They typically have thickness of $<0.1\ \mu\text{m}$, whereas thick film is several times more. Thin films are typically made using sophisticated vacuum-based techniques, whereas thick films are using less intricate and inexpensive techniques. Thin films have desirable active/functional properties, while thick films have enhanced surface protection [3].

The proper classification and definition of all coating types and manufacturing methods is challenging due to the variety of process mechanisms and the emergence of hybrid deposition processes. Coatings can be classified in different ways considering various aspects such as, by material – metallic coatings (metal, alloys), non-metallic coatings (organic or inorganic materials); by application – protective coatings (anodic or cathodic coatings), decorative coatings, technical coatings (corrective coatings, catalytic coatings, ablation coatings, optical coatings); by manufacturing methods – galvanizing (electroplating coatings, chemical coatings, conversion coatings), immersion coatings (hot dip coatings, gel coatings, paint coatings), spray coatings, cladded coatings, crystallizing coatings. These can be formed by utilizing a single technique or a combination of techniques [4]. Martin [5] has suggested four main categories of thin film deposition such as atomistic growth, particle deposition, bulk coating, and surface alteration.

Coatings can be of single layer or multiple layers. The single layer coatings consist of one layer, and it is applied with a single process or technological operation. It could be a single constituent coating (element or compound), such as chromium and titanium nitride, and multicomponent coating, such as alloying additives and titanium carbonitride, etc. The multilayer coating may consist of layers of single material separated by a distinctive sublayer, or layers of distinct

materials [4] (Fig. 2). The typical objective of applying multilayer coatings is to enhance the protective, aesthetic, or other functions.

Solar energy harvesting through thin film photovoltaic cells have gained a lot of attention due to their flexibility and applicability in modern applications such as building-integrated photovoltaics (BIPV), floating solar photovoltaics (FPV), submerged photovoltaics, agri-voltaics and space applications [6].

Materials have been found to behave differently when particle sizes reach to nano and quantum levels, offer astonishing physical, chemical, and optical properties. The physical characteristics of nanomaterials are diverse such as, (i) energy bandgap flexibility and interchangeability via altering the nanoparticle size, (ii) improved optical path as a result of numerous reflections, and (iii) considerable decrease in the recombination possibility of charge carriers due to the smaller pathway to travel for light-generated carriers.

Nanomaterials offers opportunities to alter the conversion of solar energy by enabling low-priced and highly efficient devices. Two extensive methods based on nanostructures are being discovered for photovoltaics: (1) considerable decrease in material usage and/or related final costs; (2) photovoltaic devices with a greater optimum efficiency than that found through the Shockley–Queisser analysis.

Many investigations have been performed to enhance different aspects of PV solar cells through various nanomaterials as highlighted by the published books and articles [8–11]. Three types of common nanostructured solar cells and their benefits are shown in Table 1. With the advent of nanotechnology, extensive research has been done to synthesize PV films of nanometric grain size and thickness with various production methods and materials [12,13].

Carbon comes in many forms, such as diamond and graphite, as well as fullerene molecules, nanocrystalline graphite (nc-G), nanotubes, glassy carbon, semicrystalline carbon black, and graphene, etc. (Fig. 3). The valence electrons in carbon ([He] $2s^22p^2$) allows three main bond configurations such as sp^3 tetrahedral bonds, sp^2 planar bonds, and sp sigma bonds. The sp^2 and sp^3 bonds may arise not just only in crystals (such as graphite and diamond) but also in amorphous solids.

Carbon allotropes and nanomaterial have been extensively studied in surface engineering due to their excellent properties. Specifically carbon nanotubes, graphene and its derivatives, fullerene and carbon dots have revolutionized many industries, their significance has also been acknowledged by the Swedish Academy [14,15]. The physical features that characterize carbon coatings include the sp^3/sp^2 ratio, the cluster and presentation of the sp^2 phase, and the hydrogen content. In non-hydrogenated films the properties – density, band gap, hardness and young's modulus are proportional to sp^3 percentage of carbon, because sp^3 bonds facilitate higher packing density and robustness. Although hydrogenated films might contain a high number of sp^3 bonds, but the mechanical strength and density diminish with the increasing hydrogen content [16,17]. Carbon have shown remarkable potential to replace the harmful and scarce materials by its abundant nature and extremely favorable electrical and optical characteristics. Hence carbon nanomaterials in thin films solar cells are the focus of this article.

2. Coating mechanisms

In coatings, target is the source material from which films are formed, precursors are the chemicals that are used to make the film stoichiometry and substrate represents the surface on which the thin or thick film material is deposited. The substrate features and deposition method have a substantial influence on the growth behavior of the films of desired thickness. Various process parameters influence the thin film's characteristics, such as material properties, deposition method and equipment, processes parameters etc. [20].

The key criteria for an adoptable manufacturing method is low cost, which consist of capital expenditure (CAPEX) for the machinery required and operational expenditure (OPEX) comprising the energy utilized, cost of material use, quality control, and treatment cost of

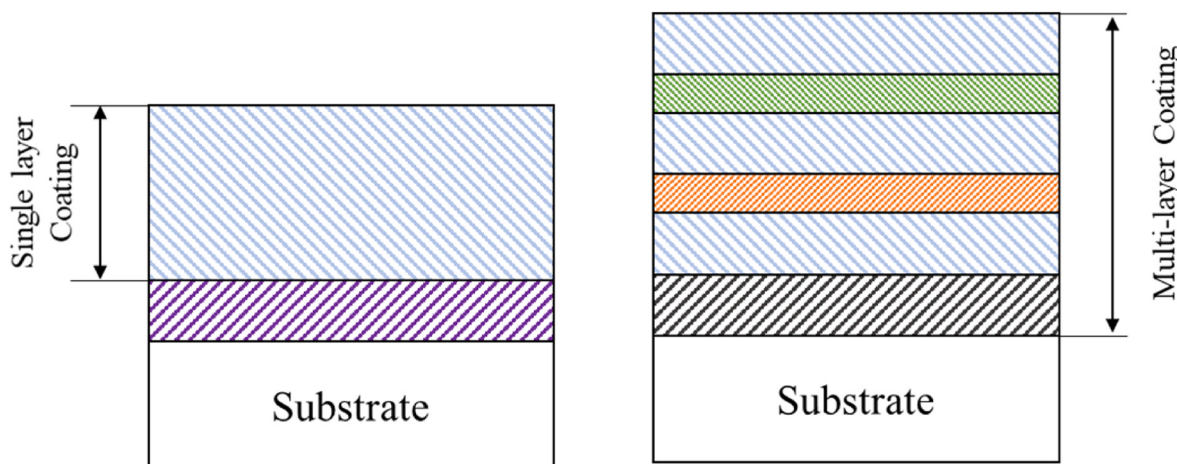


Fig. 2. Single layer and multilayer coating structure (blue: coating layer; green: sublayer; orange: sandwiched layer; purple: intermediate layer; black: primary layer) [4].

Table 1

Nanostructured solar cells: (a) Quantum Dots (b) Nanowires (c) Mesoscopic [7].

Quantum dot solar cell	Nanowire solar cell	Mesoscopic solar cell
Benefit: Multiple exciton generation Tunable bandgap Low-temperature fabrication Challenges: Charge/transport through QD array Monodispersity of QDs QD long-term stability	Benefit: Reduction in minority-carrier lifetime Reduced material usage Reduced reflectivity Challenges: Positional stability of dopants Achieving high areal density Top contact	Benefit: Use of low dielectric materials, use of metal oxide electrodes Lightweight absorber layers Cheap Challenges: Stability of morphology Photostability of polymers/dyes Charge transport in polymer phase

hazardous waste produced during the manufacturing. High yield, high quantity, and reproducibility, as well as better utilization of material, considerably reduced the manufacturing cost [24].

Deposition of thin film coatings can occur through a suitable precursor transport mechanism, such as the direct application of a liquid onto the substrate, exposing the substrate to a reactive gas, or transferring atomic clusters through ballistic means under vacuum conditions. Coatings can be directly grown on the substrate material or through liquid coatings with additional processing can be applied. Synthesis methods can be categorized based on the physical state of the precursor material, the mechanism of transforming the precursor into thin film and the deposition situations. Deposition processes are usually categorized into two main types – liquid deposition (solution based) and vapor deposition. Both deposition paths can also be merged e.g., in two step production methods. The vapor deposition techniques, is usually further classified into two main categories: physical and chemical (Fig. 4) [21].

The term, physical form, pertains to the state or condition in which the precursor exists during the deposition process. Solution processes enable the deposition of thin films at normal atmospheric pressure and require minimum equipment cost. Solution processing involves the use of a solution as a carrier for a specific material; it might be physical (for materials or nanoparticles dispersions) or chemical (for perovskites). In this context, a solution is a solvent, which is typically a liquid or a combination of liquids that have the ability to dissolve solutes.

Solutes can consist of molecular or polymer organics, ionic constituents, nanoparticles, or a mixture of any of them. Numerous solution methodologies for depositing thin films depend on the generation of a wet liquid film by mechanical methods. The wet film is subsequently dried, typically under standard pressure and low temperatures (<120 °C), resulting in the formation of a solid film with the specified material and thickness. After deposition, dry or semi-dry films can be treated with thermal annealing or curing at high temperatures in ovens. This process serves to eliminate any remaining solvent, induce recrystallisation, or alleviate film strain. Environmental variables, solution chemistry, rheology, and drying microfluidics processes can collectively affect the quality of the final material phase and morphology. Solution-based methods involve the application of inks that contain precursor substances and appropriate solvent systems. These inks are then applied to a substrate using numerous techniques such as spin coating, blade coating, slot-die coating, spray coating, or inkjet printing. Solution-based techniques are still dominating field due to their rapid process optimization and ease to use, as well as their easily integration with research laboratory settings. Furthermore, research on solution-based techniques is usually driven by the goal of achieving low-cost, high-throughput roll-to-roll production. Whereas solution-based techniques for perovskite-based PV have proven to be successful in the laboratory, their adoption in industrial processes is complicated. Furthermore, vapor-based fabrication processes dominate the thin-film PV industry. Solution-based methods are hard to use in large-scale industrial

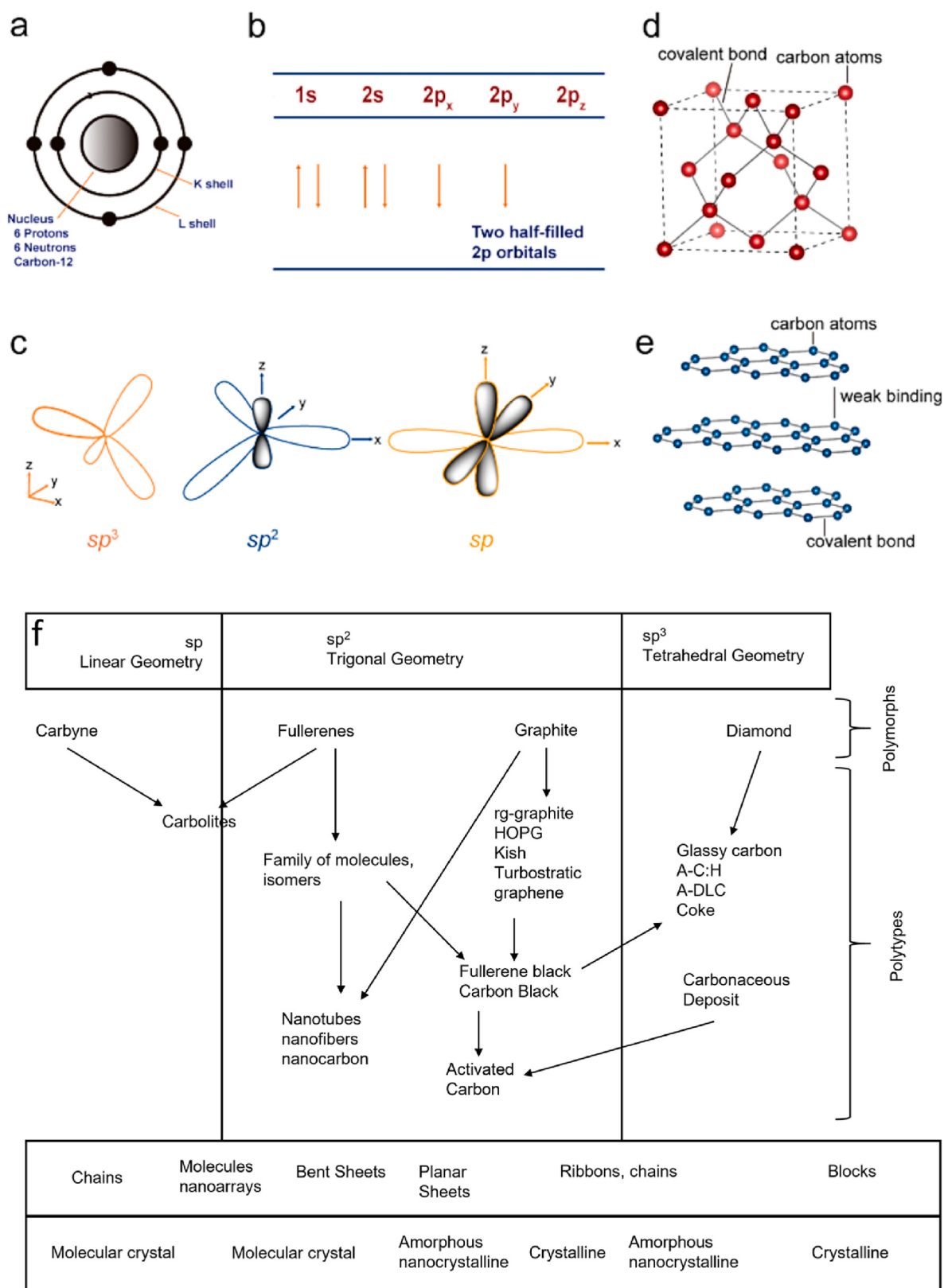


Fig. 3. (a) Schematic of carbon atom (b) electron structure of carbon (c) demonstrates the sp^3 , sp^2 , and sp hybridized atoms (d) atomic structure of diamond (e) atomic structure of graphite (f) polymorphs and polytypes of carbon [18,19].

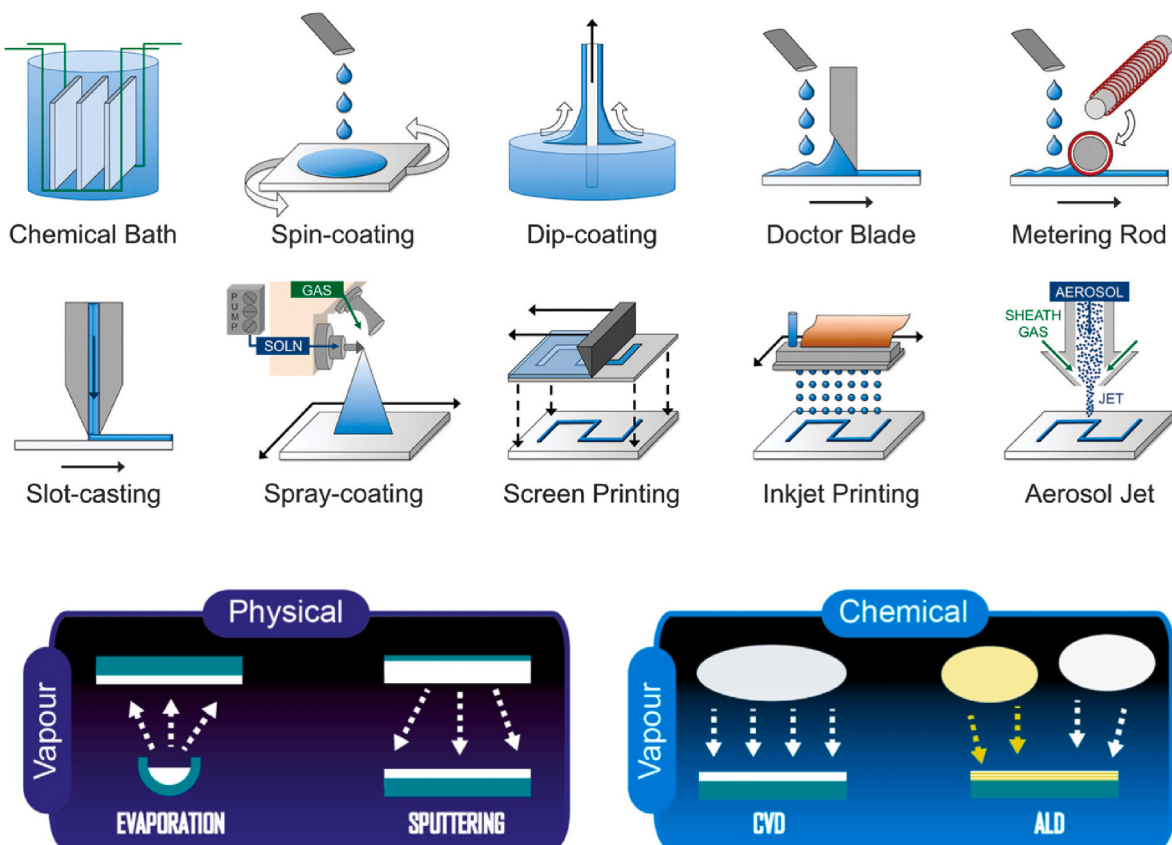


Fig. 4. Thin film deposition techniques [21,22].

fabrication because precursor materials, solvents, and the processing environment all interact in complicated ways. This establishes an extensive number of process parameters that need to be optimized, controlled, and monitored during fabrication. When processes are shifted to the large areas desired for PV applications, they need to be controlled more extensively [23–25].

In film coating industries, solution-based deposition processes have been proven to enable roll-to-roll deposition rates of hundreds of meters per minute. A probable decrease in productivity with high throughput, as well as stringent requirements for solvent treatment and solution quality control. They can all serve as a counterbalance to the advantages of the rapid deposition rates. In addition, the production process can incur considerable operational costs as a result of the management of toxic solvents, despite the fact that it is challenging to quantify. Recently Agresti et al. [25] have done a qualitative evaluation of various solution-based coating and printing techniques for PV and provided a summary as shown in Table 2.

Vapor-based processing utilizes techniques that do not involve solvents but instead rely on the evaporation or sublimation of precursor materials under vacuum conditions. This results in the development of a very uniform thin layer when the vapor condenses on a substrate. On

the other hand, vapor-based methods depend on a small set of process parameters, which are primarily the deposition rates of the precursor materials, the specific process conditions (such as pressure and system design), and the substrate conditions (such as temperature and surface conditions). This allows for relatively straightforward monitoring, control, and replication of the process. Significant advantages of vapor-based deposition include the possibility of high process control that leads to high precision and uniformity needed in thin-film fabrication as well as not having to recycle and treat solvents or ensure the often-expensive quality control for ink formulations. The resulting high reproducibility and high yield can lower the OPEX for quality control. Based on overall costs, the key differences among vapor and solution processing are the production costs, which are primarily influenced via throughput and production, and the CAPEX related with the vacuum devices. Vapor-based deposition methods are more cost-effective than solution processing, as they are simpler to obtain high production yields at both the research and industrial scales. The established thin-film PV industry (e.g., CdTe, CIGS, as well as the organic PV and OLED industry) is the primary archetype for scalable, high-yield, and high-throughput perovskite PV manufacturing, which is primarily based on vapor phase processing. While it is frequently asserted that solution-based

Table 2

Summary of the printing and coating methods. Low grades are indicated as ▼, medium grades as ◆, and high grades as ▲ [25].

Technique	S2S	R2R	Speed	Material Yield	Patterning	Uniformity	Ink Versatility
Spin coating	▲	▼	▼	▼	▼	▲	▲
Blade/wire bar coating	▲	▲	▲	▲	◆	◆	▲
Slot die coating	▲	▲	▲	▲	◆	▲	▲
Inkjet	▲	▲	◆	▲	▲	▲	◆
Spray coating	▲	▲	▲	◆	◆	▲	▲
Screen printing	▲	▲	▲	▲	▲	▲	▼
Chemical bath	▲	◆	◆	▲	◆	▲	▼
Gravure	◆	▲	▲	▲	▲	▲	◆

processing ensures reduction in production and capital expenditure costs, their fundamental techno-economic analysis indicates that vapor phase processing can compete with solution processing in both categories for high deposition rates and large-scale manufacturing tools [23–25].

The present PV sector significantly depends on vacuum deposition methods to coat silicon solar cells such as amorphous silicon for heterojunction devices or anti-reflective coatings, are commonly applied using chemical vapor deposition (CVD) technologies. Thin-film solar cells, such as copper indium gallium selenide (CIGS), are primarily fabricated via thermal co-evaporation, whereas CdTe solar panels are created by a high-throughput vapor transport deposition (VTD) technique. To date, sequential vapor-phase processes may offer the highest, however, still too slow dynamic deposition rates. Research on new high-rate deposition concepts like closed-space sublimation, flash sublimation, or sputtering approaches as well as the exploration of industrial designs for evaporation sources has just started and needs to be emphasized [23–25]. Hence comprehensive discussion and recent advancement, focused on carbon nanomaterials and PV, for both of these vapor-based methods are discussed further.

2.1. Physical vapor deposition (PVD)

In the PVD process, diffusion, agglomeration, condensation coalescence, and nucleation arise on the surface of the substrate, leading to the development of a coating. The precursor is introduced into a highly energetic and entropic environment, causing clusters, atoms, or particles of the precursor to detach from the surface of the solid material [26,27]. The entire system is enclosed within a vacuum deposition chamber to facilitate unrestricted particle movement between the source and substrate. Due to the inherent tendency of particles to exhibit linear motion, films that are deposited using physical methods often exhibit a directional growth pattern, as opposed to a conformal one. Two common PVD procedures are magnetron sputtering and thermal evaporation [28]. Magnetron sputtering, deposit thin films in which the ultimate structure is determined not only by the energy of the sputtered atoms but also through their surface diffusion and interaction characteristics. The primary research emphasis has been analyzing the energy of sputtered atoms via investigating the impact of different parameters in the PVD process, such as input pressure, deposition rate, and composition of the deposition atmosphere, cleanliness level of the vacuum chamber, substrate temperature, substrate materials, distance from source to substrate, incidence angle, substrate angle, and the energy of the precursor atoms/particles/clusters that are ejected. These parameters are examined to understand their influence on growth and the relationship between the structure and properties of the material [29,158]. The influence of disorders, surface roughness, and grain boundaries can play a crucial role in the properties of thin films. A general comparison of thermal and sputtering processes is given in Table 3 [21].

In a recent study, Voznesenskaya et al. [30] studied carbon nanostructured coating with different PVD methods on polyurethane and compared their effects on several properties such as the contact wetting angle, coating thickness, topology, microstructure, and roughness. Zia et al. [31] conducted a review of graphitic carbon nanoparticles manufactured via various PVD techniques (arc system, sputtering), their characteristics and applications in various fields. They also came up with a four-stage growth model for graphitic particles, which means the particles go from being seeds to coalescence to atomic groups to granular structures on the substrate surface (Fig. 5). Additionally, they noted that isolated graphitic carbon particles could be established via

Table 3

Comparison of general condition and parameters for evaporation and sputter PVD deposition

Condition/Parameter	Evaporation	Sputter
Vacuum (mbar)	<10 ⁻³	<10 ⁻³
Input energy source	Heat	Ion bombardment (plasma)
Target/Evaporation temperature	Melt temperature of evaporant	<100C (active cooling)
Approximate kinetic energy of ejected cluster/atom/particles	0.2 eV	1–10 eV
Deposition rate		1–10 nm.s ⁻¹

magnetron sputtering and laser vaporization. Particle synthesis is influenced by various system features and operating parameters, including target to substrate distance, target current, pressure gradient and chamber size.

Stueber et al. [32] reviewed the nanoscale multilayered PVD thin films and concluded that extremely fine structural ordering is necessary for these films. Also, grain growth and coherent layer interface significantly affects the hardness. Furthermore, to comprehend the deformation mechanisms in nanostructured coatings, the correlations among the residual stress, fracture elastic properties, toughness, and macroscopic thin film properties (for example interactions among the dislocations or cracks and stress fields) involve more comprehensive investigation (Fig. 6). They also reported the optimized interface volume for protective coatings. The multilayer thin films physical properties can also be improved by overlaying nanoscale gradients in the chemical arrangement, growing coatings with substrate temperature gradients, or interfacial engineering, which involves adjusting substrate bias-induced stress relaxation or intermixing at layer interfaces.

Bakhsheshi-Rad et al. [33] investigated the duplex coating of zinc oxide (ZnO) and multiwalled carbon nanotubes (MWCNTs), produced by PVD in conjunction with dip coating. The thickness of inner ZnO layer is 1.1 μm consisting spherical particles while the outer MWCNTs layer of 10.2 μm. They claimed that the ZnO coated single layer and bare magnesium alloy had lower compressive strengths than the duplex coating. They compared the rate of corrosion on Mg alloy with simulated body fluid (SBF) solution with single layer ZnO coating and duplex coating and concluded significant reduction in corrosion rate with duplex coating (Fig. 7).

Arpit Agrawal et al. [34] investigated the multiple nanocomposite layer of graphene-copper coatings on Kapton foils formed by DC magnetron sputtering (Fig. 8). They embedded graphene particles between copper layers as opposed to cover the entire layer surface. It was observed that the sample of ten-layer develops a crack pattern channel, whereas the sample of four-layer produces microcracks. Specifically, the stress of film cracking improved by 121 % in the case of four-layered copper films and 50 % in the case of ten-layered copper films (channel cracks) when graphene reinforcement was incorporated. Moreover, experimental evidence of an enhancement in deformation stress and fracture deflection resistance suggests that the presence of graphene particles influences the plastic region in close proximity to the crack tip.

Zhang et al. [26] fabricated one dimensional (1D) composite of CNTs with tungsten coating by PVD method. Pure Tungsten vapors were evaporated from the filament and carried by H₂ gas to nanotubes, however the diameters of these composite nanowires were not uniform. In another study Ji et al. [35] investigated a novel reinforced carbon nanocomposite coating through two step method. Vertically aligned carbon nanotubes (VACNT) films were developed through plasma

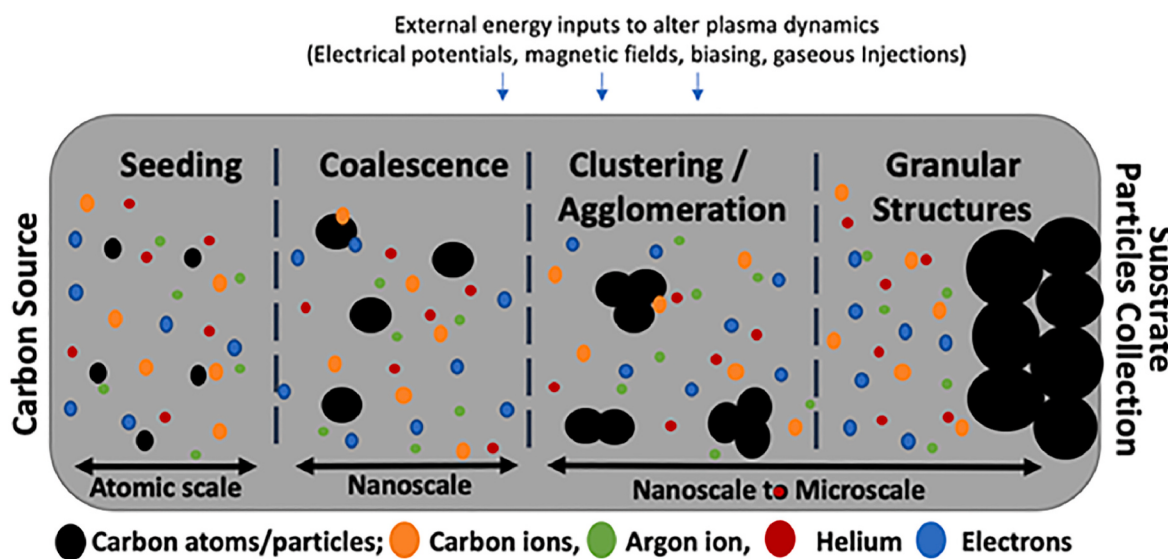


Fig. 5. A generalized 4-step mode to produce the in-situ particle growth procedure in PVD approaches. Particles grow from seeding to amalgamation and form clusters of atoms before accumulating on the surface of substrate in a granular structure [31].

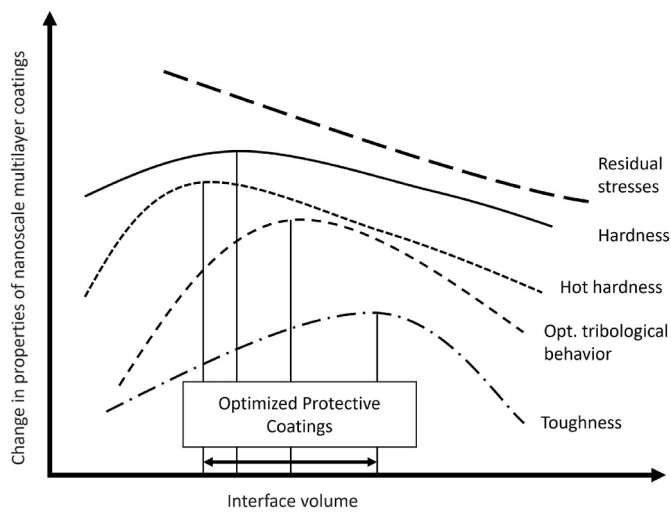


Fig. 6. Variation in characteristics of multilayer nanoscale coatings as result of interface volume [32].

enhanced CVD and catalyst films, containing inert elements were utilized to reduce the density of the VACNT films (Fig. 9). The two-step approaches to utilize VACNT films as a foundation for applying multi-functional nanocomposite coatings. This is because of the distinctive characteristics of the VACNT architecture, which prevents CNTs from being damaged during the premixing procedure. Films were further modified by Ag impregnation, and also nanocomposites of Pt-CNT, Ag-CNT and DLC-CNT.

The composite catalyst film used in this work is an easy and inexpensive way to change the VACNT film's density. However, some big Ag particles developed during the sputtering development may have an effect on how well the composite coating is deposited. Other elements,

such as Cu or Ti, should be investigated in order to improve catalyst film control. In an ideal state, the 1D nanocomposite coating should possess characteristics derived from both the matrix and the reinforcements. Because of their distinct architectures, these nanocomposite structures may offer highly different properties that can be employed as electrodes, biosensors, and so on [35].

Magnetron sputtering with varying deposition time of amorphous carbon material on single-crystal sapphire substrate was investigated by Li et al. [36]. They studied the thickness and optical properties of the coating and reported its suitability for optoelectronic industry. Barreto et al. [37] investigated multilayer graphene (MLG) thin films produced by sputtering method. The transition of carbon atoms from amorphous to graphene occurs via diffusion across the catalyst metal; then carbon atoms were dissolved in the metal as graphene. They found nonlinear absorption of the films and hence it can be used as optical limiters.

Mrkvica et al. [38] modified the PVD method by enhancing fixture design with additional rotation of the process. They reported that the added fixture reduced friction and eliminated shadow effect. They compared the coatings from 3-fold to 4-fold rotation and found that the grain growth and continuation of the coating remained constant, thereby it increased the quality.

Utilizing an inert or reactive gas over a broad pressure range, pulsed laser deposition (PLD) is an adaptable technique for fabricating nanoscale films of multi-element. It has been extensively explored for DLC since its first attempt with PLD in 1980s. The target's superficial layer is instantly heated by the intense laser and the atoms of carbon in the thin layer can get enough kinetic energy to skip the limitation, to develop the carbon plasma in vacuum. Plasma's expansion direction is always at 90 % to the surface of target. The DLC coating forms on the substrate as the particles cool. DLC films may be doped with additional elements using either a doped graphite target or an ambient gas. When required, a negative bias and substrate heaters are implemented. Amorphous carbon films with pulsed laser deposition was initially investigated by Ref. [39] in 1996.

The basic approach is straightforward however it is ineffective for

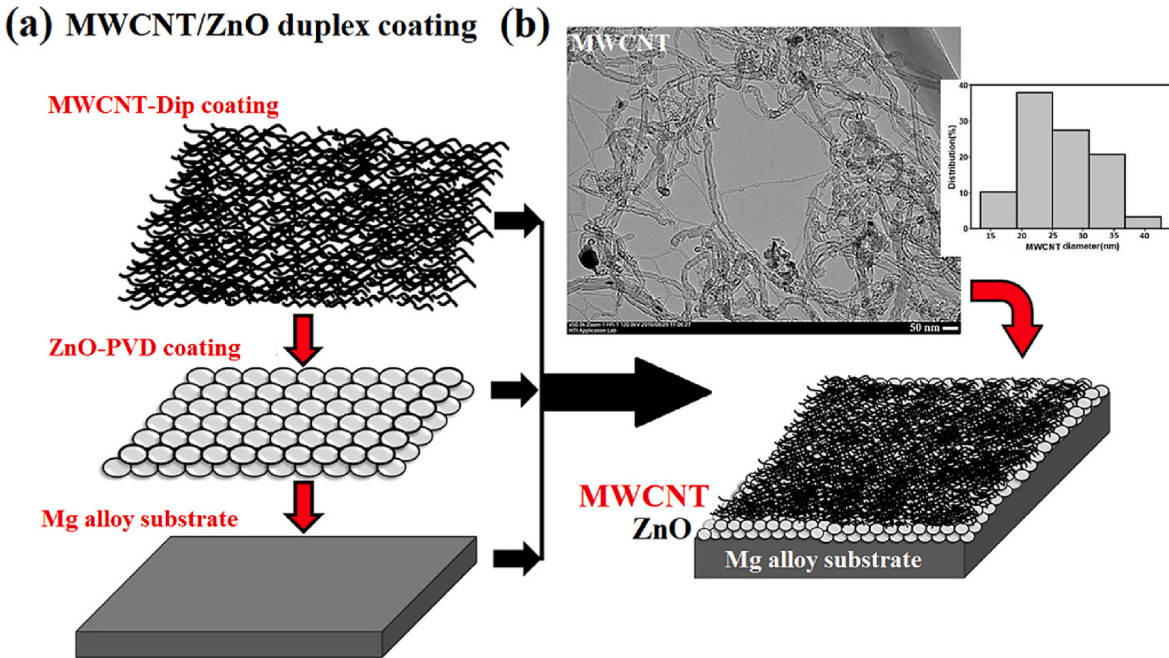


Fig. 7. (a) Demonstrates the schematic ZnO/MWCNT duplex thin film coating through PVD in combination of dip coating and (b) MWCNTs powders TEM image [33].

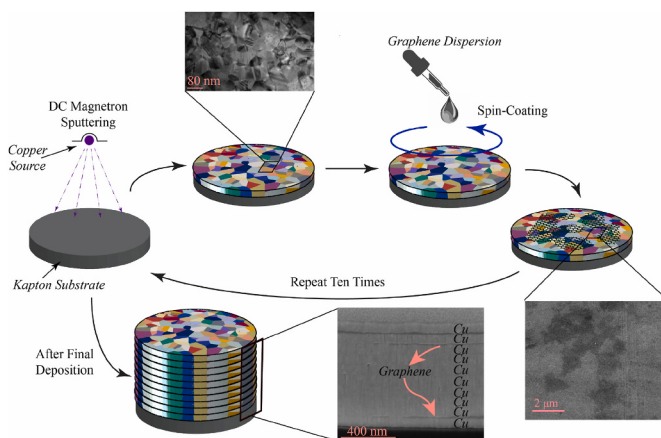


Fig. 8. Procedure for developing the graphene-copper nanolayer composites. The copper was coated through the DC magnetron sputtering on Kapton. The spinning method of coating was utilized to disperse the graphene nanoparticles on the copper deposited surface. The SEM was utilized to examine the dispersion of Graphene over the copper layer and to study the cross-sections of the invented composites. TEM was utilized used to examine crystallinity and apparent grain morphology of copper layers [34].

large surface areas larger size than 3 cm. Furthermore, ambient gas can influence the forward-directed dispersion of the laser-induced plume, increasing the homogeneity of PLD-grown films. The deposition velocity is greater in a multi-laser scan as opposed to a single-laser scan (Fig. 10). But dividing a single laser beam into many beams significantly lowers the influence of each beam, which is very detrimental to the formation of sp^3 bonds in DLC films. However, the relative transfer among the substrate and plume can also be accomplished through the fixing of laser beam when the substrate is moved. The plasma axis is perpendicular to the tangential plane of the micro region surrounding the ablated spot. Thus, as the laser moves in a radial direction along the cylindrical target, the plume continuously deflects against the substrate plane. By rotating or shifting the substrate, it is possible to obtain a large-area film that is uniform throughout. Comprehensive description, effective parameters and application of PLD for DLC is reviewed by Lu et al. [40], and also highlighted all the major affecting paraments (Fig. 11).

Shakerzadeh et al. [41] investigated the effect of plasma parameters on carbon films with DC double bend filtered cathodic vacuum physical vapor deposition. They found that the desired orientation strongly relies on the densities of plasma. At greater nanocrystals, plasma densities, develop a quite minimal ion energies in comparison to lesser density of plasma. Furthermore, it was noticed that at lower mass densities and higher ion energies, tubular nanostructures are developed whereas at high ion energies nanostructures like graphene were more stable. During

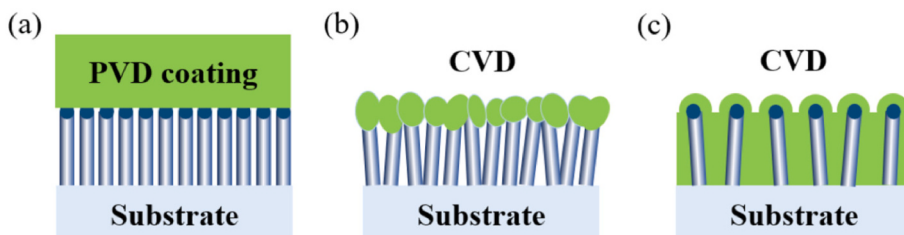


Fig. 9. Graphical images of the common composite structures coated through CVD and PVD methods. (a) Surface of the VACANT film deposited through PVD coating (b) CNTs tips deposited through CVD coating (c) well-organized nanocomposite coating was established through CVD coating penetrating inside the VACANT film [35].

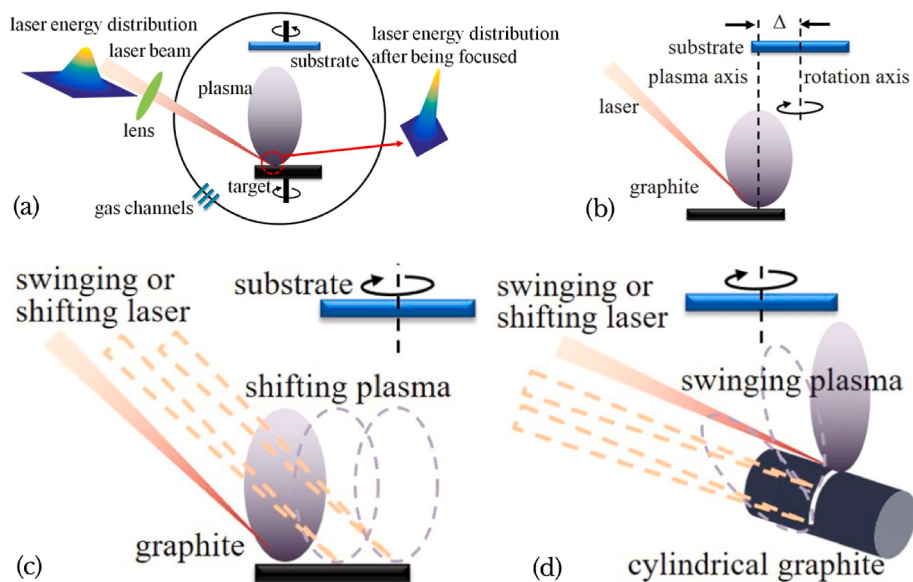


Fig. 10. Schematic of standard pulsed laser deposition procedure and procedure for achieving homogeneous PLD-grown DLC films [40].

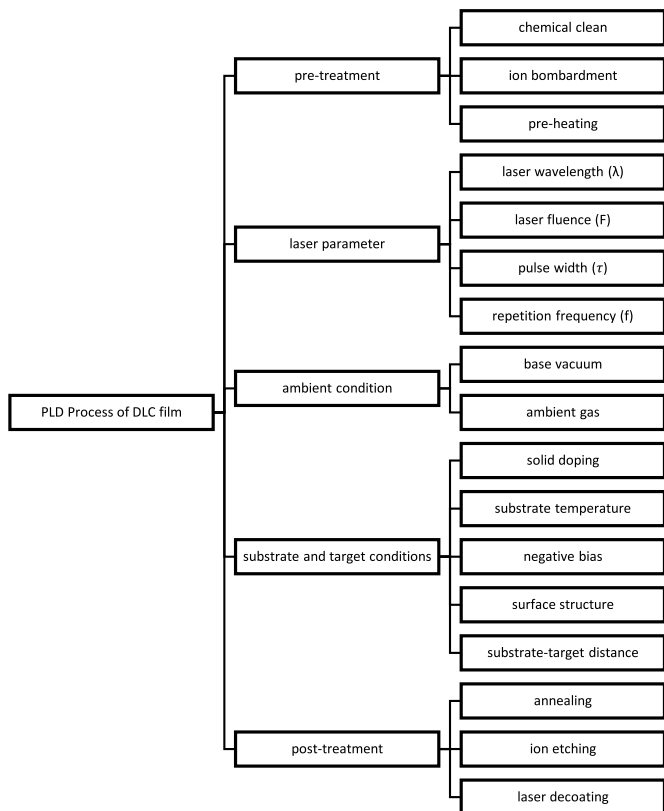


Fig. 11. Factors affecting the PLD development of DLC films [40].

deposition, the ion beam travels as a convergent beam within the magnetized duct and a divergent beam as it leaves. Thereby manipulating the gap between the holder of substrates and the magnetic duct outlet, the impacting ions density can be regulated. To measure the density of ion a Faraday cup was utilized. By selecting appropriate distance among the magnetic filter and sample, plasma profiles of two ion density that are five times from one and other were obtained and utilized in this work (Fig. 12).

2.2. Chemical vapor deposition (CVD)

CVD is a commonly employed approach for engineering and processing materials where thin films are developed on a substrate through a chemical reaction of gas-stage precursors. In comparison to PVD it is a superior, because it relies on chemical reactions that allow for adjustable deposition rates and products with high quality. In most cases, the coating materials such as metal oxides, carbides, and hydrides are chemically adsorbed onto the substrate [3]. CVD is a famous technology for optoelectronics, biomedical electronics, and surface modification applications because it normally doesn't demand high-vacuum operational conditions. Regardless of the variations in CVD types, the basic procedure is identical and involves the same basic steps (Fig. 13). At first, the reactant gases are transferred into the reactor, they either initiate the gas-phase reactions to produce interim reactants and vapor by-products through uniform reactions, or directly diffuse via the boundary layer to the substrate. In both scenarios, reactant gases and interim reactants adsorb onto the hot substrate surface and diffuse across the surface. Afterward, mixed reactions at the gas-solid boundary enable continual thin film development by means of nucleation, growth, and coalescence, in addition to the development of a reaction byproducts. Lastly, gaseous products and unaltered species desorb from the surface and escape from the reaction zone. Moreover, the presence of a mixed reaction is crucial in cases where the deposition reaction relies solely on the surface catalysis of the underlying substrate, for example in the context of catalytic graphene growth on a metal surface. In short, firstly, transmission of the gaseous precursor into the reaction chamber occurs, then precursor molecules penetrate via the boundary layer and then attached to the development sites on substrate. Again, the frequency of chemical reaction catalyzed through the surface of substrate, followed by the removal of reaction developed by-products from the reactor. Finally, it forms the nucleation, growth, and the amorphous crystallization thin films on the substrate [3,43]. The main types of CVD are vertical and horizontal CVD, atmospheric pressure and low-pressure CVD, cold wall and hot wall CVD, initiated CVD, photo-assisted and laser-assisted CVD, plasma-enhanced [44], hot-filament/wire CVD, oxidative CVD, metal organic CVD, and atomic [45] and molecular layer deposition [43].

Qiu et al. [46] have recently reported the development of perovskite in a atmospheric or low vacuum pressure condition. The precursor vapor can be evaporated from solid particles or formed as a vapor through the ultrasonication of a precursor solution. Modified CVD deposition of

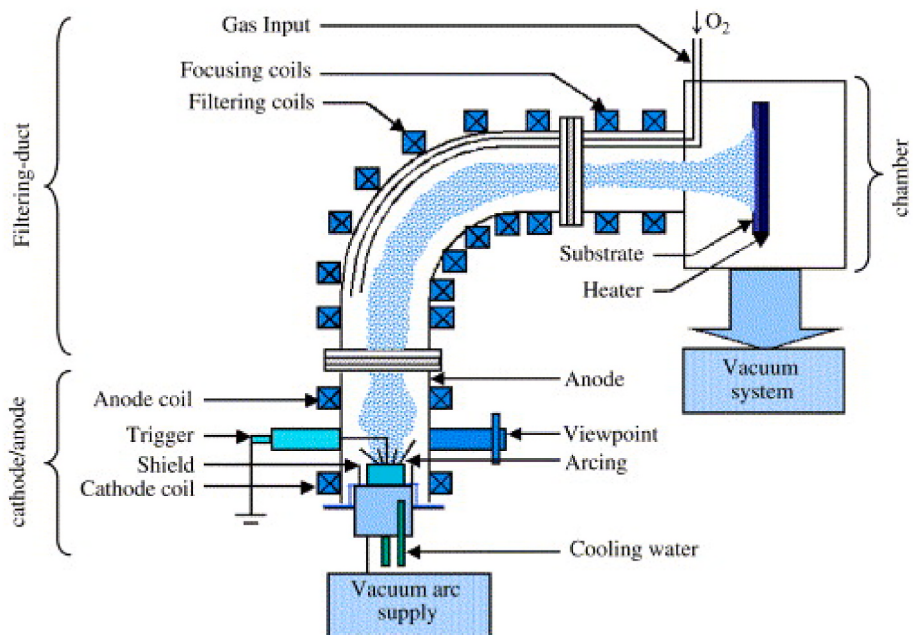


Fig. 12. Schematic of filtered cathodic vacuum arc deposition procedure. Plasma is developed via using arc on a target of graphitic. The microdroplets developed in the arc procedure are filtered through the magnetic duct. The plasma alters as it escapes the duct. Therefore, by controlling the distance among the substrate and the magnetic duct exit, the density of impacting ions on the substrate can be managed [41,42].

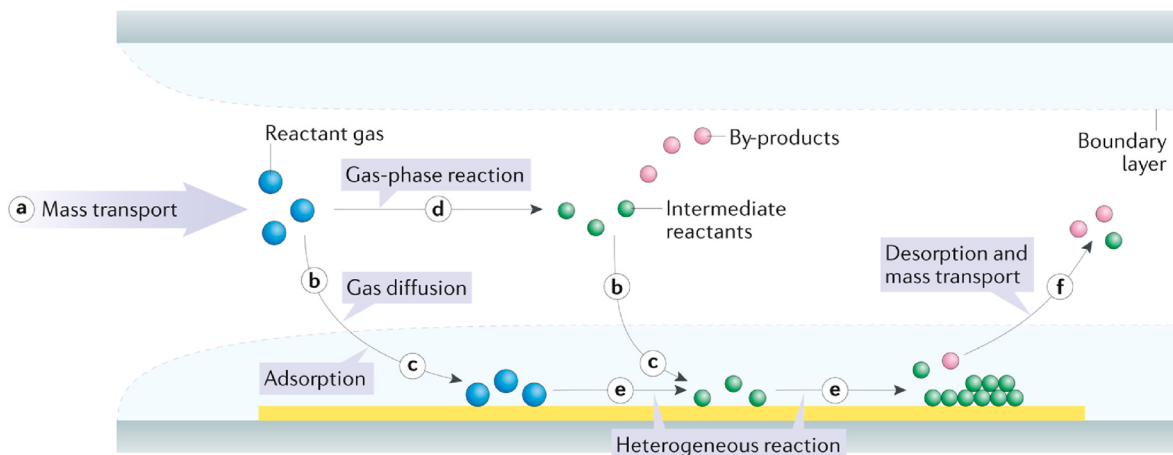


Fig. 13. Diagram of general primary steps of common CVD procedure. Initially reactant gases are transferred in the reactor (step a). afterward there are two likely ways for the reactant gases: directly diffusing over the boundary layer (step b) and adsorbing on the substrate (step c); or creating transitional reactants and by-products through the gas phase-reaction (step d) and existence deposited on the substrate by diffusion (step b) and adsorption (step c). Surface diffusion and heterogeneous reactions (step e) occur on the surface of substrate prior to the creation of thin films. Lastly, by-products and unreacted groups are desorbed from the surface and removed from the reactor as exhausts (step f) [18,43].

perovskite materials can be classified into multiple categories based on the development of reaction mechanisms, which include varying furnace designs, precursor positions, temperature zone control, and pressure control (Fig. 14). Improvements in elements engineering in vapor deposited perovskite thin film for PV cells, have been reviewed by Lin et al. [47].

Carbon material has been proved to be a viable substitute because of its affordability, stability, resistance to ion migration, hydrophobic nature, and appropriate work function (5.0 eV). Carbon-based supercapacitors have emerged as highly attractive candidates for commercialization. As previously stated, the use of affordable carbon electrodes, HTM free structure, long-term stability, and simple fabrication methods have made it beneficial for attaining large-scale production [48].

Precursor, catalyst, pressure, temperature, and growth time are generally the main controlling variables in CVD process [49]. In general, carbon-containing hydrocarbon is used as the carbon source. This hydrocarbon breaks down into carbon clusters on the metal catalyst substrates. These clusters then combine by diffusion and aggregation to develop graphene. The intricacy arises in achieving control over the uniformity of the layer and obtaining a single-crystal domain across large areas on a macroscopic scale. The hexagonal form of graphene is widely recognized as the most thermodynamically viable morphology, mostly because of its highly symmetrical arrangements. Robertson and Warner [50] stated the development of hexagonal, few-layer, single-crystal graphene on solid Cu foils with ambient pressure CVD. Transmission electron microscopy and Raman spectrum investigations verified that the as-grown, few-layer graphene had five to ten layers.

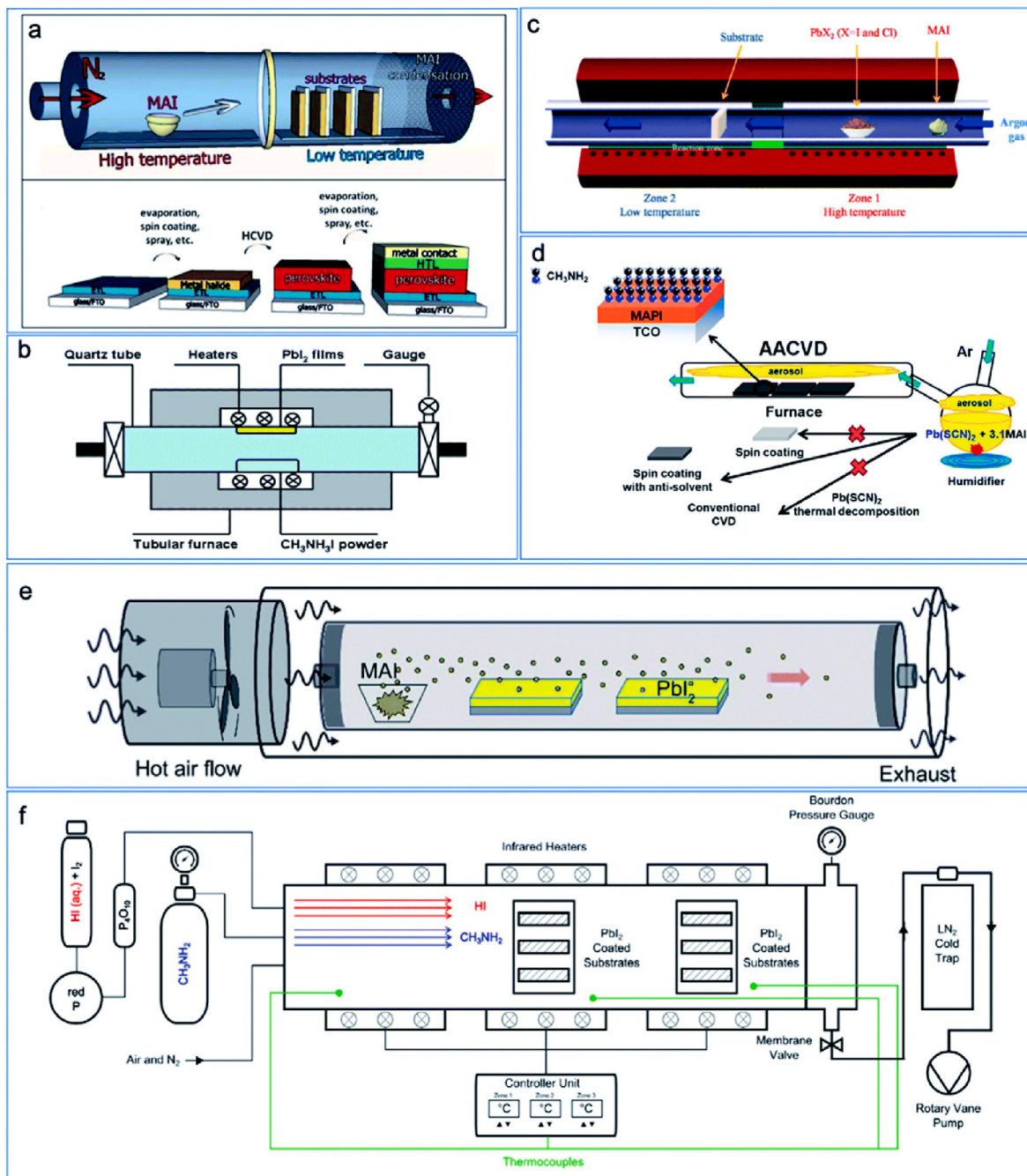


Fig. 14. Schematic diagram exhibiting the numerous types of altered CVD to prepare perovskite materials (a) Double-zone HCVD procedure (b) Single-zone HCVD procedure (c) One-step HCVD procedure (d) Ambient pressure AACVD procedure (e) Ambient pressure double-zone HCVD procedure (f) MA gas with HI vapor-based CVD procedure [46].

Electron diffraction of individual crystals indicated that they were single crystals with AB Bernal stacking. It should be noticed that the hexagonal graphene crystals were only 2.0–5.0 μm in size [51] (Fig. 15).

Sung et al. [52] initially developed perovskite solar cells (PSCs) using graphene as the transparent conducting anode, and utilized CVD for the synthesis of graphene layer. The graphene films were incorporated into inverted, p-i-n devices positioned on glass substrates. In order to enhance the capacity of the graphene electrode to interact with liquids and facilitate the application of other layers in the device, another layer of MoO₃ was applied. This additional layer also served to alter the properties of the graphene by reducing its sheet resistance from approximately 2000 Ω/cm^2 to 500 Ω/cm^2 (Fig. 16b). This decline in sheet resistance contributed to a substantial improvement in the device

efficiency which increased its power conversion efficiency (PCE) from 0 to 17.1 % (Fig. 16c), which is comparable to the efficiencies of devices based on Indium tin oxide (ITO), which have an efficiency of 18.8 %. CVD synthesized graphene can be utilized as the uppermost electrode in PSCs by a dry transfer technique to create semi-transparent devices. However, they proved that when tested under extreme bending circumstances (1000 cycles of bending), the device made of graphene maintained almost 90 % of its initial PCE, while the device made of ITO preserved less than 40 % of its initial PCE (Fig. 16e). The authors credited this enhancement to the exceptional resilience of graphene against mechanical distortion, suggesting its substantial potential in the development of flexible PSCs. Other research support the idea that graphene is effective in conducting charges and can be used as a

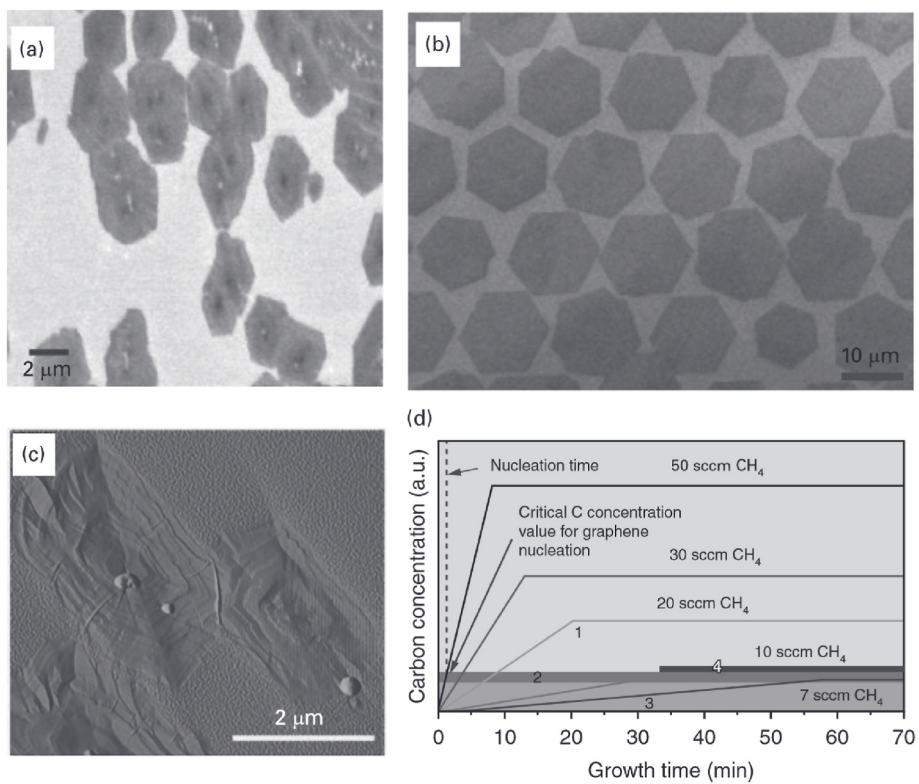


Fig. 15. Graphene hexagonal granules on Cu solid surface (a) SEM images of few-layer graphene domains on a Cu surface (b) Seeded graphene grains growth (c) Image of AFM amplitude of hexagonal graphene grains (d) Carbon concentrations graphs in the Cu film zone as a result of reaction time, demonstrating the relation among experimental situations and the grown graphene data. Regions 1, 2, 3 and 4 demonstrates the growth, nucleation, no growth of graphene, and growth of regular-shaped graphene, respectively [51,155–157].

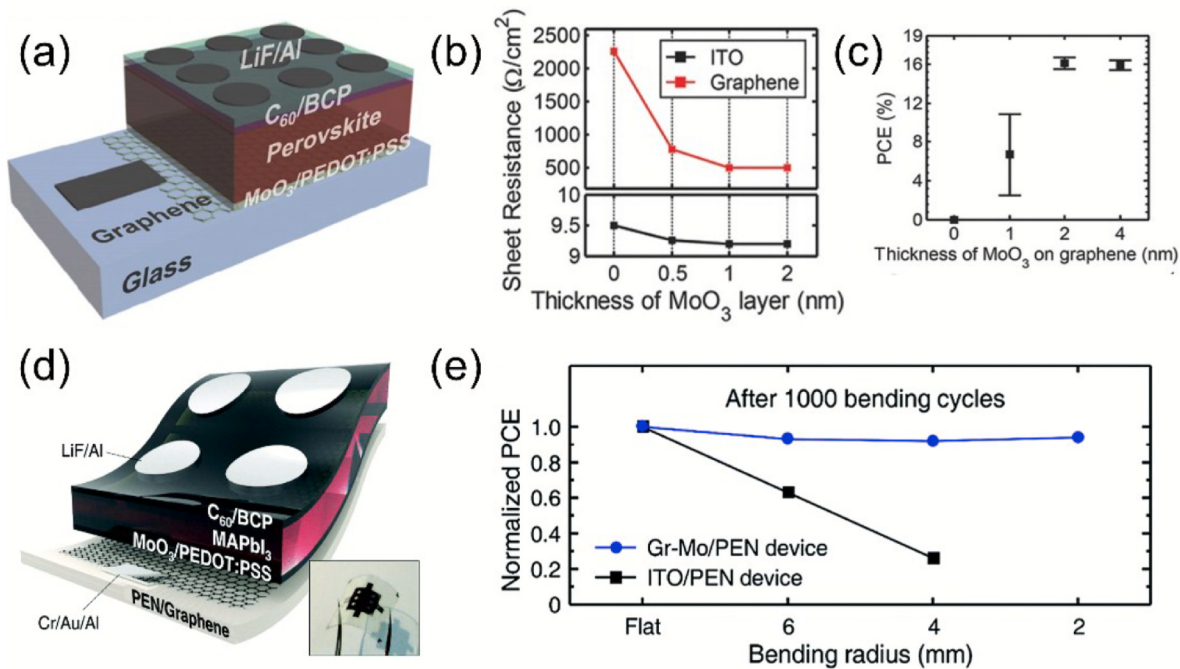


Fig. 16. CVD-grown graphene electrodes for PSCs (a) Schematic of an inverted MAPbI₃ PSC employing graphene as a visible electrode (b) Relationship among sheet resistance and MoO₃ dopant thickness for graphene-based and ITO visible electrodes (c) Relationship among mean PCE and MoO₃ dopant thickness for graphene-based visible electrodes (d) Device structure of graphene-based flexible PSCs (e) Normalized PCEs of the graphene and ITO-based devices after 1000 cycles of bending with numerous radii: flat, 6, 4, and 2 mm [53].

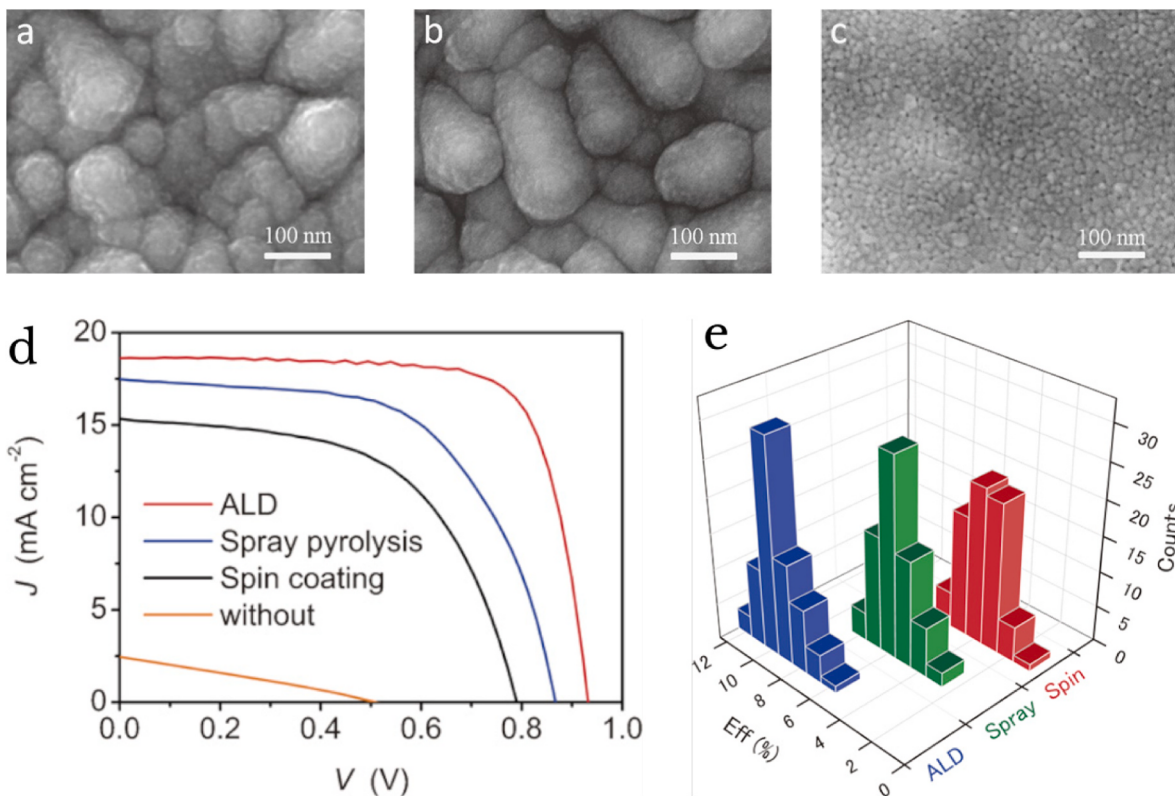


Fig. 17. (a) (Top-view FE-SEM images of TiO₂ compact layers produced on FTO electrodes through various preparation procedures: (a) ALD, (b) spray pyrolysis, and (c) spin coating. The mean thickness of TiO₂ is around 50 nm in every sample.) (d) J-V curves of perovskite solar cells established on various compact TiO₂ blocking layers. (e) Efficiencies histograms for several compact TiO₂ layer-based perovskite solar cells [55].

substitute for ITO in PSCs [53].

Jeon et al. [54] conducted an experiment to use carbon nanotubes generated using CVD in PSCs. They achieved this by entirely replacing both electrodes of the device with carbon nanotubes. They attained a maximum device PCE of 7.3 %. The authors propose a trade-off among price and performance, claiming that although their device has comparatively low performance, their carbon-based electrodes can substantially reduce materials prices in PSC modules by 66 % when implemented on a large scale [53].

The layer of absorber in PSCs is generally coated through solution processing techniques, which include spin-coating, because they are simple to use for manufacturing purposes. Nevertheless, a limited degree of control over the process of solution processing can lead to the production of films that exhibit substantial variations in terms of their morphology, structure, and porosity. Moreover, the substantial utilization of organic solvents in solution-based fabrication gives rise to environmental and health issues. Thermal evaporation, a type of vapor deposition technology, can produce consistent films on surfaces that are rough or not uniform. However, the high capital expenditure and energy cost related to high vacuum equipment make it challenging to apply this technique to large-area devices [53].

Wu et al. [55] established this outcome by fabricating devices with a 50 nm compact TiO₂ ETL by three distinct deposition procedures: spray pyrolysis, spin, and ALD coating. The mesostructured solar cells achieved PCEs of 12.56 %, 8.76 %, and 6.52 % using the three methodologies mentioned (Fig. 17). The authors attributed the enhanced performance of the ALD-based devices to a decrease in interfacial charge recombination and a lower density of nanoscale pinholes in the compact ETL.

CVD graphene sheet typically consists of many crystals and exhibits electrical characteristics that are less superior compared to the exfoliated counterpart. This is primarily attributed to the existence of grain

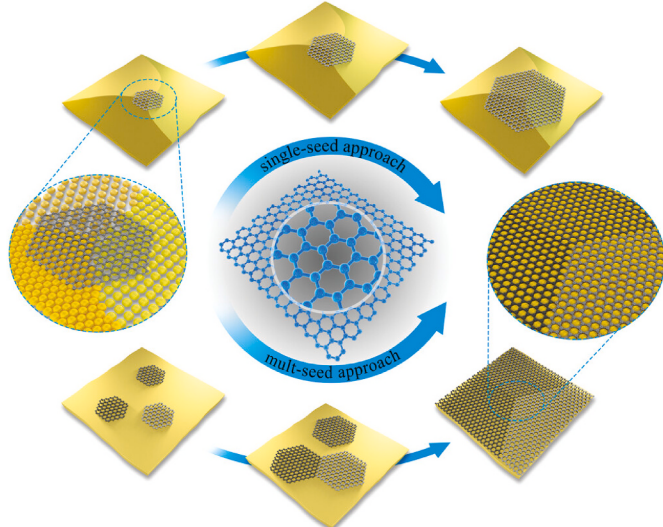


Fig. 18. Two methods for the regulated growth of single-crystal graphene. The upper is the single-seed method, where regulation of the nucleation density is serious to grow graphene single crystals as long as possible and the lower is the multi-seed method where the presentation of graphene nuclei must be aligned to assure the seamless integration of neighboring graphene islands without creating damaged graphene grain boundaries [58].

boundaries, which serve as significant causes of intervalley scattering [56]. Therefore, the primary objective is to produce single-crystal graphene devoid of any structural abnormalities. Single-crystal graphene can be produced through two methods: either by the lateral expansion on the substrate from a single-nuclei (single seed), or by the seamless

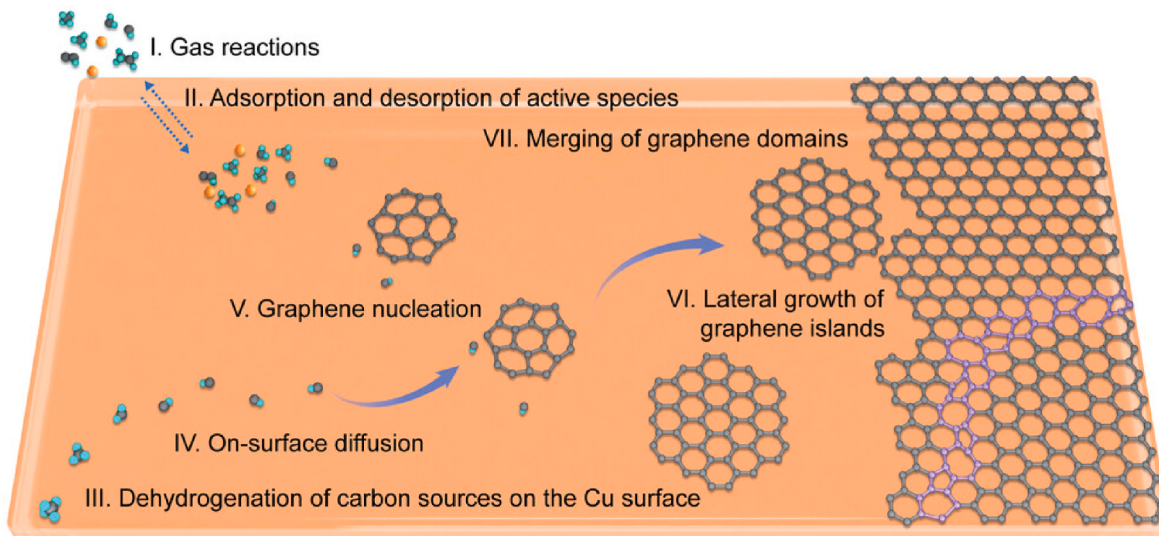


Fig. 19. Graphene Growth mechanism on Cu. I: Gas reaction. II: Desorption and adsorption of active species from the substrate surface. III: Carbon sources Dehydrogenation on the Cu surface. VI: Active species diffusion on surface. V: Nucleation of Graphene. VI: Lateral growth of graphene islands. VII: Combination of neighboring graphene domains [58].

merging of several nuclei with aligned orientation to form a single-crystal domain. First method deals by reducing the number of nucleation sites (Figs. 18 and 19), by methods such as polished copper foil, pre-oxidized copper, or annealed copper foil. It is apparent that the process of growth from a single seed may demand a significant amount of time, however the new development by Wu et al. [57] recommends that the kinetic limit can be overcome. In contrast to that, the process of merging several graphene grains in an epitaxial alignment has the capability to produce a uniform film of single-crystal graphene. This can be achieved in a significantly shorter period of time related to the growth process starting from a single nucleus. The primary objective of the single nucleus approach is to effectively reduce the nucleation density. Ideally, the growth process occurs exclusively from a single seed, thereby eliminating the presence of grain boundaries. The effectiveness of achieving single-domain growth can be attributed to the surface design of the catalytic substrate. The nucleation density of graphene is contingent upon the availability of carbon for graphene growth and the presence of active sites for graphene nucleation [51].

Ni and Cu are the most popular metals among the others for producing uniform and high-quality graphene. Nickel-catalyzed, multilayer graphene could be utilized for stretchable transparent electrodes when graphene thickness is required for adequate conductivity [59]. Li et al. [60] fabricated large graphene films using CVD on copper foils. The resulting graphene films were mainly composed of a single layer and <5

% consisting of double or triple layers. Single layer graphene film developed on Cu is more suitable for high-mobility field-effect transistors. Reina et al. [59] explored a low cost and scalable procedure for graphene films with ambient pressure CVD on polycrystalline Nickel surface. The formed single layer and multiple layer graphene films were of high structural quality and their size was only limited by CVD chamber size. Due to its extremely low carbon solubility, a surface catalyzed, self-limiting technique can be utilized to create a uniform, single-layer graphene throughout the whole copper surface. Also one limiting factor for CVD is the melting point of copper [51,60,61].

Gomez De Arco et al. [62] synthesized transparent thin graphene films by CVD on the nickel surface for organic photovoltaic application and concluded that the synthesis method provides high conductivity, stability low cost, electrode/organic film compatibility and flexibility. Vlassiouk et al. [63] produced huge single crystal graphene using a CVD approach in CH₄, and Ar atmosphere as catalysts, and Cu foils as substrates and hydrogen as a co-catalyst. Single crystal graphene was produced by varying the partial pressures of hydrogen and methane. The resulting graphene was around 10 μm in size, and it demonstrated weak adhesion to the copper foil substrates, that facilitated in the sequential removal of the substrates and the development of prototype devices [61]. The primary factor contributing to the inferiority of polycrystalline graphene is widely attributed to the presence of grain boundaries. Large grain size will result in a reduced number of grain boundaries, leading to

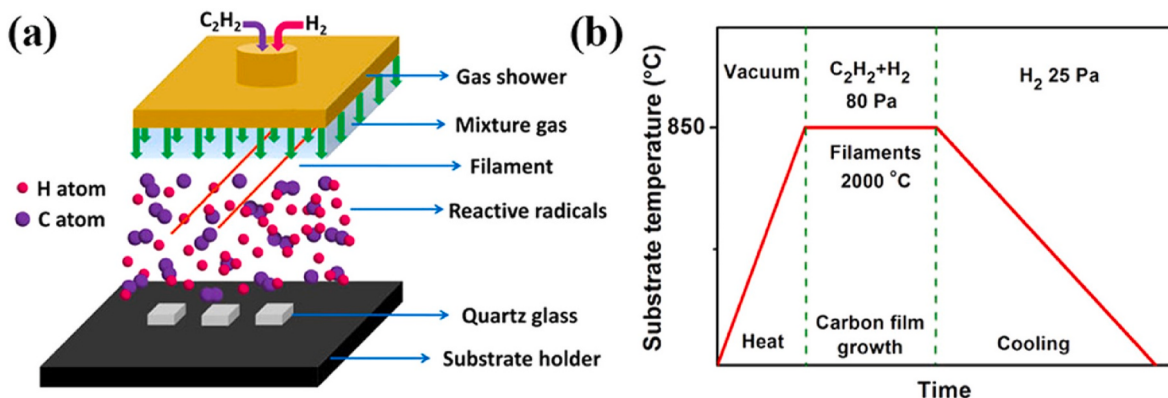


Fig. 20. (a) Diagram of HFCVD system. (b) Schematic Procedure for the preparation of carbon film containing all three steps and its key parameters [64].

improved performance. However, the cost of commercially available single crystal substrates or catalysts is not economic for widespread use [61].

Zhai et al. [64] investigated the structural and chemical properties and the impact of hydrogen on the electrical and structural characteristics of carbon films formed on quartz glass using hot-filament chemical vapor deposition (HFCVD). They reported that HFCVD is a promising approach for producing a-C and nanocrystalline graphene films on glass surfaces and can be used for a wide range of applications. A turbo-stratic structure was seen in a-C films that were formed using 50 % H₂ dilution ratio, that was the outcome of the augmentation of the interlayer gap of sp² aromatic clusters. The graphene films developed by HFCVD on glass demonstrated excellent electrical properties and had a carrier mobility of 36.76 cm²/(Vs) and a resistivity of 5.24 × 10⁻³ Ωcm over 1 cm² area, which was similar to the results obtained from other methods. It was also observed that the nanocrystalline graphene films had a lower conductive activation energy compared to a-C films (Fig. 20).

Another method for the formation of porous graphitic thin films with radio frequency magnetron plasma CVD with silicon target under 0.8 Pa Argon environment was reported. Later annealing was done under Nitrogen atmosphere at 650 °C, decreasing the porosity of the film. Such films demonstrated good gas sensitivity, especially to water vapor and ammonia. The gas sensing capabilities of the carbon film exhibited a significant resemblance to those of reduced graphene oxide [65]. Liu and Wöll [66] reviewed the metal-organic frameworks (MOFs) based thin films and reported the new modifications and techniques used to control film's thickness, homogeneity, morphology and dimensions. They found that even though MOF films have potential for various applications its commercialization is still a long way.

The plasma generator is the main element of the plasma enhanced chemical vapor deposition (PECVD) system and may be divided into three primary categories based on the power source used for plasma generation: microwave plasma (often at 2.45 GHz), radio frequency (RF) plasma (typically at 13.56 MHz), and direct current (DC) plasma. Microwave (MW) plasma refers to a form of high-frequency electromagnetic radiation that operates within the gigahertz range. So far, MW-PECVD has been widely utilized in the production of graphene and its related materials, including CNTs and diamond films. The RF generator's energy is connected to the plasma through three primary modes: the propagating wave (W) mode, evanescent electromagnetic (H) mode, the propagating wave (W) mode, and the electrostatic (E) mode W-

mode. The H-mode inductively coupled plasma (ICP) offers the benefit of a high-power density and a greater plasma volume, resulting in elevated growth rates. On the other hand, E-mode capacitively linked plasma has relatively little energy, it cannot be employed as a separate supplier of plasma. Another frequently used source is dc glow plasma because of its straightforward setup. DC glow plasmas can be created using two different geometric designs: pin-to plate, and parallel-plate which can develop nonuniform and uniform plasma sources respectively.

Gaseous substances play a crucial role in the production of graphene and its derivatives, which can be classified into three distinct functional groups. (i) The carbon-containing gaseous precursors supply carbon radicals to facilitate the development of graphene through plasma-enhanced reactions. (ii) Gases like H₂ and O₂ are introduced as amorphous carbon etchants in order to generate outstanding graphene and its derivatives. (iii) Gases like N₂ and NH₃ are commonly employed to perform the doping process on as-grown graphene that can modify its electrical characteristics. During the plasma-enhanced process, the source gas undergoes activation through the energetic electrons produced in the plasma. The process of ionization, excitation, and dissociation of the source gases takes place within the low-temperature plasma. Initially, the ionization processes occur through the interactions between high-energy electrons and molecules of gas. Secondly, the ions with high energy, which are produced during ionization processes eventually engage in reactions with molecules of the source gas. These radicals have higher reactivity compared to atoms or molecules in their ground state, enabling the synthesis of graphene and its derivatives on surfaces with or without a catalyst, even at low temperatures. Detailed mechanism of graphene synthesized using PECVD is discussed by Li et al. [44] (Fig. 21).

Kim et al. [67] developed highly transparent coatings of hydrogenated amorphous carbon via PECVD. The films were formed at room temperature and by using methane source gas. The films were exhibited the high transparency across a wide spectrum, ranging from ultraviolet to infrared, with a transmittance of approximately 90 % (Fig. 22). It also has an optical bandgap of around 3.7 eV and have young's modulus as ~78GPa and density of ~1.9 g/cm³.

Liu et al. [68] investigated the impact of growth temperature, cooling rate, and methane flow on the production of graphene coatings on cemented carbide surfaces. They concluded that, for optimal growth include methane flow rate of 10 sccm, a growth temperature of 1000 °C,

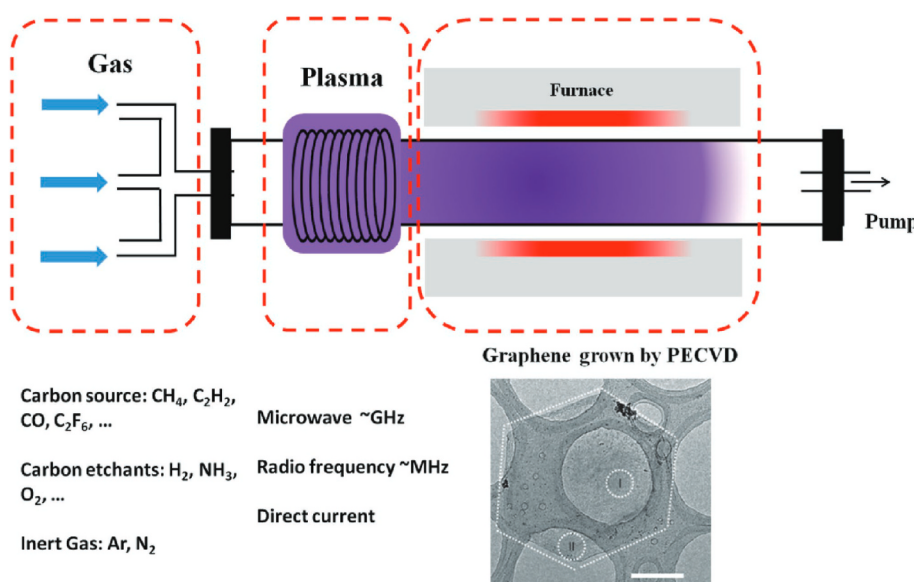


Fig. 21. Illustrates experimental setup schematic for PECVD comprising three main elements – vacuum heating system plasma generator system and gaseous system [44].

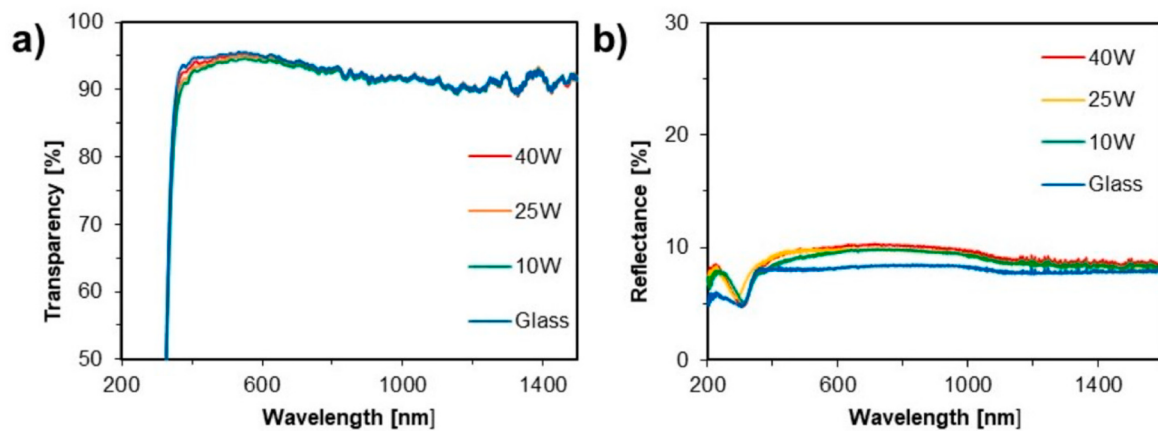


Fig. 22. (a) Transmittance and (b) reflectance spectra of the a-C:H coatings Developed through the variable RF power ion source [67].

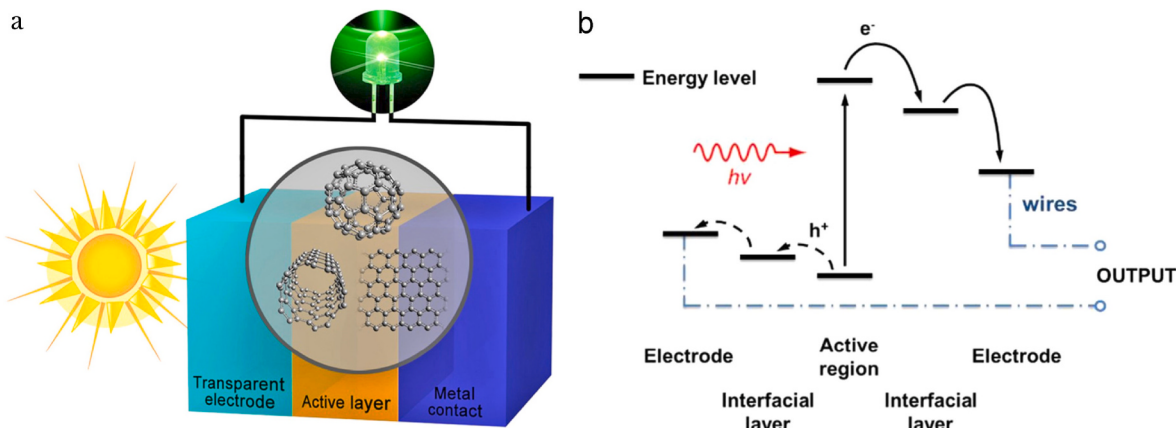


Fig. 23. (a) Diagram of a photovoltaic device based on nano-carbons that converts solar energy to electricity (b) Outline of photovoltaic process [69].

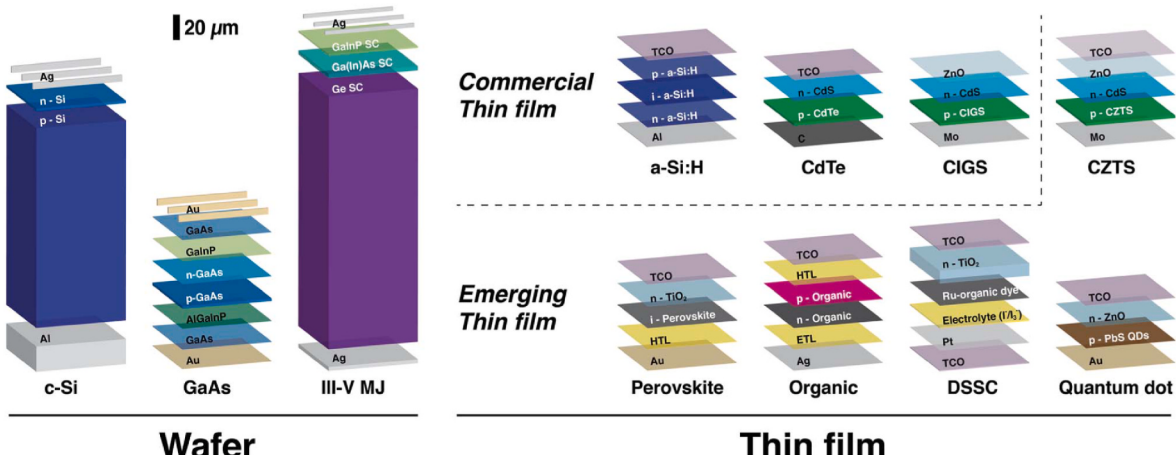


Fig. 24. Typical solar PV technologies, divided into wafer-based and thin film [70].

and a cooling rate of 15 °C/min and the rise in methane flow can lead to increase graphene layers number. Also, the inverse relation between the applied frictional load and coefficient of the graphene friction was found.

3. Photovoltaic (PV) solar cells

PV solar cells directly transfer light energy into electricity. Its process typically consists of three main steps: the creation of excitons, the split of

excitons, and the transit and cluster of charge carriers (Fig. 23). Various materials are utilized to perform these operations. Active materials absorb photons to produce excitons and establish heterojunctions for exciton separation. Subsequently, the produced electrons and holes are conveyed and gathered at the anode and cathode. The energy level difference among the active materials (typically a semiconductor) and the materials used for electrodes can have a major impact on the device's performance. Interfacial layers are necessary when there is a considerable difference in energy levels among active and electrode materials.

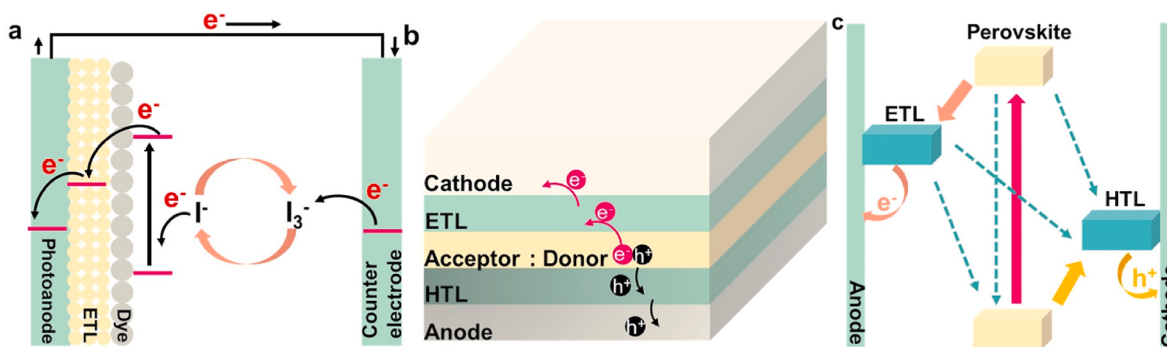


Fig. 25. Diagrams showing the working process and structure of (a) DSCs, (b) organic solar cells (OSCs), and (c) PSCs [72].

These layers serve to decrease the barrier for carrier injection from the active area to the electrodes and minimize the probability of electron-hole reintegration.

PV technologies can be widely divided into two clusters: wafer-based and thin-film based. Former are made from semiconducting wafers and may be carried without the use of an extra substrate; whereas later are made up of films that have been placed on a glass, plastic, or metal substrate. Thin films can be further classified as commercial and emerging technologies [70] (Fig. 24).

Third generation PV technologies are frequently defined as those that are based on organic materials and do not depend on traditional single-p-n junction technology. They are as follows: (i) the Gratzel-invented dye-sensitized solar cells (DSSC), which are electrochemical cells that need an electrolyte; (ii) multi-function cells made from cluster IV and III-V semiconductors; (iii) hybrid techniques that combine organic materials with nanostructured inorganic semiconductors like TiO₂ or deposit inorganic quantum dots into a semiconducting polymer matrix, and (iv) all-organic solid-state techniques (Fig. 25). In organic materials, photon absorption results in the creation of an exciton, which is a bound electron-hole pair. As a result, organic materials that absorb light through optical means do not immediately produce free electron and hole carriers that may easily cause a current. Rather, the excitons must detach before they can produce a current. One distinguishing characteristic of organic semiconductors is the excitonic nature of their optical characteristics [71].

In general, thin flexible solar cells are bendable, twistable, and are made on flexible substrates. In these cells low-temperature manufacturing (below 150 °C), less thicknesses, and adjustable colors have gained significant attention [72]. In the standard arrangement of organic solar cells (OSCs) (Fig. 25 (b)), an active layer consisting of a p-type donor and an n-type acceptor, such as poly (3-hexylthiophene): phenyl-C61-butyric acid methyl ester (P3HT:PC61BM), is sandwiched between the anode and a cathode, that has two charge transport layers. Highly conductive materials, such as poly (3,4ethylenedioxythiophene): poly (styrene sulfonate) (PEDOT: PSS), are used as the anode and the active layer in a device called HTL. These types of layers split by the anode and cathode, respectively. ETL and HTL transfer electrons and holes to the cathode and anode, respectively, to produce voltage and current. OSCs, on the other hand, often have low power conversion efficiencies (PCEs) [72]. Single junction photovoltaic solar cells (PSCs) can be classified into two primary configurations: n-i-p and p-i-n. In these configurations, the letters n, i, and p represent donor-type, intrinsic, and acceptor-type semiconductors, respectively. In the planar (n-i-p) architecture, a layer called the electron selective layer (ESL) is coated onto a transparent conducting glass. That is then followed through the deposition of the LHP layer. The hole selective layer (HSL) is coated onto the LHP film and then covered by a metal contact. In the p-i-n layout, the bottom contact exhibits selectivity towards holes, whereas the ESL is positioned on top [73]. OSCs are constructed from conjugated organic small molecules and are generally called polymers.

They are a viable choice for large surface area, flexible solar technology with mechanical structure, due to their low temperature, and solution-based production. To solve the weaknesses of bilayer OSCs, the bulk heterojunction was created, which combined the donor and acceptor into an interpenetrating framework. One major disadvantage of the bilayer design is that excitons generated within a film must travel a significant distance to reach the interface, despite the precise processes required to build the film. It makes sense that films with greater thickness would have a higher capacity to absorb light, produce more exciton, and result in solar cells that are more efficient. However, thicker films would be useless if the majority of those excitons never convert to free carriers [74].

In the past few years, a lot of progress has been made in optoelectronic devices like OSCs, organic light-emitting diodes (OLEDs), smart windows and field effect transistors (FETs). Transparent electrodes are key component in all above of optoelectronic devices. Indium-doped tin oxide (ITO) is generally utilized to make transparent conductive films (TCFs) as it has a minimal sheet resistance of 10 Ωsq⁻¹ and visible transmittance of ~93 % [76]. However due to its restricted deposition conditions, require for a relatively uncommon element, and poor chemical stability in acidic and basic environments. Also, ITO isn't readily available to meet the growing demand for flexible cells and electronics. To meet the requirement, other options should be investigated as an alternative of ITO. Graphene is a substantially suggested because of its high electrical conductivity and optical transmittance in the visible and near-infrared (NIR) range [77]. Due to the high electron mobility of graphene (200,000 cm²V⁻¹s⁻¹), single-layer graphene can attain a potential sheet resistance of 30 Ωsq⁻¹ [78]. Also, graphene demonstrates high chemical stability and outstanding flexibility, but the production of large-area single-crystalline graphene without any faults or toxins remains an extremely difficult task. All such limitations reduce the graphene conductivity, which restricts its utilization in different devices. The properties of high conductivity and high transparency plays a vital role in optoelectronic applications. The transmittance of materials is dependent on their absorption and reflection properties. Single-layer graphene has the capability to demonstrate a transmittance of up to 97.7 % inside the visible region, owing to its remarkably low reflection of less than 0.1 % in this spectral range [78,79]. An essential property of optoelectronic materials is the existence of a straight band gap, allowing electronic transitions among the conduction and valence bands to take place without the need for phonons [75].

CNTs can be semiconducting or metallic with almost ballistic conduction depending on the different chirality. It has been discovered that semiconducting CNTs are often p-type and have a high expected mobility. As the conduction electron states of SWNTs are one-dimensional, the local density of states of these materials contains well-spaced and symmetric structures known as van Hove singularities. In metallic nanotubes, the fundamental energy gap is zero, but in semiconducting nanotubes, it is approximately 0.5 eV. By mixing CNTs with varying diameters and chiralities, a continuous response across a wide

Table 4
Properties of carbon allotropes [75].

Material	Hybridization	Crystal Structure	Conduction Type	Band gap (eV)	Work function (eV)
Graphite	sp^2	Hexagonal	Semi-metallic/semi-conducting Metallic/semi-conducting Insulator Semiconductor Semiconductor	0	5.0
Graphene	sp^2	—		0–0.3	5.0
CNT	sp^2+sp^3	Cylindrical		0.3–2.0	4.5–5.1
Diamond	sp^3	Cubic		5.5	5.45
Fullerene (C_{60})	sp^2+sp^3	Cubic		1.6	4.6–5.0
a-C	sp^3+sp^2	—		0.2–0.3	4.9

Table 5
List of numerous end purposes, their main features, and the suitability of every material (“✓” = superior, “–” = good, “✗” = poor) [80].

Applications	Key Features	Nanotube	Graphene	Metal Nanowires
Touch Panels	Flexibility	✓	✓	✗
	Patterning	✓	✓	✓
	Sheer Resistance	✓	—	✓
	Transparency	—	—	✓
LCD	Surface	—	✓	✗
	Roughness	—	—	—
	Ionic Impurities	✗	✗	✗
	Conformal	✓	✓	✗
OLED/Solar Cell	Coating	—	—	—
	Color/Haze	✓	✓	✗
	Work Function	✓	✓	✗
	Sheet Resistance	✗	✗	✓
	Surface	—	✓	✗
	Roughness	—	—	—
	Stability	✓	✓	✗

spectral range can be achieved [75]. Properties of common carbon allotropes are mentioned in Table 4. Moreover, the suitability of nanotubes and graphene and metal nanowire in different applications is highlighted in Table 5.

4. Carbon nanomaterial in thin film photovoltaic solar cells

The market for photovoltaic systems is currently dominated by silicon wafer-based solar cells, due to their high PCE, exceptional stability, extended lifespan, scalability of the procedures, and high ratio of cost to performance.

Carbon materials have gained significant interest because of their adjustable structures with suitable Fermi levels, affordable cost, copiousness, and a range of exceptional characteristics, such as notable mechanical strength, promising electrical and thermal conductivity, chemical stability, and superior high charge carrier mobility. Carbon nanomaterials (e.g., graphene, fullerene, and CNTs) have since been utilized as additives, charge transport layers, and electrodes (both counter and window electrodes) in many types of PSC device topologies. The tunable characteristic of the perovskite bandgap is desirable as it provides the possibility to optimize the light absorption in the resulting photovoltaic cells, potentially by utilizing multiple-layered perovskite tandem solar cells. The PSC is derived from studies on DSSCs and usually utilizes either a mesoporous structure or a planar heterojunction structure. A planar heterojunction structure is produced by placing a perovskite thin film among two charge transport layers, specifically an electron transport layer (ETL) and a hole transport layer (HTL), without using a mesoporous scaffold. The ETL and HTL are both essential for the device's functioning since they facilitate effective charge conduction to the anode and cathode, respectively [81].

Mismatches in energy levels across layers in PSCs are another hurdle that needs to be addressed. Hole-electron pairs are formed by the absorption of light in perovskite (Fig. 26). Electrons are carried via the ETL, while holes are carried through the HTL. Using electron transition as an instance, when the lowest unfilled molecular orbital level (LUMO) of the perovskite layer is significantly greater than the LUMO level of ETL, it will cause in an excess energy loss. Nevertheless, when the LUMO level of the perovskite layer is less than the LUMO level of the ETL, the transfer of electrons to the ETL becomes challenging due to the presence of a significant energy barrier (Fig. 27). Therefore, reducing the disparity in energy levels is crucial for conserving energy and enhancing the efficiency of PSCs. The cost of producing polymer-based organic solar cells is only roughly one-third that of silicon cells, and they are

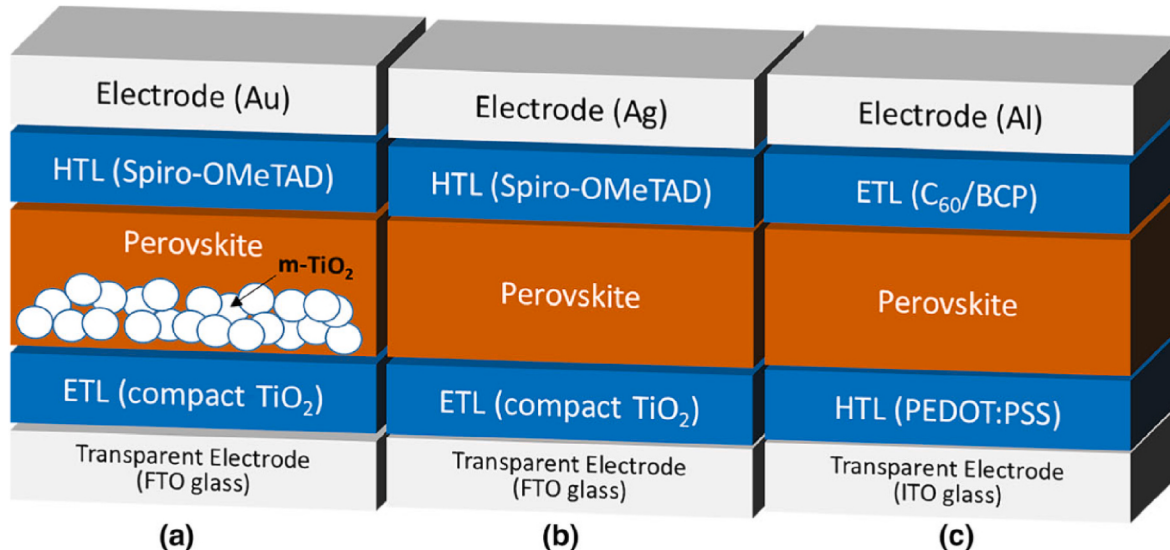


Fig. 26. (a) Mesoporous perovskite solar cell device architecture with transparent electrode (b) Traditional planar heterojunction perovskite solar cell (n-i-p) (c) reversed planar heterojunction perovskite solar cell (p-i-n) [81].

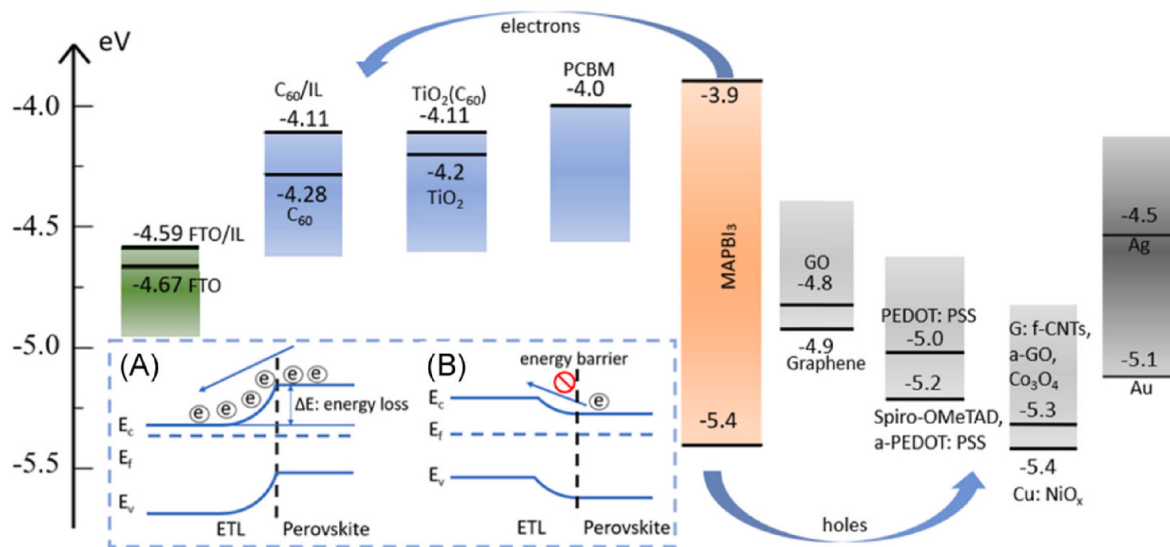


Fig. 27. Energy level of every layer in PSCs. (a) energy is lost when LUMO magnitude or level of perovskite is much higher to ETL. (b) energy obstacle occurred when LUMO magnitude or level of perovskite is lesser than ETL. (CNT, ETL-electron transport layer, FTO-fluorine-tin oxide, GO-graphene oxide, LUMO-lowest unoccupied molecular orbital level; PSC-perovskite solar cell; PEDOT:PSS-poly (3,4 ethylenedioxythiophene) polystyrene sulfonate) [83].

more versatile. They can be devised using molecules and are reusable [75]. Recently Wang et al. [82] and Li et al. [48] has comprehensively reviewed perovskite solar cells and modules.

Energy levels of carbon nanomaterials are not only well-suited for usage as PV cells but can also be tailored throughout a large range by specifying a molecular structure. They also feature efficient structures at the atomic and mesoscopic levels, which contributes to their high conductivity. All functional layers should be made flexible for thin film solar cells. Furthermore, interactions among flexible electrodes and active layers via low-temperature processing are important for changing the structure and interface of all functional layers, hence altering solar power device performance [72].

Utilizing CNTs in a passivated charge chosen contact system must also be balanced against the use of 1D and 2D materials like graphene flakes, black phosphorous, or MoS₂, which have proven to create an expanded porous grid and operate as carrier selective contacts. However, the future of carbon nanotubes in photovoltaics is promising, and the barriers to application are fast disappearing [74]. Ku et al. [84] initially incorporated carbon into the perovskite solar cell architecture, using carbon black/graphite as a counter electrode in a hole-conductor-free PSC architecture to achieve a PCE of 6.64 %.

4.1. Carbon nanotubes (CNTs)

CNTs are categorized as single walled CNTs (SWCNTs, $n = 1$), double-walled CNTs (DWCNTs, $n = 2$), and multi-walled CNTs (MWCNTs, $n \geq 3$), based on the number of layers (n). SWCNTs can be distinctly characterized by the chiral vector ($C_h = n\mathbf{a}_1 + m\mathbf{a}_2$). The variables a_1 and a_2 represent the unit cell vectors of the lattice, while n and m are integers. SWCNTs are characterized as zigzag ($m = 0$), armchair ($m = n$), or chiral (other situations) based on their rolling angles and SWCNT's electrical characteristics are influenced by their chiral vectors. These can be metallic ($m = n$ or $m - n$ is a multiple of 3) or semiconducting (in other cases) [72].

The CNT films thickness would be selected to provide a layer with substantial lateral electrical conductivity while maintaining the highest level of transparency towards incident light. It is being considered to substitute for conventional conductive materials (such as ITO, FTO, ZnO, or CdS) in coatings and circuits.

On the basis of the production environment, Sun et al. [85] classified CNT and graphene based thin-film manufacturing into three phases: solid, liquid, and gaseous. To fabricate solid phases, CNTs and graphene adhered to a solid wafer are transferred to an elastic substrate.

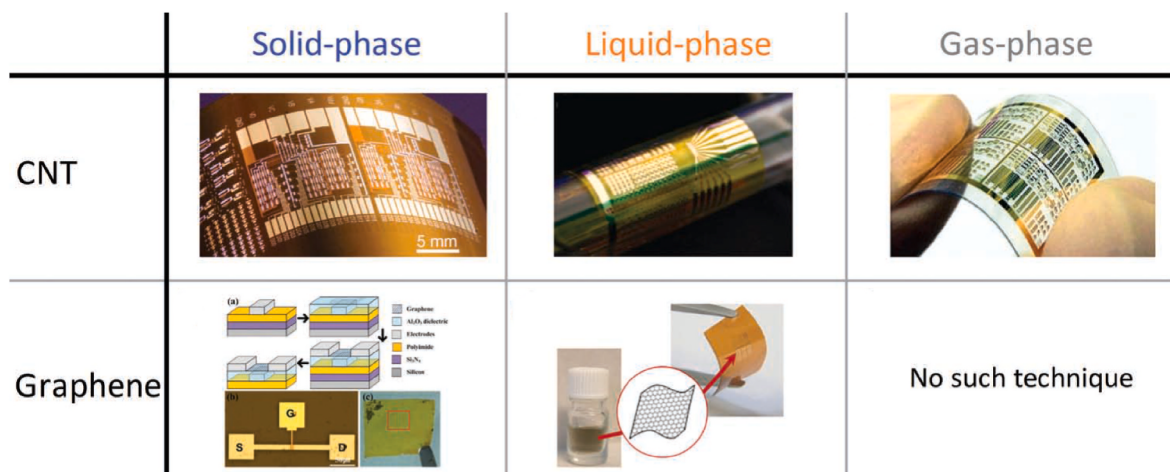


Fig. 28. Solid, liquid and gas phase manufacturing for CNT and graphene [85].

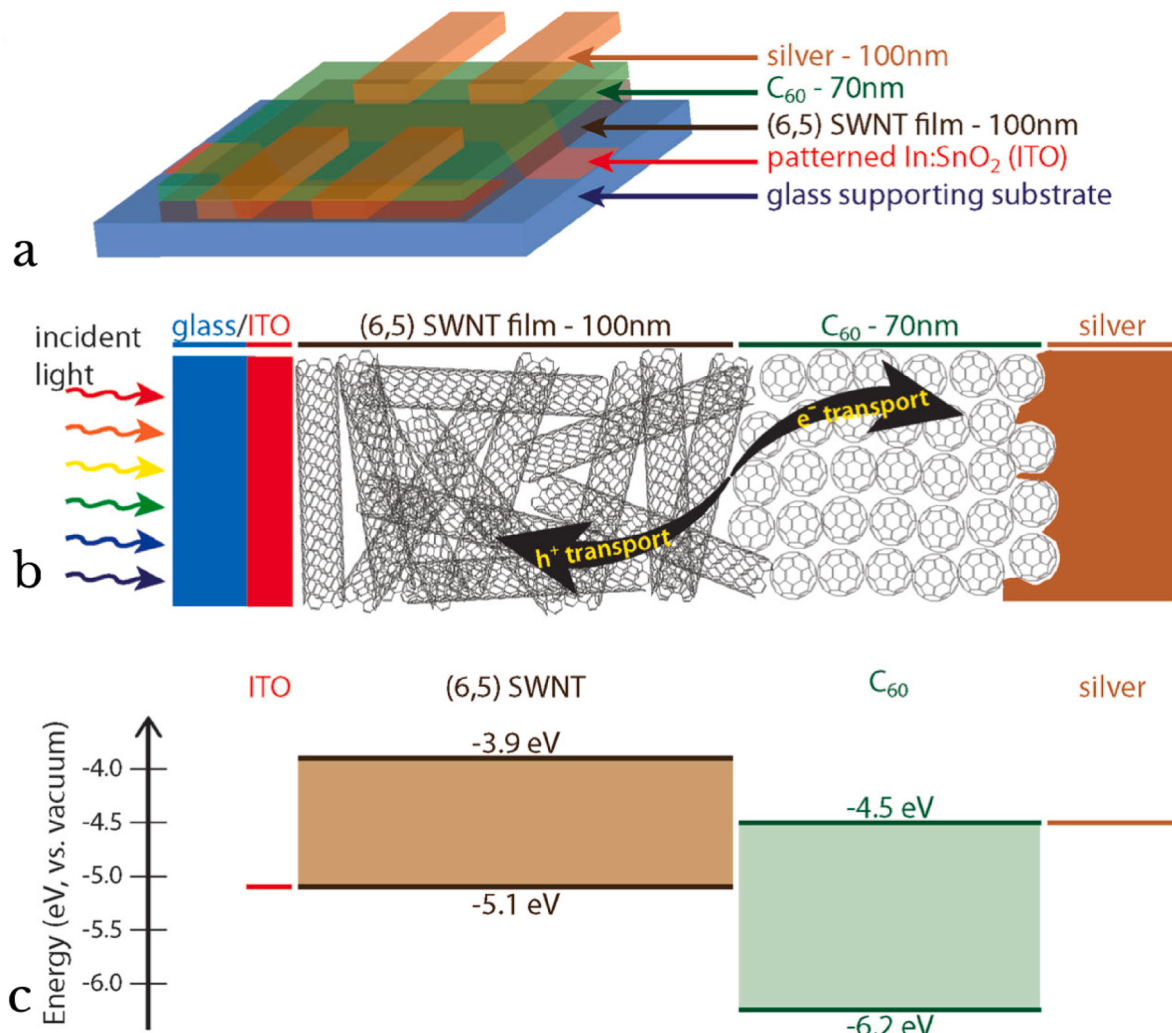


Fig. 29. demonstrates the energy diagram and schematic of polymer free CNT photovoltaic device. Layer 3D device architecture (a) that permits for the creation and investigation of several devices from a SWCNT film, and cross-sectional diagram (b) Focusing the directional transportation of charge carriers (c) Energy diagram of the device demonstrating a type-II heterojunction [86].

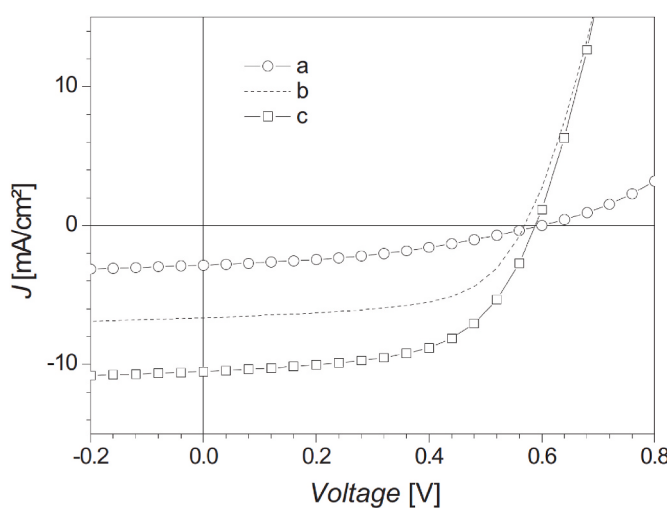


Fig. 30. Current-density-voltage curves for various forms of the active layer in the photovoltaic cell: a) amorphous P3HT and PCBM, b) amorphous P3HT and PCBM annealed at 150 °C for 5 min, and c) pristine nanostructured P3HT and PCBM. The measurements have been worked in simulated AM1.5 situations at 100mWcm⁻² [88].

Liquid-phase techniques consist of spin coating, inkjet printing, nano-imprinting, di-electrophoresis, and others, a flexible substrate is coated with CNTs or graphene that are dispersed in a solution. For gas-phase development, a thin film of CNT is produced in a gaseous environment and subsequently transferred in dry form to a substrate to fabricate elastic devices, but no such method was reported for graphene (Fig. 28).

Jain et al. [86] used a 100 nm (6,5) SWCNT layer and reported that the exciton diffusion length was measured using photocurrent measurements in bilayer devices or ultrafast spectroscopy, and it has been found to be 5–10 nm. As a result, the SWCNT films used in all high-performance SWCNT/fullerene solar cells are only a few nanometers thick (Fig. 29). However, Bindl et al. [87] predicted that an internal quantum efficiency of 100 % can be achieved with a 4 nm thick screen [74].

Berson et al. [88] incorporated SWCNTs and MWCNTs to a poly 3-hexathiophene (P3HT):PCBM active layer combination in separate devices, resulting in a 100 % increase in J_{SC} (Fig. 30). However, a balance was found between the J_{SC} and fill factor (FF) as well as between the J_{SC} and V_{OC}, resulting in PCE of 1.3 % for SWCNTs and 2 % for MWCNTs, correspondingly. The adjustment was explained by the fact that CNTs with large aspect ratios had more short circuit connections.

CNTs as the active layer of OPVs have also been reported in the literature. CNTs have shown potential for reduced brittleness that can limit device lifespan of ITO and have the potential overcome the

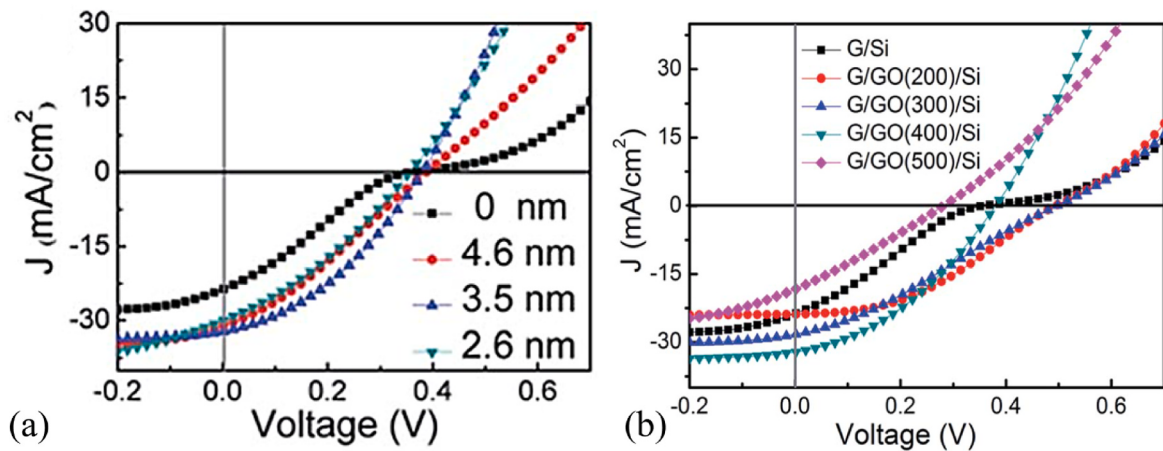


Fig. 31. Graph of J_{sc} and voltage for (a) different layer thickness and (b) G/GO annealing temperature [92].

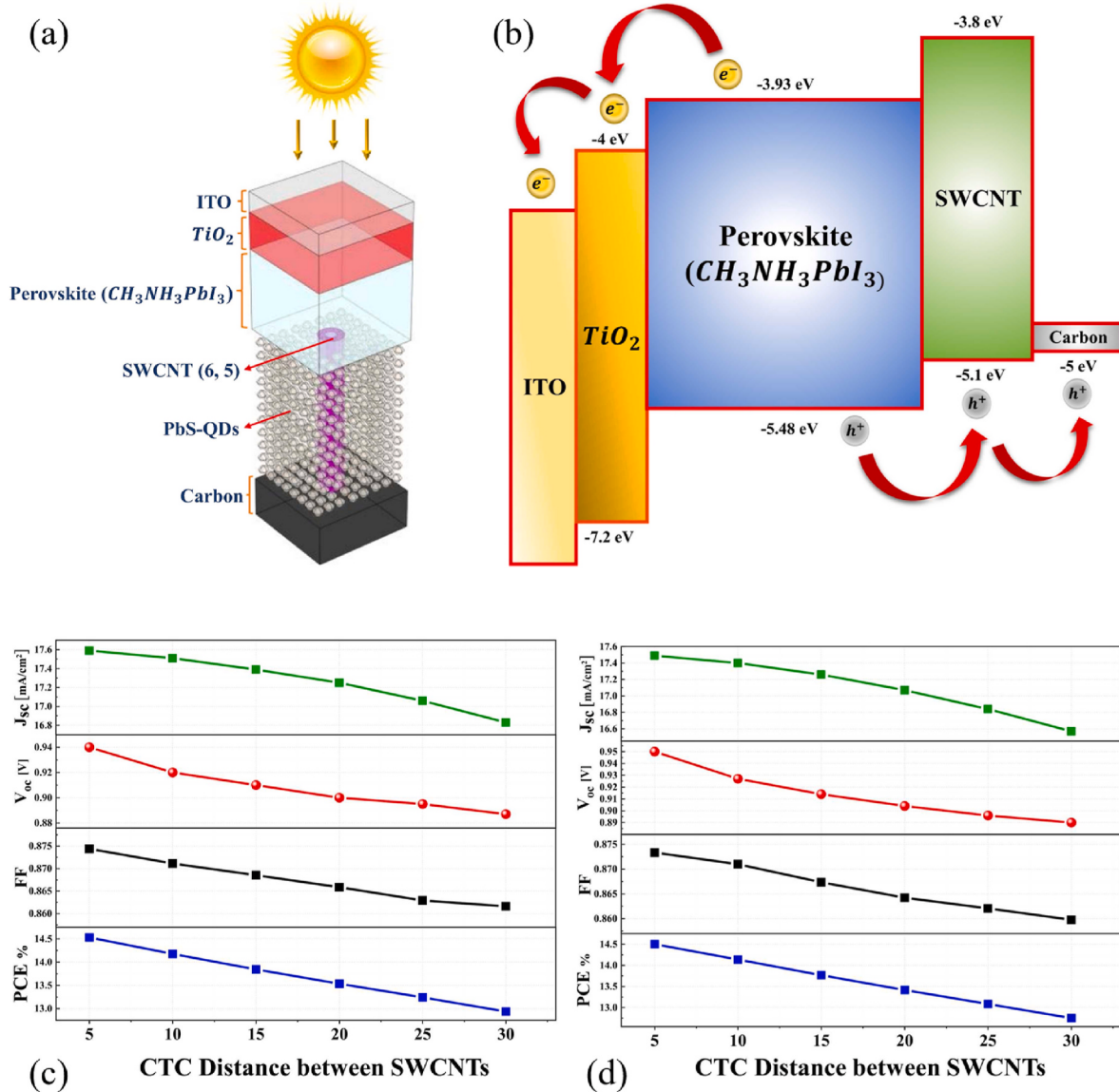


Fig. 32. (a) Schematic structure of the projected PSC with the (6,5) SWCNT as the HTL contained via PbS-CQDs (b) Band diagram of the projected PSC structure with SWCNT based HTL, Electrical parameters for (c) 800 nm and, (d) 1200 nm CNT length with 5–30 nm CCDs [101].

shortage of indium. However, there are still barriers to their widespread adoption including long-term stability and reliability, low-yield mass production, and a less cost-effective production process [89–91].

Initial investigations involving CNTs acting as acceptors for porphyrins produced monochromatic PCE values of 435 nm amounting to 8.5 %. After that, CdS nanoparticles were covalently bonded to CNTs, resulting in a 25 % internal quantum efficiency in the subsequent photoelectrochemical behavior. Additionally, CNTs were combined with CdTe nanobelts and Si nanowires to fabricate nanostructured iterations [89]. While both semiconducting and metallic CNTs can function as efficient carriers of charge, only semiconducting CNTs with a limited band gap can function as sites for charge separation, while metallic CNTs can increase the short circuit current and serve as recombination centers, suggesting that monodisperse semiconducting CNTs are more appealing in this application [89]. Jiao et al. [92] and Yang et al. [93] used GO as an interfacial layer to upgrade the efficiency of a solar cell. They increased the annealing temperatures to attain greater PCE values. Using the GO film reduced the PCE from 2.13 % to 0.2 %, however increasing the annealing temperature to 400 °C improved the efficiency by up to 5.2 % (Fig. 31) [94].

It was also reported that electrodes composed of 99.9 % pure metallic SWCNTs performed 50 times better than 99.9 % semiconducting SWCNTs and performed similarly to control ITO-based devices. The improvement was predominantly attributable to an increase in J_{SC} . In the investigation, nitric acid was used to dope SWCNT films to decrease irregularity and sheet resistance. This significantly reduced PCE for semiconducting SWCNTs in comparison to metallic SWCNTs that are treated similarly to nitric acid treated semiconducting SWCNTs due to their lower sheet resistance [95,96].

Guo et al. [97] used annealed ion irradiation graphene in ammonia for n-type doping, whereas fluoropolymer was employed by Lee et al. [98] as the p-type doping layer and as a supporting layer for graphene transfer. Huang et al. [99] employed alkali carbonate salts (Li_2CO_3 , Na_2CO_3 , K_2CO_3 , Rb_2CO_3 , and Cs_2CO_3) to regulate a graphene-CNT composite film's work function. The composite film's work function decreased from 5.1 to 3.4 eV upon doping with Cs_2CO_3 . In OPVs, these doped composite materials may be utilized as cathodes. Conversely, when composite films are exposed to oxygen, the doping impact of alkali carbonate salts on graphene will progressively diminish [100].

Fooladvand et al. [101] suggested a PSC structure made up of a bottom-up layer with a 100 nm thick carbon film as the back contact layer (BCL). They used CVD on a thin layer of carbon to produce SWCNTs. Then, they fill the gap space among SWCNTs with lead sulfide colloidal quantum dots (PbS-CQDs) material to build a composite of nanotubes and PbS-CQD on a thin carbon sheet. The glass substrate is covered with ITO after being washed for 15 min in an ultrasonic bath with acetone, isopropanol, and ionized water, which formed the ITO glass layer. After that, it was dried using nitrogen gas and placed in an oven at 120 °C, then TiO_2 layer placed. They fabricate the MAPbI_3 perovskite layer using the Lewis base conduction approach, as explained

by Ahn et al. [102]. Fooladvand et al. investigated electrical parameters with two different 800 nm and 1200 nm HTL heights (Fig. 32) and reported the best overall values for PCE, FF, V_{oc} and J_{sc} values were 19.98 %, 0.86 %, 0.94 V and 24.45 mA/cm^2 respectively. Also, the maximum PCE was obtained with nanotubes and PBs-CQDs of 800 nm, in addition leading to superior cell stability.

Bernardi et al. [103] applied the active layer of combination of carbon nanomaterials. Their cell structure was Al (100 nm) as the top contact followed by CPV (120 nm), TFB (10 nm), poly (3,4-ethylene dioxythiophene) polystyrene sulfonate (PEDOT:PSS) (40 nm) and lastly ITO. Initially, they concluded that large diameter semiconducting SWCNT (s-SWCNT) with fullerene derivative (PCBM) cannot provide PV conversion and are unsuitable for PV operation due to type-I alignment, on the other hand the high van der Waals attractive force between small-diameter nanotubes caused extensive bundling and poor morphology leading to maximum efficiency of ~0.4 % using either PC₆₀BM or PC₇₀BM. Further they added reduced graphene oxide (rGO) as a third material phase to induce exciton dissociation at the interface with PCBM or s-SWCNT and reported the phase combination PCBM/rGO/s-SWCNT with $d > 1.2 \text{ nm}$ can simultaneously achieve favorable morphology and exciton dissociation. They reported the best device active-layer composition was of PC₇₀BM (95 wt %)/rGO (2 wt %)/s-SWCNT (3 wt %, $d > 1.2 \text{ nm}$), achieving power conversion efficiency of 1.3 %, with short-circuit current (J_{sc}) of 3.1 mA/cm^2 , an open circuit voltage (V_{oc}) of 0.75 V, and a FF of 0.55, (Fig. 33b). They also evaluated J_{sc} , V_{oc} , FF and the power conversion efficiency upon aging

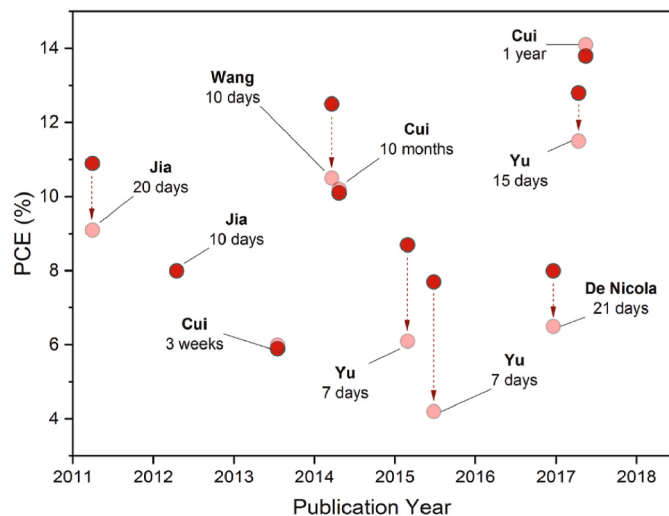


Fig. 34. Optimization of CNT-silicon solar cells stated to be stable for a minimum of 7 days. pink data points demonstrate the starting efficacy of devices while red data points demonstrate the efficacy after the indicated time [104].

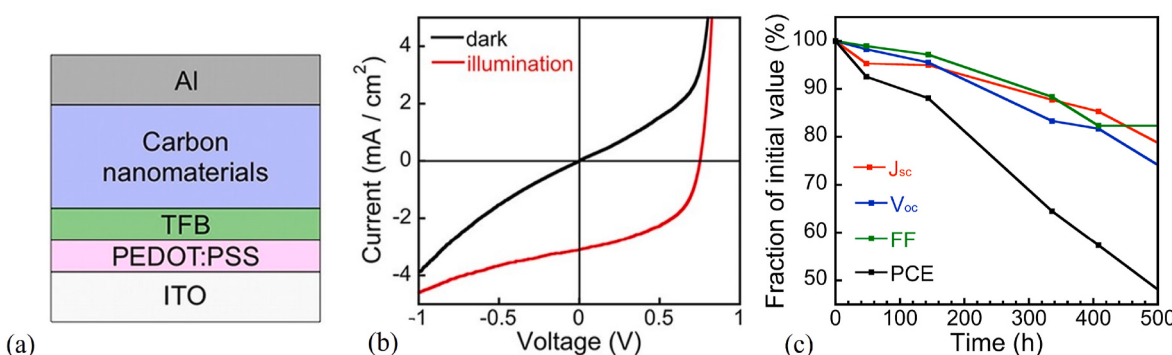


Fig. 33. (a) Carbon nanomaterial based solar cell structure (b) Current-voltage curves (c) Evolution of device characteristics [103].

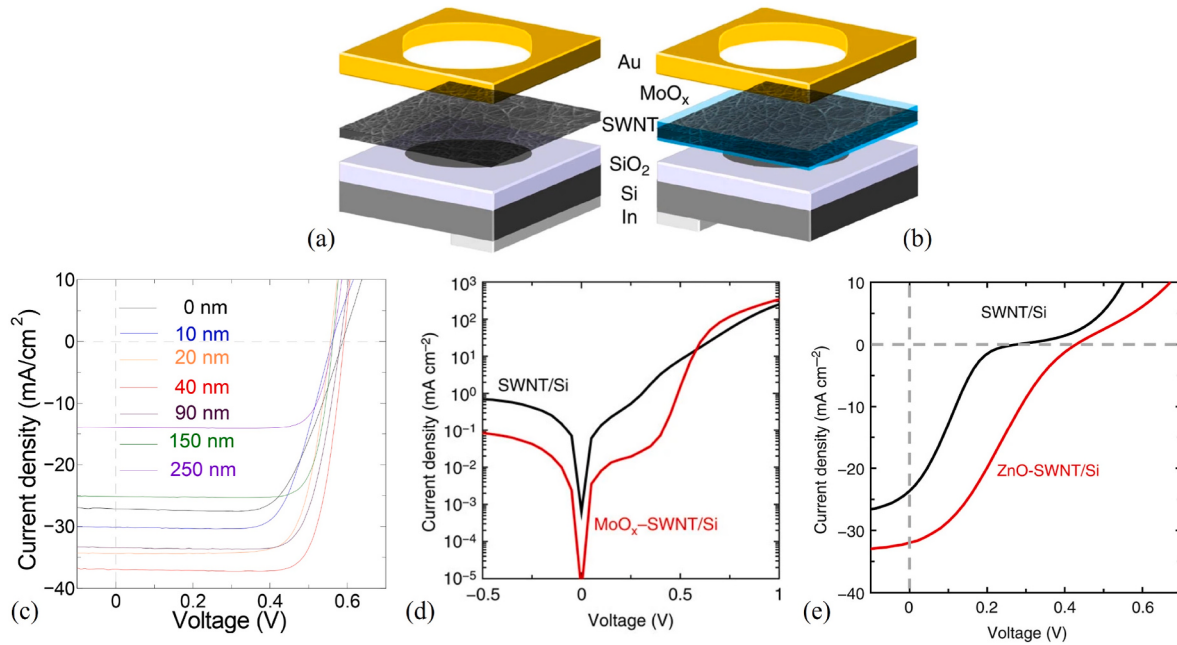


Fig. 35. Photovoltaic working of n-SWCNT/p-Si solar cells. J-V curves for the n-SWCNT/p-Si solar cells with (red line) and without (black line) a ZnO layer [105] (a) current density voltage (J-V) curves for MoO_x-SWCNT/Si solar cell as a function of the MoO_x layer thickness. (b) Log-plot of the dark current before (black line) and after (red line) the deposition of the MoO_x coating. (a,b) Schematic diagrams of the pristine-SWNT/Si and MoO_x-SWNT/Si solar cells, respectively [105].

of a non-encapsulated device in air (Fig. 33c).

Tune and Flavel [104] emphasized the variance between high efficiency CNT-silicon solar cells and stability. Numerous short-acting doping schemes and novel gating obtain high efficiencies, which are improbable for mass production and will therefore remain in the laboratory. As shown in Fig. 34, however, the efficiency of virtually all CNT-silicon solar cells that have been found to degrades over time, including those with these nonvolatile dopant schemes. Still, studies conducted to address the issue is limited.

Wang et al. [105] increased the performance of SWCNT solar cells by

using metal oxide layers to facilitate effective carrier transport (Fig. 35). Metal oxides resulted in decreased deficit of incident solar light and enhanced photocurrent, respectively act as an antireflection layer and an effective carrier dopant. Consequently, the use of MoO_x and ZnO layers in both SWCNT/n-Si and n-SWCNT/p-Si heterojunction solar cells lead to an improvement in their photovoltaic performance. This improvement results in very high photovoltaic efficiencies of 17.0 % and 4.0 % for the corresponding cells. The findings indicate that including multifunctional metal oxide layers with SWCNT could enhance the performance of electrical devices. The growth of SWCNTs on an n-Si substrate was achieved by the floating catalyst CVD approach. The thickness of the SWCNT film was manipulated by adjusting the time. These materials serve as antireflection layers to enhance optical absorption, carrier dopants to minimize series resistance, and effective carrier transport layers to reduce the Schottky barrier.

Tune and Shapter [106] examined solar cells composed of haphazardly arranged thin layers of SWCNTs over n-type monocrystalline silicon (Fig. 36). The films are produced through the process of vacuum filtration using aqueous solutions of Triton X-100 and large diameter arc-discharge SWCNTs. Their findings demonstrated a significant correlation between film thickness and the observed outcomes, with average transmittance greater than ~70 %. The primary factor contributing to this correlation is the sheet resistance of the SWCNT film. Doping with SOCl₂ largely reduces sheet resistance, resulting in an enhanced in short circuit current density, OCV, and FF.

Habisreutinger et al. [107] created a composite layer consisting of CNTs and polymer to reduce the negative effects of heat degradation. The incorporation of CNTs into the polymer composite functions as an insulating layer, hence enhancing the thermal stability of the PSCs. With this composite structure, they achieved power-conversion efficiencies of up to 15.3 % with an average efficiency of 10 ± 2 %. They also noted hysteresis in the current–voltage curves due by yet unknown causes (Fig. 37).

The PCE achieved a value of 15.3 %, with an average efficiency of 10 ± 2 %. Yoon et al. [108] employed a hybrid HTL composed of CNTs and PEDOT:PSS to reduce the number of empty spaces for positive charges. The composition with the best performance exhibited effective surface and photoluminescence quenching capabilities, achieving a PCE

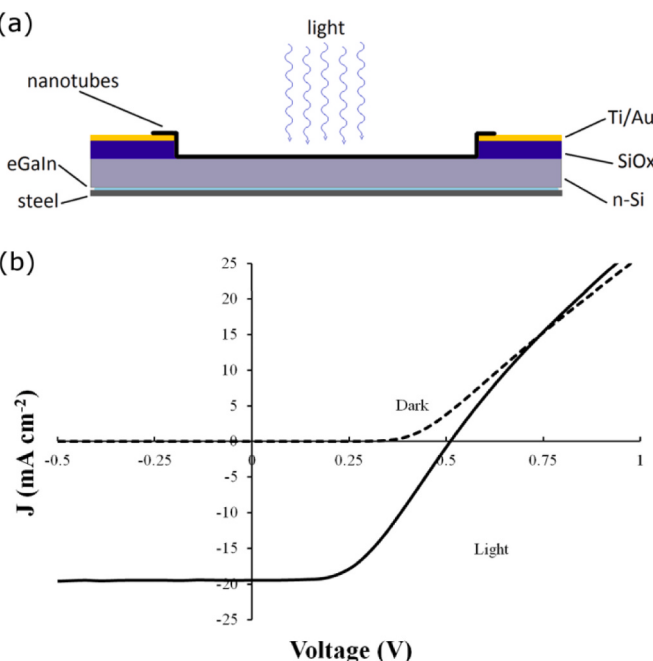


Fig. 36. (a) Device schematic; (b) JV curve of a typical SWCNT-Si solar cell [106].

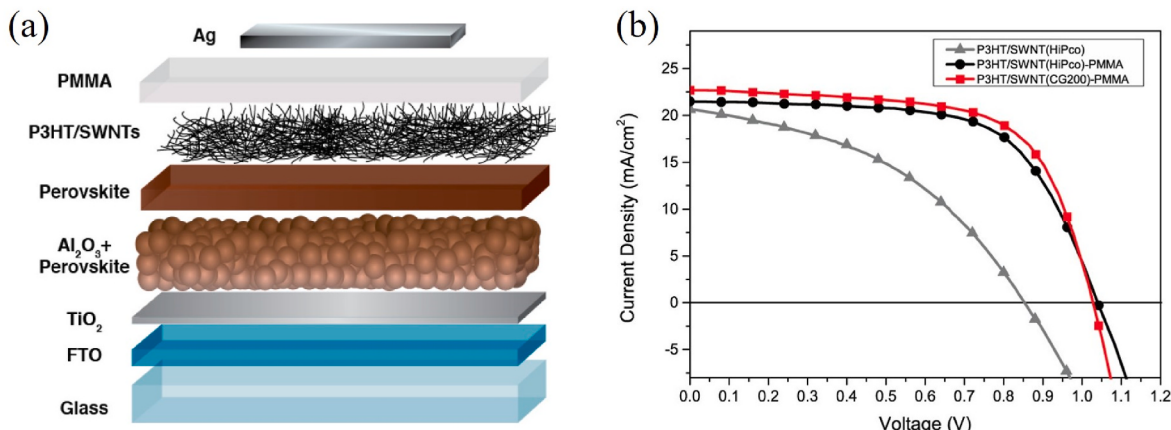


Fig. 37. (a) Schematic demonstration of the solar cell with a carbon nanotube/polymer composite as hole-transporting structure. (b) Plots of the current–voltage features of the best-performing devices with a HTL consisting of P3HT/SWNT(HiPco)-only (gray triangles); the stratified P3HT/SWNT(HiPco)-PMMA structure (black circles); and the P3HT/SWNT(CG200)-PMMA stratified HTL (red squares), examined as forward bias to short-circuit at a rate of 0.24 V/s [107].

of 16.0 % and little hysteresis.

Apart from graphene and carbon nanotubes, other carbon allotropes have also been investigated for the enhancement of thin film solar cells. Hollow carbon spherical nanoparticles such as fullerenes and quantum dots have gained a lot of attention [109–116]. C₆₀, also known as buckminsterfullerene, was the first carbon nanomaterial to be effectively synthesized. Kroto et al. [117,118] did this via laser ablation of graphite in an extreme helium flow rate. Carbon nanotubes (CNTs) were later obtained as a byproduct of fullerene synthesis, as the earliest methods used to create CNTs were either designed for producing fullerenes or based on existing procedures for fullerene manufacture. CNTs were discovered and synthesized on a wide scale using an arc discharge approach [119,120], laser ablation [121] and later by pyrolyzing metal carbonyls in the existence of other hydrocarbons [122]. The synthetic techniques used to produce carbon nanomaterials sometimes lack precise control over all the structural characteristics, leading to raw materials that exhibited significant variation in both the physical and electrical properties. Chiral vectors and diameter have a significant influence on the electrical structure of carbon nanotubes. During the CVD

creation of graphene, multiple graphene layers in the final film can be adjusted by carefully selecting the metal and growing environment [89]. The structure of spherical fullerene is composed of pentagons and hexagons. The C₆₀ fullerene is made up of 12 pentagons and 20 hexagons, with 60 bonds out of 30 conjugated double bonds, and it has excellent heat and pressure stabilities as well as chemical reactivity. C₆₀ has good electrical conductivity (10⁻⁴ S/cm) and is quite transparent. Fullerenes (C₆₀ and C₇₀) and their derivatives have a high electron affinity and are commonly employed as electron acceptors of photoactive layers in OSCs. Furthermore, because of their excellent carrier mobility at ambient temperature and proper energy levels, they can operate as electron transport layers in PSCs. PC₆₁BM, which is a derivative of C₆₀ functionalized with a side group containing a phenyl and butyric acid methyl ester, was synthesized to enhance its solubility. To boost photovoltaic performance, C₇₀ derivatives were also included into OSCs. Fullerenes are rarely used in flexible DSCs; instead, CNTs and graphene are generally utilized in fiber and planar shapes [72]. It is generally known that C₆₀ is a more effective charge separator and a stronger electron acceptor. Because semiconducting CNTs produce perfect

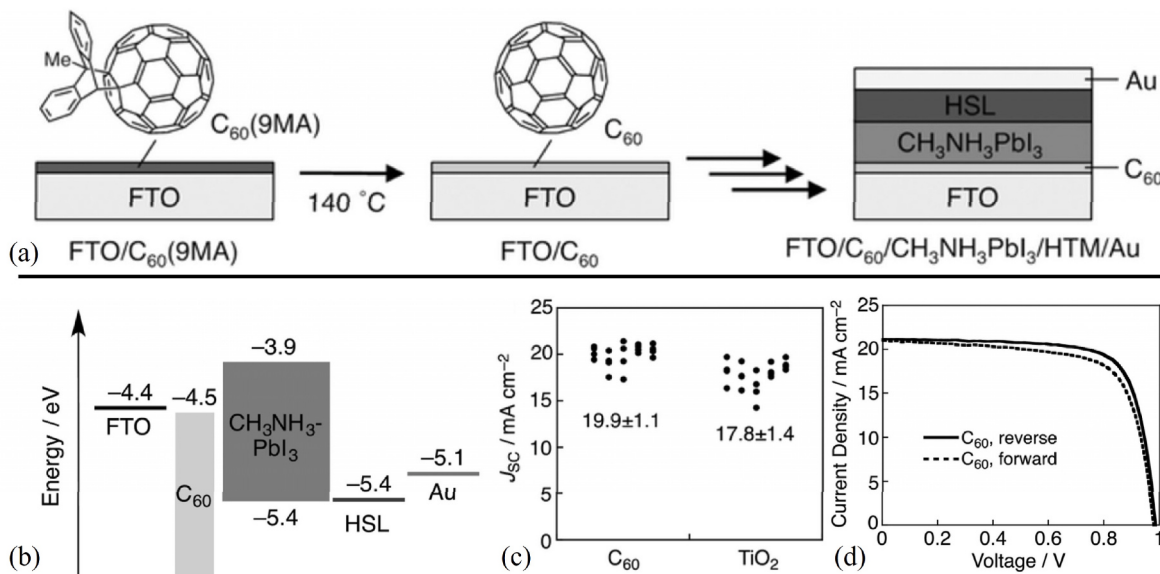


Fig. 38. Diagrams of thermal transformation of C₆₀(9 MA) to C₆₀ in the film state and device structure of perovskite solar cells. (b) energy graph of the FTO/C₆₀/CH₃NH₃PbI₃/HSL/Au device. (c) Photovoltaic parameters, J_{SC} of 20 devices of FTO/C₆₀/CH₃NH₃PbI₃/HSL/Au and FTO/TiO₂/CH₃NH₃PbI₃/HSL/Au. (d) Current density–voltage curves under various examining direction, reverse (solid line) and forward (dotted line), for the best-performing devices of (a) FTO/C₆₀/CH₃NH₃PbI₃/HSL/Au [123].

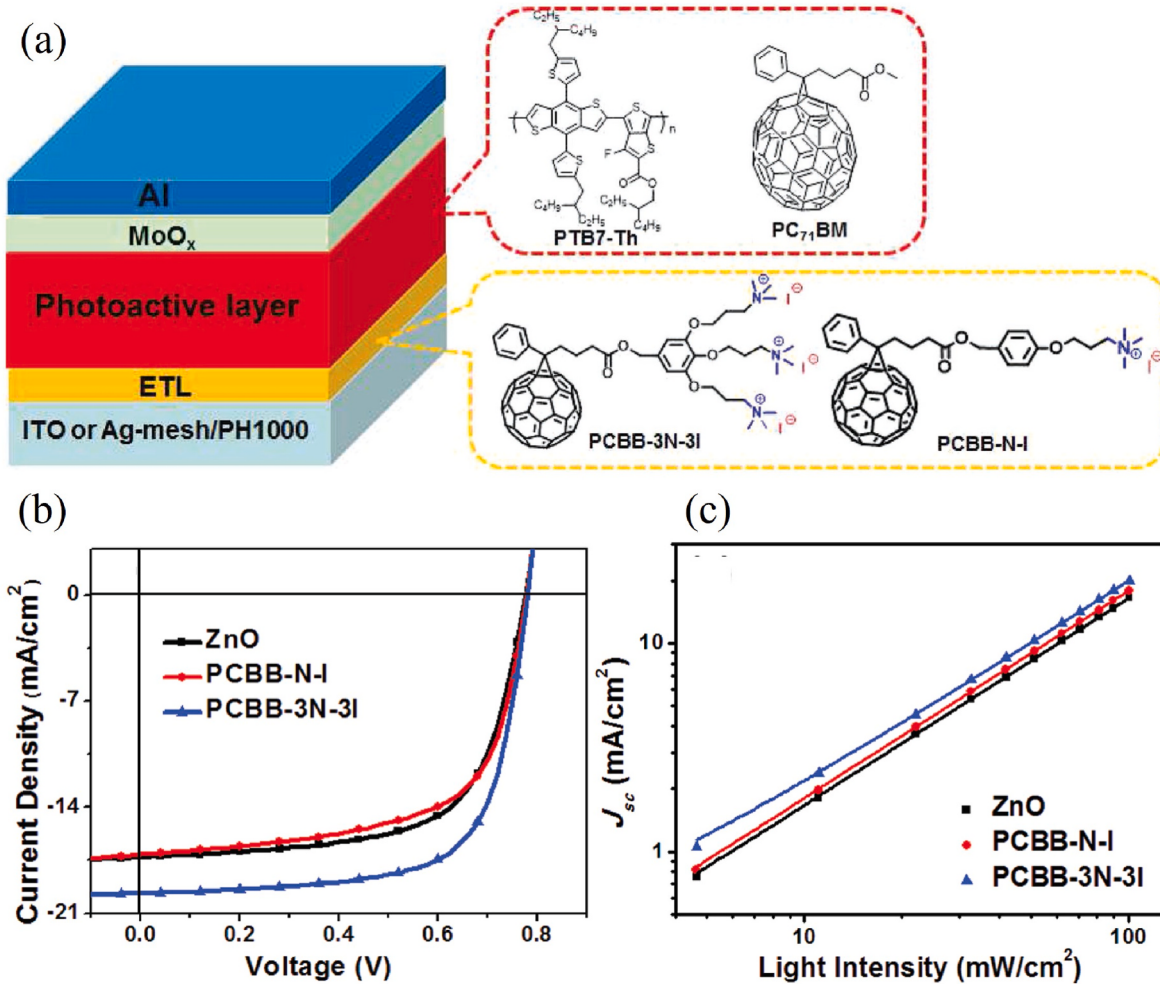


Fig. 39. Left: device structure of overturned PSCs Right: Molecular structure of photoactive layer and fullerene electrolyte based ETL. a) J-V curves of the PSCs based on various ETLs under the illumination of AM1.5G 100 mW cm⁻². c) J_{sc} and d) Voc versus natural logarithm of light intensities fitted through a linear relationship for the optimized PSCs with altered ETLs [127].

heterojunctions, they can serve as a good substitute for C₆₀. Additionally, CNTs can be employed to increase carrier mobility in P₃OT-nitrogen-doped MWCNT cells to effectively remove charges [75]. Fullerene-based electron selective layers (ESLs) have been modified using different substances, including decamethylcobaltocene, oleamide, carbon, and innovative two-dimensional carbon compounds like graphdiyne [73].

C₆₀ is commonly employed to enhance the electron extraction efficiency of the ETL. Tian et al. [124] employed a C₆₀ modified TiO₂ layer to reduce the energy imbalance among ETL and the perovskite layer [83, 125]. Jeng et al. [126] investigated fullerene (C₆₀) in PSCs with spin coating method. Umeyama et al. [123] were the first to utilize C₆₀ thin films as the electron selective layer (ESL) in normal n-i-p perovskite solar cells (PSCs). This was achieved by exposing the pre-prepared glass/FTO/C₆₀-9-methylanthracene structure to a thermal retro-Diels-Alder reaction. The PSC device showed the maximum PCE of 15.0 %, which was superior to that of the device with the compact TiO₂ as an ESL (12.9 %). The hysteresis behavior in J-V curves of the C₆₀-based device was impressively suppressed compared to the TiO₂-based device due to the enhanced electron selective collection ability of fullerene (Fig. 38).

Fullerenes and their compounds were subsequently implemented as ETL for OSCs. An inverted OSC utilized an n-type self-doping fullerene electrolyte with [6,6]-Phenyl-C₆₀ as the backbone, serving as the ETL (Fig. 39). The photoactive layer consisted of PTB7-Th:PC₇₁BM (PCBB-

3N-3I). It exhibited an improved PCE of 10.04 % and 10.62 % when used for flexible and rigid devices, respectively. Also, they reported that selecting thermal-annealing-free PTB7-Th:PC₇₁BM as the photo-active layer, the inverted PSCs with PCBB-3N-3I ETL could be fabricated at room temperature, showing the best PCE of 10.62 %, which was \approx 20 % higher than that of the device with ZnO as ETL [127].

The TiO₂/C₇₀ ETL, which is sandwiched among TiO₂ and perovskite material, exhibits favorable surface morphology, effective electron extraction, and an excellent quality perovskite film. These characteristics can be ascribed to the appropriate nano-size and exceptional electronic properties of the C₇₀ molecules. The PCE of the TiO₂-based PSC equivalents was enhanced by 28 % as compared to the immaculate ones [72, 128].

Yang et al. [129] explored methods to enhance the effectiveness and reliability of solar cells containing PCBM by introducing graphene quantum dots (GQDs). An optimal concentration of GQDs manifested in a PCE rise of around 20 %. The scientists also suggested that including GQDs could improve the fracture resistance of the PCBM. The modifications in the structure of device result in the cells reaching a stabilized PCE of more than 17 %. Additionally, 80 % of the initial PCE is maintained after 300 h of exposure to light, indicating a promising approach for creating solar cells that are both efficient and stable. Tiong et al. [130] conducted a study to explore the potential of SWCNTs as a restricting layer for the perovskite film. The aim of study was to improve the grain size of the perovskite layer and thereby increase the PCE of the

solar cells. The study achieved a PCE of 16.1 %. The research conducted by Zheng et al. [131] on boron doping of the MWCNT layer has the potential to significantly reduce the devices cost. Thus, the utilization of carbon nanotubes (CNTs) can provide enhanced stability to the PSCs, thereby minimizing the manufacturing expenses and ensuring comparable performance levels, with a goal of achieving a competitive performance [81].

Xie et al. [132] incorporated a minute quantity of graphene quantum dots (GQDs) into the SnO_2 film to enhance its conductivity. The electrons produced by the GQDs occupied the trap states in SnO_2 formed during the solution process. Consequently, the PCE increased to 20.23 % with minimal hysteresis [83]. Geng et al. [133,134] investigated the impact of graphene oxide quantum dots (GOQDs) as an excellent-quality interface on graphene/n-Si solar cells. By utilizing GOQDs, it is possible to modify the interfaces characteristics of Gr/Si Schottky barriers solar cells (SBSCs) and establish a unique barrier at the interface. They achieved excellent efficiency Gr/Si solar cells through carbon quantum dots (CQDs) as an interface modifying layer. The CQDs interlayer had the dual purpose of blocking electrons and facilitating the movement of holes. This resulted in a higher reversed saturation current and a significantly improved V_{oc} , hence enhancing the effectiveness of the solar cell. The PCE of the Gr/CQDs/Si solar cells is 6.52 %. The highest power conversion efficiency was obtained by precisely regulating the thickness and diameters of the interlayer made of quantum dots of 26 nm and 4–7 nm, respectively, without use of chemical doping. Their findings demonstrated that the utilization of nano-TiO₂ resulted in a PCE of 9.97 % [94].

4.2. Graphene derivatives

Graphene is a honeycomb-structured single layer of sp² hybridized carbon. Every carbon atom is attached to three nearby carbon atoms by s bonds in a typical graphene structure, and the electrons in the p orbitals of every carbon atom are placed adjacent, to create a delocalized conjugated big p bond. Graphene has a thickness of 0.335 nm. Graphene is often synthesized and studied in monolayer, bilayer, and thick films [72, 135].

The utilization of graphene as the absorbing layer presents major challenges due to its poor metallic characteristics and absorption coefficient arising from the lack of a band gap, it also hinders efficient carrier production and separation. Single-layer graphene has a significant sheet resistance (several k Ω) and a low work function (4.4 eV). Because of the low work function, the barrier height can be lowered, decreasing the internal electric field, and preventing electron-hole pairs from splitting. However, in the case of high sheet resistance, the series resistance might be substantial. A small portion of photons (30–40 % of visible light, or 350–800 nm) are absorbed by the flat silicon wafer [94].

As early as 2007, a DSSC device showcased the initial implementation of a graphene-based electrode in a solar cell by using rGO as electrode [136]. While pure graphene does not possess a distinct band gap, different types of chemically modified graphene substances have been employed in the active layers of OPV devices. An initial endeavor involved utilizing GO as an acceptor material, along with donor polymers like P₃HT and P₃OT, in a straightforward combination [89]. Ma and Zhi [78] reviewed the optoelectronic properties and application of graphene-based transparent conductive films (G-TCFs). They focused on decreasing sheet resistance, maintained transmittance of G-TCFs and

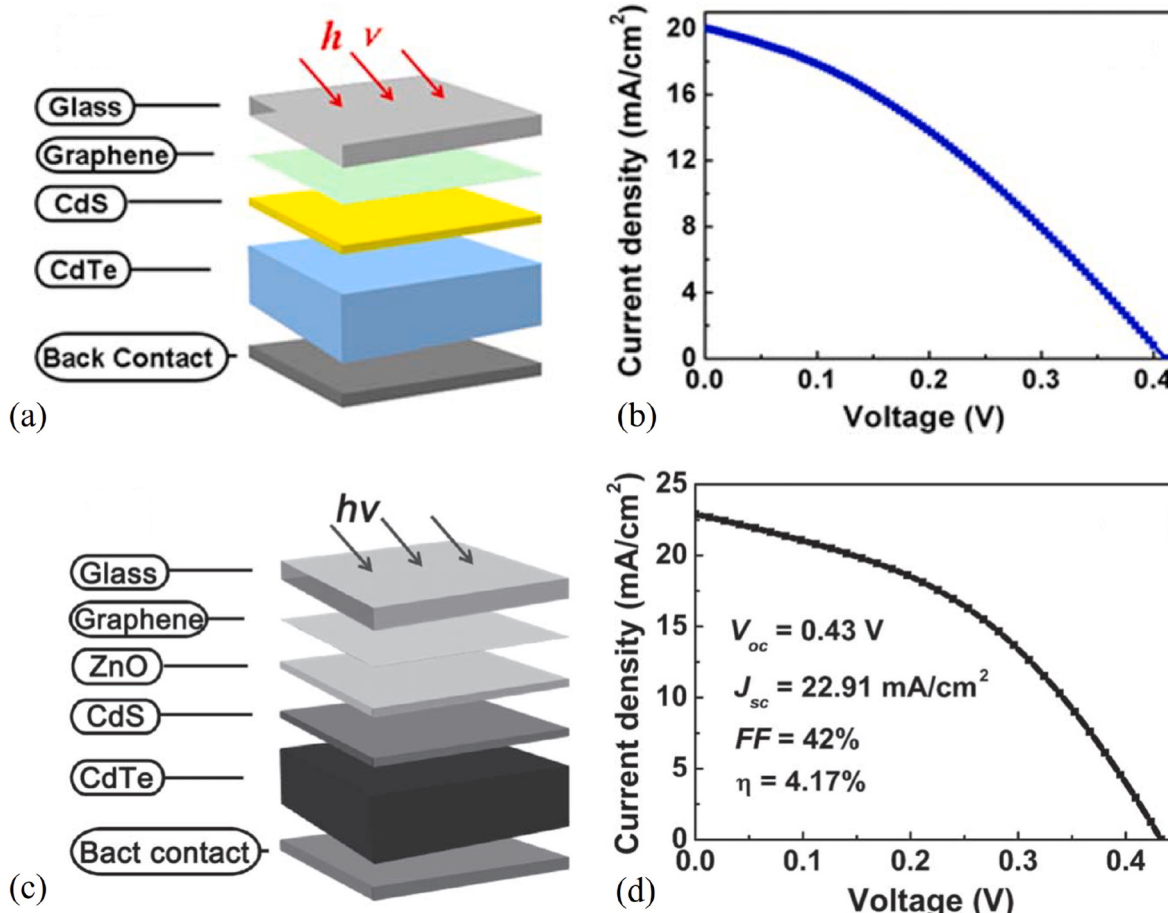


Fig. 40. (a) Schematic diagram and (b) J-V characteristics of the glass/graphene/CdS/CdTe/(graphite paste) solar cell c) Schematic diagram and d) J-V characteristics of the glass/graphene/ZnO/CdS/CdTe/(graphite paste) solar cell [137].

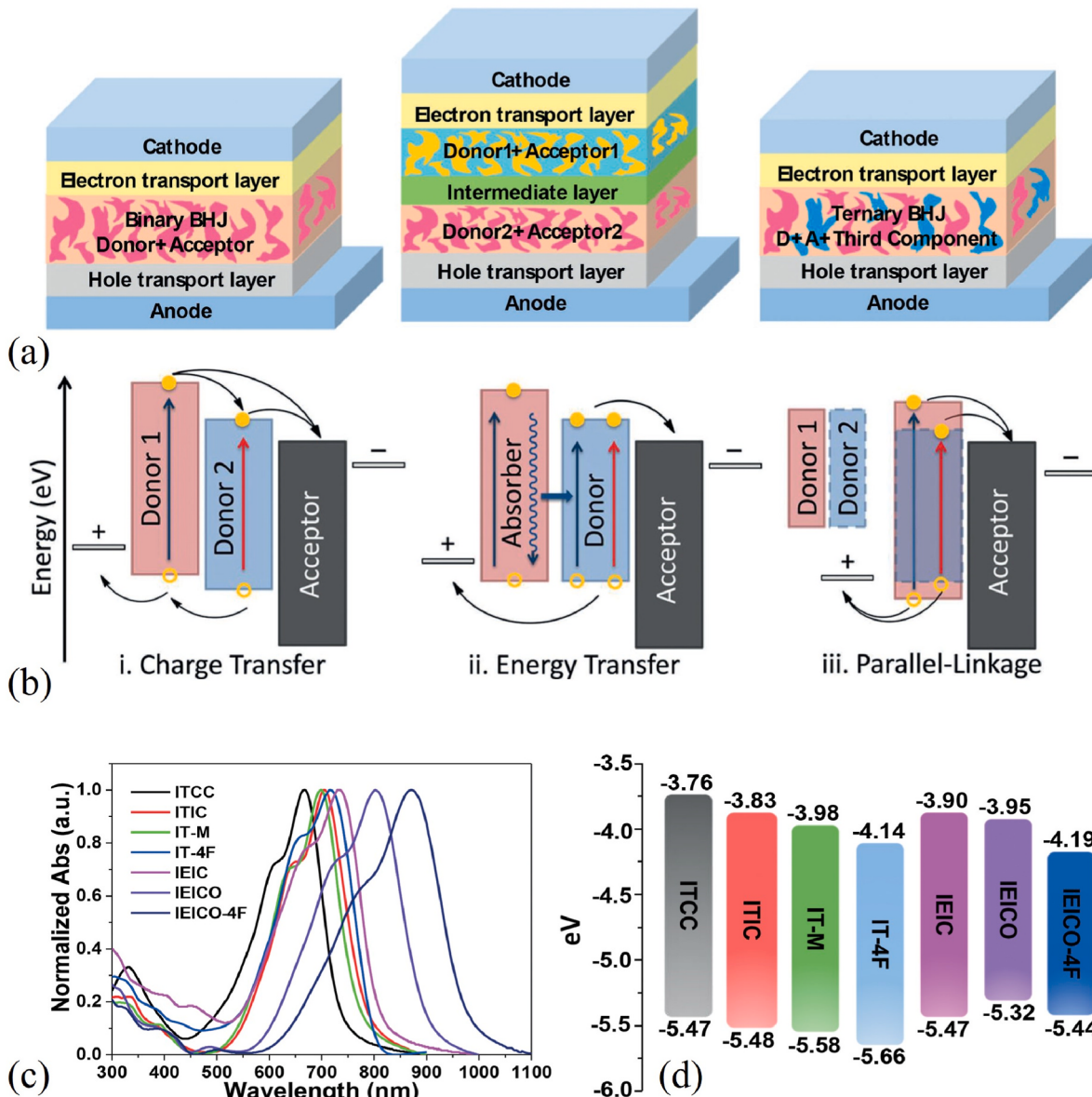


Fig. 41. Conventional structures diagrams of binary bulk heterojunction, tandem device and ternary device. Three fundamentally different mechanisms in ternary OSCs: charge transfer, energy transfer, and parallel linkage. a) Normalized absorption spectra and b) energy level diagrams of different nonfullerene acceptors, such as ITIC, ITCC, IT-M, IT-4F, IEIC, and IEICO-4F.

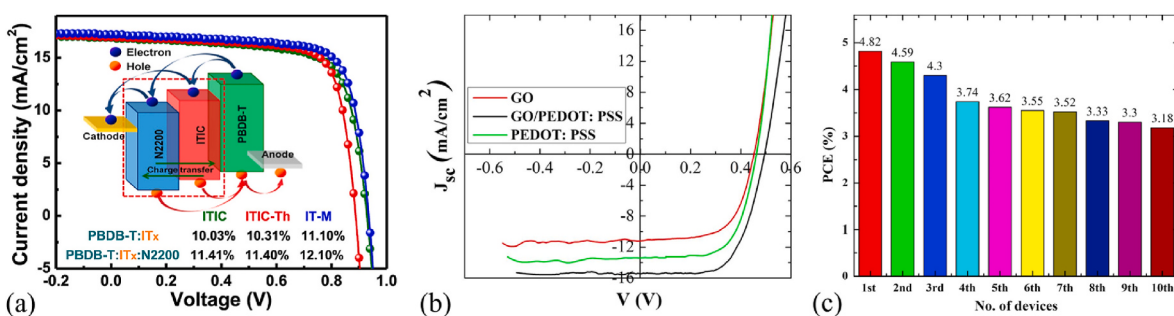


Fig. 42. (a) PCE of ternary OSCs for PBDB-T:ITx:N2200 approaches 11.41 %, 11.40 % or 12.10 % with ITIC, ITIC-Th or IT-M, respectively [143] (b) J-V characteristic of BHJ OSCs with various HTLs under light conditions. (c) Statistical distribution analysis bar chart of the fabricated ten (10) sets of organic solar cell based on GO/PEDOT:PSS composite HTL [144].

highlighted that their flexibility, stretchability, and self-healing should be the focus of research. They compared the different G-TCFs along with the deposition methods and improvements. Bi et al. [137] presented the first effective CdTe device incorporating graphene, considering the comparable work function of graphene and FTO (Fig. 40). The researchers synthesized graphene on a copper foil using atmospheric pressure CVD and subsequently transferred it to a glass substrate. They observed the JV characteristics of the device having graphene but without ZnO include a photocurrent density (J_{sc}) of 20.06 mAcm^{-2} with V_{oc} of 0.41 V and FF of 34 %, and an overall PCE of 2.81 %. The addition of a ZnO barrier layer in the cell results in better performance, with an efficiency rise to 4.17 % ($V_{oc} = 0.43 \text{ V}$, $J_{sc} = 22.91 \text{ mAcm}^{-2}$, FF = 42 %).

Liang et al. [138] documented the application of a Cu nanowire/graphene back contact for a CdTe solar cell. Subsequently, the graphene was combined with Cu nanowires that were synthesized by hydrothermal methods. The solution was applied to the CdTe layer using a brush, resulting in a device efficiency of 12.1 % [139].

Three organic materials are the part of ternary blend in the form of either donor:donor:acceptor ($D_1:D_2:A$) or donor:acceptor:acceptor ($D:A_1:A_2$) combination, generally can provide a better device operation than its binary blend counterpart [140,141] (Fig. 41). In general, it is simple to ascertain that the ternary strategy to increase the stability of the device originates from the morphology adjustment in the active layer. For the ternary strategy to enhance the stability of the device, it is imperative that the third component can generate a more secure morphology within the active layer. To produce a more stable active layer morphology, it is proposed that the third component be miscible with the donor polymer and partially miscible with the crystallizable acceptor [140,142]. An et al. [143] introduced the polymer acceptor N2200 as a 3rd part in the PBDB-T:ITIC non-fullerene binary system to create ternary OSCs. In order to create fullerene-free ternary OSCs, a polymer acceptor called N2200 is added as the third component to the PBDB-T:ITIC mixture. This combination results in an impressive power conversion efficiency (PCE) of 11.41 % and exceptional stability even in air conditions. The higher performance of ternary OSCs, in comparison to binary cells, can be primarily attributable to improved photon harvesting and better shape of the active layers. By substituting ITIC with a

comparable acceptor such as ITIC-Th or IT-M in the ternary OSCs, it is possible to attain optimal PCE of 11.40 % or 12.10 % for PBDB-T:ITIC-Th:N2200-based or PBDB-T:IT-M:N2200-based cells, respectively.

Hilal and Han [144] included a GO layer among the PEDOT:PSS layer and the electrode to create a bilayer structure for the hole transit layer. It was discovered that the extra GO layer can function as a barrier, preventing oxygen and moisture from passing through to the PEDOT:PSS layer. Consequently, the device utilizing a hole transportation layer based on GO/PEDOT:PSS bilayer demonstrated improved resistance to degradation in the presence of air [140] (Fig. 42). The catalytic capacity of pristine graphene may be restricted for the reduction reaction due to its electrocatalytic activity being mostly associated with defects and point placements. Therefore, in case of graphene, some structural

NUMBER OF GRAPHENE LAYERS

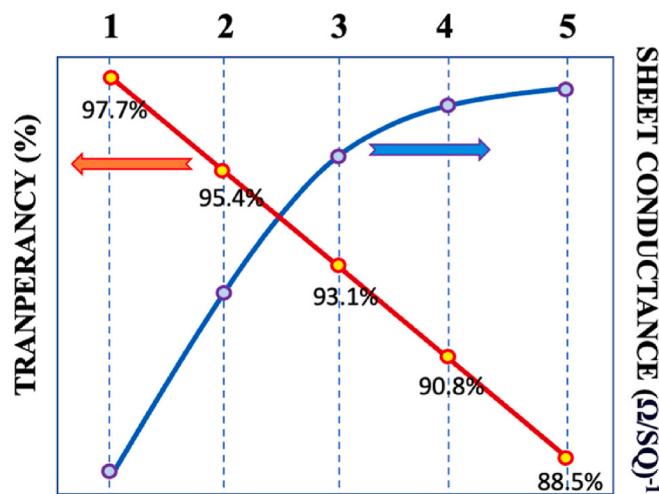


Fig. 44. Alteration of sheet conductance and transparency and as a result of the graphene layers numbers [147].

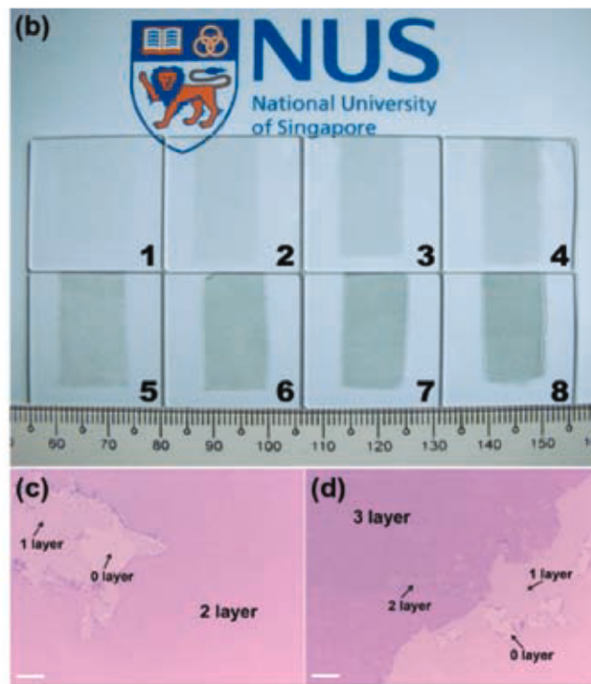
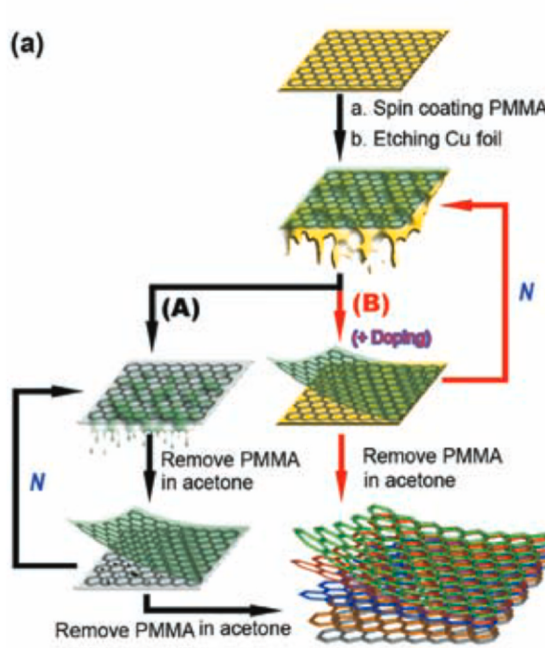


Fig. 43. (a) diagram of multilayer graphene films developed through normal wet transfer (A) and direct combining LBL assembly (B) [$N = 0,1,2,3 \dots$] (b) Optical image of multilayer graphene films from 1 to 8 layers on a quartz substrate. (c, d) General optical microscope figures of 2- and 3-layers on quartz [146].

modifications are always required. The literature primarily describes methods such as heteroatom doping, compositing with metal sulfides, and incorporating conducting polymers. An instance of flexible DSCs utilizing nano-TiC/graphene/PEDOT:PSS composites as a counter electrode on a plastic substrate through spray printing was documented. The device attained a PCE of 4.5 %, marginally surpassing that of a comparable device employing PCE of 4.3 % [72]. Liu et al. [145] created a very thin and flexible PSC utilizing a transparent graphene electrode. The device structure consisted of a PET polyethylene terephthalate substrate that was 20 mm thick, with layers of graphene, P₃HT, CH₃NH₃PbI₃, PC₇₁BM, and Ag. The fabrication procedure involved a low-temperature solution method. The flexible devices exhibited a PCE of 11.5 % together with exceptional durability and air stability. The study involved creating flexible, indium-free inverted PSCs by substituting ITO with either SWCNT or graphene, resulting in a noticeable distinction. The SWCNT or graphene-based PSCs exhibited efficiencies of 12.8 % and 14.2 %, respectively [72]. Wang et al. [146] experimentally found that with the rise in number of layer (from 1 to 8) optical transparency decreased demonstrating the inverse relation among the optical transparency and number of layer (Fig. 43). They also noticed decline in sheet and series resistance of graphene structure with the increasing of graphene layers number [147].

Liu et al. [148] experimented with 1–4 graphene layers in the Ag/P3HT:PCBM/PEDOT:PSS + Au/graphene arrangement and observed that the bi-layer graphene produced the highest efficiency [147]. Generally, the use of bi-layer and tri-layer graphene leads to the SC efficiency, as the transparency and sheet resistance characteristics of graphene are balanced by its bi- and tri-layer structures. Since the amounts of optical transmittance and sheet resistance rely on the SC structure, they reported maximum efficiency for various SCs by varying graphene layers number (Fig. 44) [147].

The doping profile of graphene includes the concentration and type of dopants significantly affects the physical, optical, and chemical properties [149]. The position of the Fermi level in graphene undergoes a shift when it is doped (Fig. 45). Unaltered graphene is a continuous semiconductor with the Fermi level located precisely at the Dirac point

of the energy band structure. Chemical doping can manipulate the Fermi level of graphene, resulting in the formation of n-type or p-type doped graphene. This process also enables the creation of a variable bandgap among the conduction and valence bands. Managing the predominant doping configurations is a viable strategy to not only improve the mobility of electrons and holes but also increased the electrical conductivity. The enhancement in the production and mobilities of electron-hole pairs decreases the rate at which charge carriers combine, resulting in more effective photo/electrocatalytic processes. Increasing the doping level results in a greater displacement of the Fermi level, leading to the formation of a stronger built-in electric field/potential within the solar cells, which serves as a driving force for effective charge accumulation. Altering the Fermi level of graphene resulted in an elevation of its work function for p-type doping and a reduction of its work function for n-type doping, comprehensive discussion of graphene doping is done by Nguyen et al. [147,150].

Graphene is generally selected for p-type doping. Therefore, an augmentation in the p-type doping of graphene results in an elevation of the graphene work function. When the work function of graphene exceeds the vacuum level or zero-energy level of the semiconductor, the conduction band (CB) and valence band (VB) at the interface between the semiconductor and the graphene semiconductor tend to curve upwards. As a result, an ohmic contact is formed at the junction between the graphene and semiconductor. As the level of p-type doping improves, the work function of graphene also rises, resulting in an increase in the band bending at the junction between graphene and the semiconductor. This enhances the current density and subsequently enhances the efficiency of the graphene-based solar cell [94]. When graphene is selected for n-type doping, leads to a reduction in the work function of graphene. Fig. 46 illustrates that when the work function of graphene decreases below the zero-energy level of the semiconductors, the CB and VB at the interface between graphene and the semiconductor bend downwards. It results in the creation of a Schottky interface at the graphene/semiconductor junction this time. As n-type doping rises, the graphene work function reduces even further, raising band bending at the graphene/semiconductor junction. As mentioned earlier, more

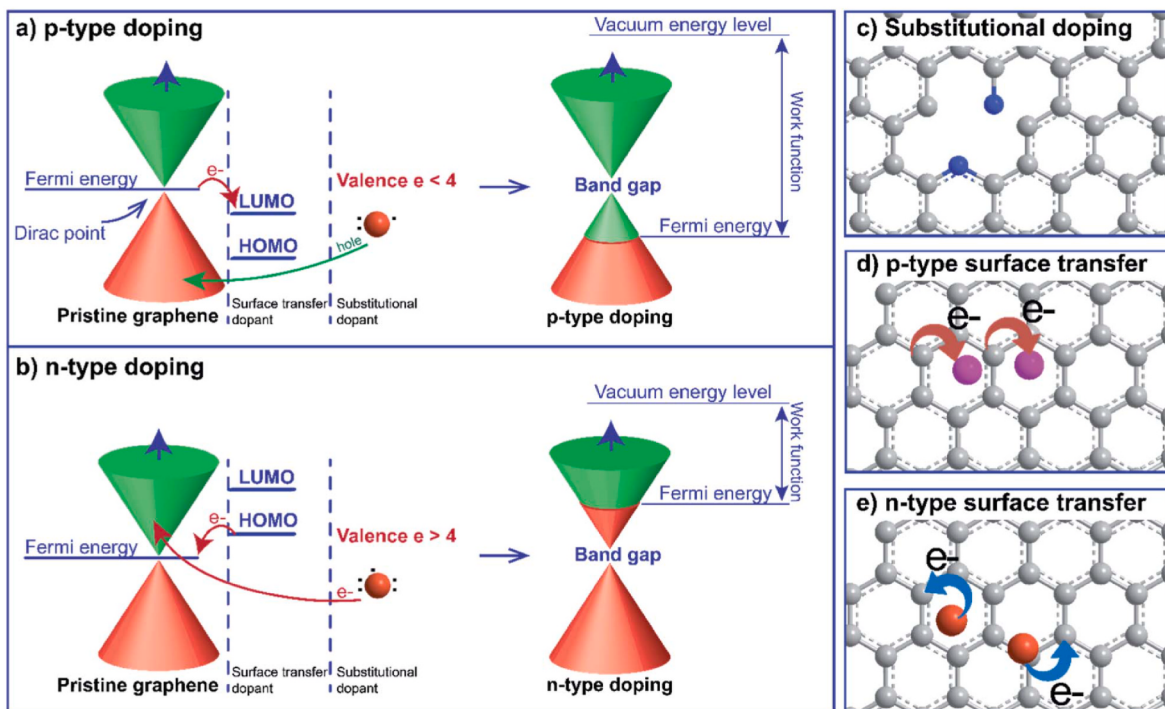


Fig. 45. Demonstrates the energy diagram of (a) expanded work function and p-type doped graphene (b) reduced work function and n-type doped graphene. Graphene doped structure by: (c) substitutional doping; (d) and reduced work function n-type surface transfer doping; (e), p-type surface transfer doping [150].

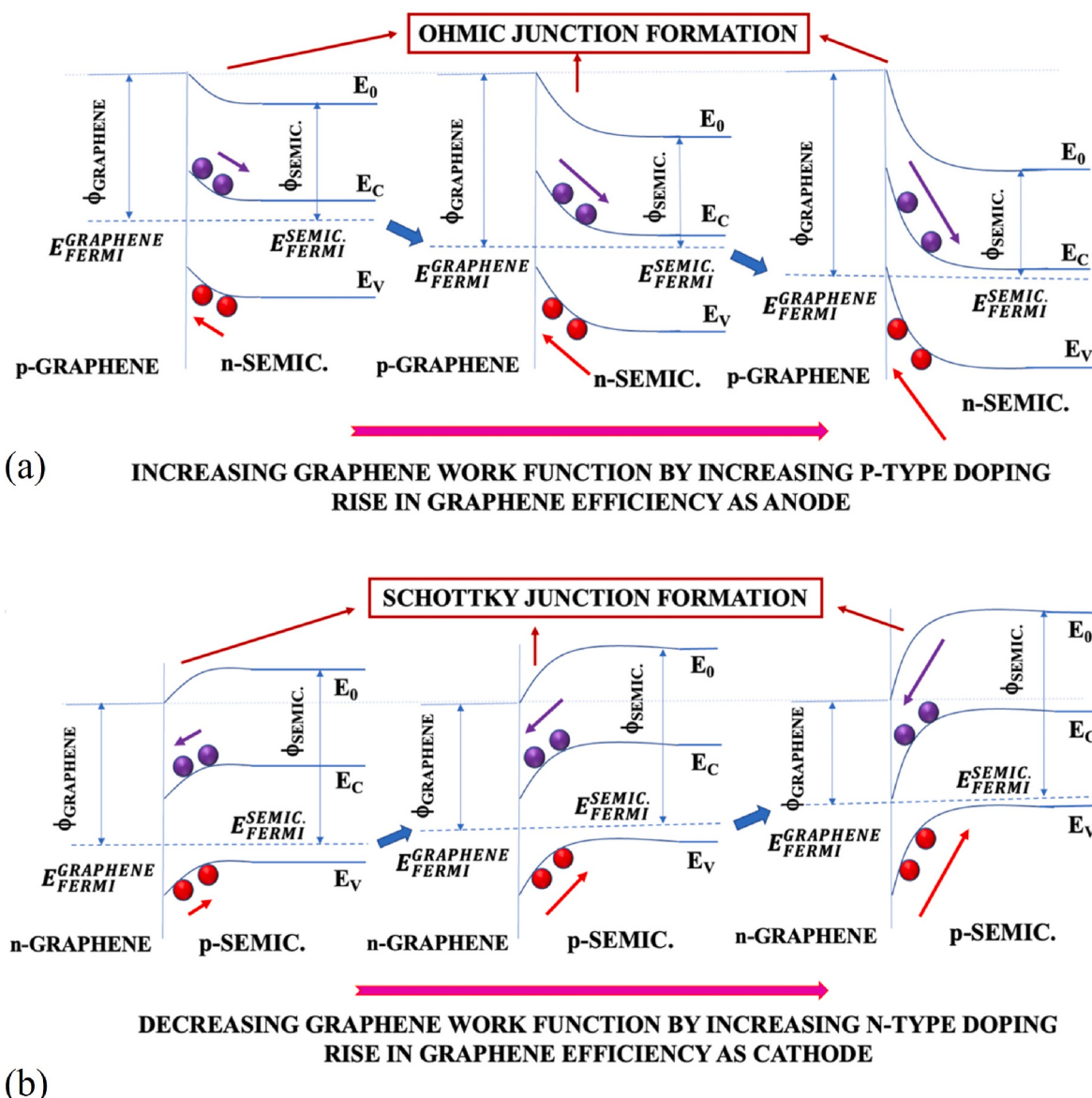


Fig. 46. (a) Alteration of junction band positioning through the p-type doping (b) Alteration of n-semiconductor/p-graphene junction band positioning through the n-type doping [147].

bending leads to faster charge transfer and absorption at graphene cathode and semiconductor anode interfaces [100,147].

Graphene has also been explored as an anode in OPVs. Graphene and ITO electrodes with transparency were used to create semitransparent OPVs. The device may be lighted from each side and has possible application in building and automotive power windows. Lee et al. [151] investigated multilayer graphene on top of a partially transparent twisted OPV (Fig. 47). It was developed with ITO, ZnO, P3HT:PCBM, GO, and multilayer graphene. They stated that the partially transparent device attains a maximum PCE of 2.5 % if it is composed of a top electrode including 10 layers of graphene, which is approximately 76 % of the PCE of the conventional opaque cell. On the other hand, when the semitransparent device made up of eight layers of graphene is lit up from the graphene side, it achieved PCE of 2.04 %. This PCE is around 62 % of the PCE of the conventional cell [100,151].

Initially, Wang et al. [136] utilized graphene films as transparency window electrodes in solid-state DSSCs. The graphene films were produced via vacuum filtering of an aqueous GO scattering, followed by thermal reduction. Graphene transparent electrodes could be included

into Schottky junction solar cells as well. Later, Li et al. [152] demonstrated through placing CVD-grown graphene on an n-type silicon (n-Si) substrate, leading in a PCE of 1.5 %. Subsequently, significant efforts have been undertaken to enhance the PCEs of graphene/Si Schottky junction solar cells [153]. Dodoo-Arhin et al. [154] conducted comprehensive study on the growth of graphene films over a wide surface area. These films were produced on copper foil substrates that were 25 μm thick using CVD with a split tube furnace. The growth procedure was performed at 1000 °C utilizing hydrogen gas at a flow rate of 10 sccm, methane gas at a flow rate of 15 sccm, and argon gas at a flow rate of 300 sccm. The procedure was carried out under ambient pressure conditions and for growth durations were set 1, 5, 10, 15, and 20 min. After the growing procedure, the sample was rapidly cooled by removing it from the hot zone of the furnace using a quartz tube. The grown graphene was placed onto SiO_2 or glass substrates using the unique bubbling approach. Furthermore, an investigation was conducted to examine the CVD graphene sheets as a counter electrode in DSSC. The J_{sc} , V_{oc} , FF, and overall conversion efficiency under AM 1.5, 100 mW/cm² lighting were 12.7 mA/cm², 544.8 mV, 57.5 %, and 3.8 %,

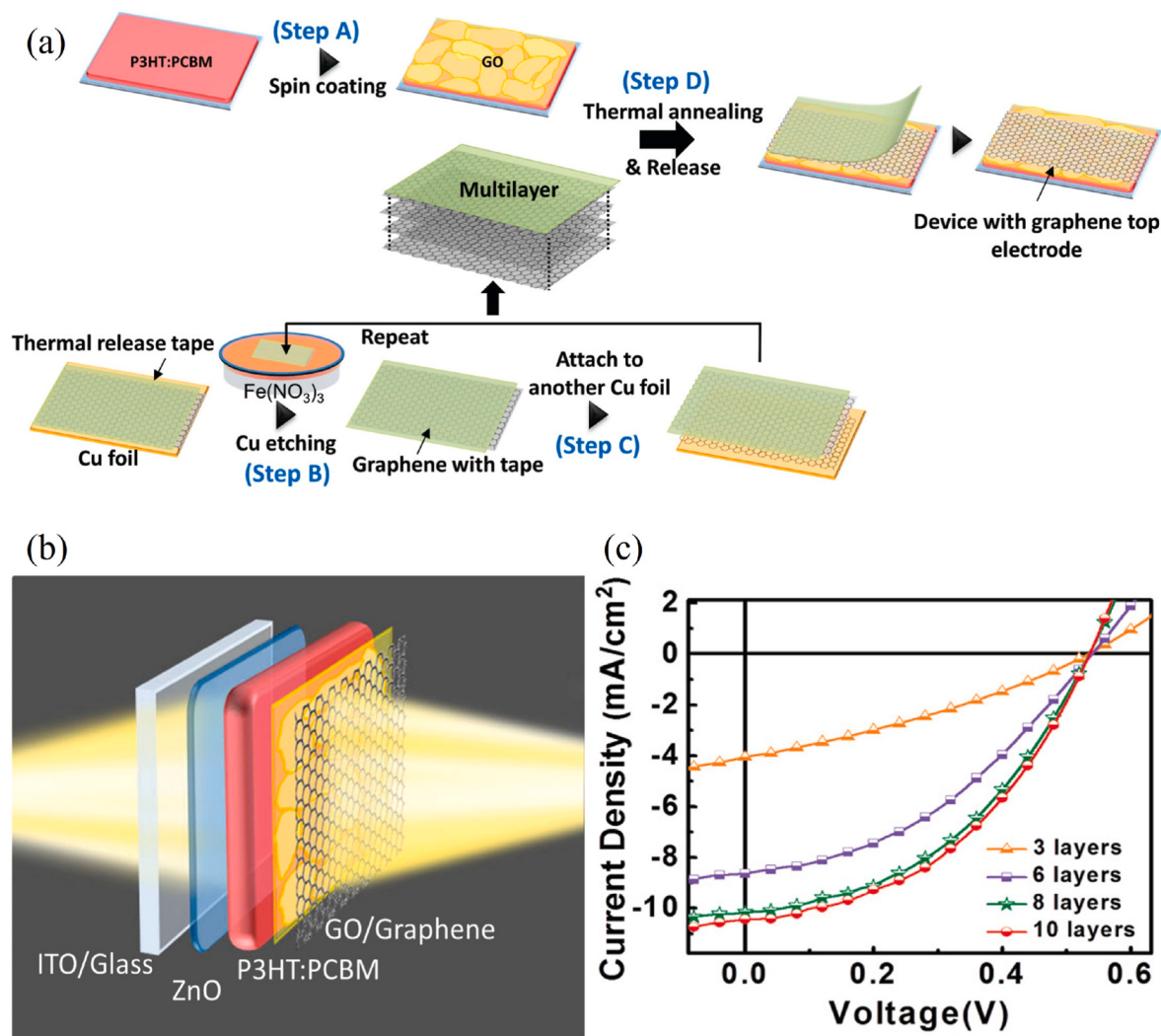


Fig. 47. (a) Development of the ITO/ZnO/P3HT:PCBM/GO device prior to placing the top electrode (step A). Top lamination procedures of graphene electrodes through the graphene film transferring (steps B, C) and thermal annealing/releasing procedures (step D). (b) Semitransparent inverted polymer solar cell with a structure of ITO/ZnO/P3HT:PCBM/graphene oxide (GO)/graphene top electrode. (c) Current – voltage characteristics of the semitransparent polymer solar cells involving of several number of top graphene layers with light shining from the ITO side [151].

respectively. Overall, the PCE of Gr/Si solar cells is still rather low when compared to traditional p-n junction solar cells. Moreover, assuming optimal circumstances and relying on theoretical calculations, the anticipated efficiency thresholds for graphene/GaAs and graphene/silicon solar cells are 25.5 % and 27.5 %, respectively. The incorporation of additional advancements from single-junction PSCs into larger PSC modules would undoubtedly accelerate progress in the field of PSC modules and move closer to field testing, potentially as an integral component of the electrical grid.

5. Conclusion

Surface engineering is a well-established method for enhancing the desired material properties, through modifying outer surface layer of the materials. It encompasses all stages of activities from the design, formation, investigation and utilization, where formation of coatings or films of the desired properties is the most investigated. Nanotechnology have enabled synthesizing films of nanometric grain size and thickness. Vapor deposition methods (such as PVD and CVD) have potential for the large-scale production. Also, research direction should be also considered on reproducibility and large-scale production of solar cells rather than just lab scale.

Solar energy harvesting through thin film photovoltaic cells have gained a lot of attention due to their flexibility and applicability in modern different applications. Numerous approaches have been developed to enhance the effectiveness of solar cells. The sheet resistance, work function, and optical transparency of graphene can be controlled via manipulating the layers numbers, photoinduced doping, chemical doping, or electrical field-effect to increase the carrier concentration, series resistance, barrier height, and optical absorption of the photovoltaic system. Interface band design can be used to improve the gadget barrier height and rate of optical carrier recombination. Also, enhancing light absorption can be achieved by integrating semiconductor nano/micro-structures, antireflection coatings, or plasmonic nanostructures. Furthermore, the solar cell exhibited a substantial enhancement in light absorption as a result of the surface texturing. Carbon nanomaterials have been noticed to possess the ability to fulfill various functions, including serving as an effective anode, cathode, buffer layer, TCE, acceptor layer, photoactive layer, donor layer, HTL, ETL, electron/hole charge blocking layer, SC stabilizing material, ternary material, surface antireflective coating, Schottky junction formation material, recombination suppressant layer, and passivating layer. Furthermore, the carbon materials' flexibility significantly enhances the lifetime of the PSC by improving its mechanical characteristic. In order to maintain

mechanical stability, it is crucial to employ suitable manufacturing techniques for dense deposition/coating and durable bendable electrode materials. Carbon materials exhibited excellent water resistance and effectively prevent water from entering the LHP layer, hence enhancing stability in humid environments. In order to achieve this, utilization of it will be crucial to develop carbon top electrodes, such as graphene and CNT networks, that are reasonably transparent. Additionally, prior to the commercialization and global launch of PSCs utilizing carbon materials, it is essential to solve crucial factors including cost, environmental impact, and high stability. The conventional layouts and deposition procedures are commonly employed in laboratory settings are not readily applicable to commercial solar cells. Efforts must be made to create and implement efficient manufacturing techniques for the production and commercialization of durable solar cells utilizing carbon materials. Carbon nanoparticles offer the possibility of using low-cost and eco-friendly carbon materials as a substitute for the pricey organic/inorganic function layer in the structure of perovskite devices. These carbon-based compounds were effectively exhibited as prospective electrode materials for improving the longevity of PSCs. Nevertheless, up till now, all the documented carbon-based PSCs have fallen behind Au-based PSCs in terms of their PCEs, short-circuit current densities (J_{sc}), and FF values. The primary factors contributing to PCEs of carbon-based perovskite solar cells PSCs are the elevated electrical resistance of the carbon electrodes and the inadequate connection among these electrodes and the perovskite interface. Introducing of conductive carbon nanoparticles can reduce the sheet resistivity of carbon electrodes. Additionally, optimizing the interaction among the carbon and perovskite phase can enhance the overall performance of the device. Moreover, the cost of producing carbon nanomaterials for the front and back electrodes of solar cells on a wide scale can be decreased by utilizing carbon materials derived from solid waste materials.

CRediT authorship contribution statement

Wajahat Ahmed Khan: Writing – review & editing, Writing – original draft, Visualization, Validation, Methodology, Investigation, Formal analysis, Data curation, Conceptualization. **Salim Newaz Kazi:** Validation, Supervision, Software, Resources, Project administration, Methodology, Investigation, Funding acquisition, Formal analysis. **Zaira Zaman Chowdhury:** Supervision, Software, Resources. **Mohd Nashrul Mohd Zubir:** Supervision, Software, Resources. **Yew Hoong Wong:** Supervision, Software, Resources. **Kaleemullah Shaikh:** Writing – review & editing. **Rab Nawaz:** Writing – review & editing. **Samr Ul Hasnain:** Writing – review & editing.

Declaration of competing interest

The authors declare that they have no known competing financial interests or personal relationships that could have appeared to influence the work reported in this paper.

Data availability

No data was used for the research described in the article.

Acknowledgments

This study was supported financially under HORIZON-MSCA-2022-SE-01-01 awarded by European Research Executive Agency with project number 101130406 (ice-Link). The authors also gratefully acknowledge the support from grants [MG 025-2022, ST 077-2022, RMF 0400-2021, ST 049-2022, RK 001-2022], Centers [Nanotechnology and Catalysis Research Center (NANOCAT), Centre of Advanced Manufacturing and Material Processing (AMMP Centre), Centre for Energy Sciences (CES), Centre of Advanced Materials (CAM)] and Department of Mechanical Engineering, Universiti Malaya to conduct

this research.

References

- [1] D.K. Dwivedi, Surface Engineering, Springer India, New Delhi, 2018, <https://doi.org/10.1007/978-81-322-3779-2>.
- [2] R.S. Walia, Q. Murtaza, S.M. Pandey, A. Tyagi, Surface Engineering: Methods and Applications, first ed., CRC Press, Boca Raton, 2022 <https://doi.org/10.1201/9781003319375>.
- [3] F.M. Mwema, T.-C. Jen, L. Zhu, Thin Film Coatings: Properties, Deposition, and Applications, first ed., CRC Press, Boca Raton, 2022 <https://doi.org/10.1201/9781003202615>.
- [4] T. Burakowski, T. Wierzchon, Surface Engineering of Metals, 0 ed., CRC Press, 1998 <https://doi.org/10.1201/9780367802325>.
- [5] P.M. Martin, Handbook of Deposition Technologies for Films and Coatings: Science, Applications and Technology, third ed., Elsevier, Amsterdam, 2010.
- [6] S. Wijewardane, L.L. Kazmerski, Inventions, innovations, and new technologies: flexible and lightweight thin-film solar PV based on CIGS, CdTe, and a-Si, *H. Solar Compass* 7 (2023) 100053, <https://doi.org/10.1016/j.solcom.2023.100053>.
- [7] M.C. Beard, J.M. Luther, A.J. Nozik, The promise and challenge of nanostructured solar cells, *Nat. Nanotechnol.* 9 (2014) 951–954, <https://doi.org/10.1038/nano.2014.292>.
- [8] F. Gao, Advanced Nanomaterials for Solar Cells and Light Emitting Diodes, Elsevier, 2019, <https://doi.org/10.1016/C2017-0-00025-3>.
- [9] S. Thomas, N. Kalairikkal, J. Wu, Nanomaterials for Solar Cell Applications, Elsevier, 2019, <https://doi.org/10.1016/C2016-0-03432-0>.
- [10] D. Ginley, T. Fix, Advanced Micro- and Nanomaterials for Photovoltaics, Elsevier, 2019, <https://doi.org/10.1016/C2017-0-01432-5>.
- [11] S. Kumar, M. Nehra, A. Deep, D. Kedia, N. Dilbaghi, K.-H. Kim, Quantum-sized nanomaterials for solar cell applications, *Renew. Sustain. Energy Rev.* 73 (2017) 821–839, <https://doi.org/10.1016/j.rser.2017.01.172>.
- [12] J. Takadoum (Ed.), Nanomaterials and Surface Engineering, first ed., Wiley, 2013 <https://doi.org/10.1002/9781118618523>.
- [13] E. Roduner, Size matters: why nanomaterials are different, *Chem. Soc. Rev.* 35 (2006) 583, <https://doi.org/10.1039/b502142c>.
- [14] The Nobel Foundation, The Nobel Prize in Chemistry 1996, NobelPrizeOrg n.d. <https://www.nobelprize.org/prizes/uncategorized/the-nobel-prize-in-chemistry-1996> (accessed November 2, 2023).
- [15] The Nobel Foundation, The Nobel Prize in Physics 2010, NobelPrizeOrg n.d. <https://www.nobelprize.org/prizes/physics/2010/summary/> (accessed November 2, 2023).
- [16] E. Broitman, L. Hultman, Advanced Carbon-Based Coatings. Reference Module in Materials Science and Materials Engineering, Elsevier, 2016, <https://doi.org/10.1016/B978-0-12-803581-8.09211-0>, B9780128035818092110.
- [17] B. Chen, X. Zhang, Q. Gao, D. Yang, J. Chen, X. Chang, et al., The development of carbon/silicon heterojunction solar cells through interface passivation, *Adv. Sci.* 11 (2024) 2306993, <https://doi.org/10.1002/advs.202306993>.
- [18] L. Lin, B. Deng, J. Sun, H. Peng, Z. Liu, Bridging the gap between reality and ideal in chemical vapor deposition growth of graphene, *Chem. Rev.* 118 (2018) 9281–9343, <https://doi.org/10.1021/cs.8b00325>.
- [19] P. Serp, Carbon. Comprehensive Inorganic Chemistry II, Elsevier, 2013, pp. 323–369, <https://doi.org/10.1016/B978-0-08-097774-4.00731-2>.
- [20] N. Kaiser, Review of the fundamentals of thin-film growth, *Appl. Opt.* 41 (2002) 3053, <https://doi.org/10.1364/AO.41.003053>.
- [21] J. Hora, C. Hall, D. Evans, E. Charrault, Inorganic thin film deposition and application on organic polymer substrates, *Adv. Eng. Mater.* 20 (2018) 1700868, <https://doi.org/10.1002/adem.201700868>.
- [22] R.M. Pasquarelli, D.S. Ginley, R. O’Hayre, Solution processing of transparent conductors: from flask to film, *Chem. Soc. Rev.* 40 (2011) 5406, <https://doi.org/10.1039/c1cs15065k>.
- [23] T. Abzieher, D.T. Moore, M. Roß, S. Albrecht, J. Silvia, H. Tan, et al., Vapor phase deposition of perovskite photovoltaics: short track to commercialization? *Energy Environ. Sci.* 17 (2024) 1645–1663, <https://doi.org/10.1039/D3EE03273F>.
- [24] R. Swartwout, M.T. Hoerantner, V. Bulović, Scalable deposition methods for large-area production of perovskite thin films, *Energy & Environ. Materials* 2 (2019) 119–145, <https://doi.org/10.1002/eem2.12043>.
- [25] A. Agresti, F. Di Giacomo, S. Pescetelli, A. Di Carlo, Scalable deposition techniques for large-area perovskite photovoltaic technology: a multi-perspective review, *Nano Energy* 122 (2024) 109317, <https://doi.org/10.1016/j.nanoen.2024.109317>.
- [26] Y. Zhang, Q. Zhang, Y. Li, N. Wang, J. Zhu, Coating of carbon nanotubes with tungsten by physical vapor deposition, *Solid State Commun.* 115 (2000) 51–55, [https://doi.org/10.1016/S0038-1098\(00\)00125-3](https://doi.org/10.1016/S0038-1098(00)00125-3).
- [27] K. Shaikh, S.N. Kazi, M.N.M. Zubir, B.A. Razak, K. Wong, Y.H. Wong, et al., Investigation of zirconium (Zr) coated heat exchanger surface for the enhancement of heat transfer and retardation of mineral fouling, *J. Taiwan Inst. Chem. Eng.* 153 (2023) 105246, <https://doi.org/10.1016/j.jtice.2023.105246>.
- [28] D.M. Mattox, Physical vapor deposition (PVD) processes, *Met. Finish.* 100 (2002) 394–408, [https://doi.org/10.1016/S0026-0576\(02\)82043-8](https://doi.org/10.1016/S0026-0576(02)82043-8).
- [29] I.V. Shishkovsky, P.N. Lebedev, Chemical and physical vapor deposition methods for nanocoatings, *Nanocoatings and Ultra-Thin Films*, Elsevier (2011) 57–77, <https://doi.org/10.1533/9780857094902.1.57>.
- [30] A.A. Voznesenskaya, A.V. Zhdanov, L.V. Belyaev, Deposition of carbon coatings by PVD-methods on polyurethane, *Mater. Today: Proc.* 19 (2019) 2270–2273, <https://doi.org/10.1016/j.matpr.2019.07.595>.

- [31] A.W. Zia, M. Birkett, M.A. Badshah, M. Iqbal, Progress in-situ synthesis of graphitic carbon nanoparticles with physical vapour deposition, *Prog. Cryst. Growth Char. Mater.* 67 (2021) 100534, <https://doi.org/10.1016/j.pcrsgrow.2021.100534>.
- [32] M. Stueber, H. Holleck, H. Leiste, K. Seemann, S. Ulrich, C. Ziebert, Concepts for the design of advanced nanoscale PVD multilayer protective thin films, *J. Alloys Compd.* 483 (2009) 321–333, <https://doi.org/10.1016/j.jallcom.2008.08.133>.
- [33] H.R. Bakhshehi-Rad, E. Hamzah, G.J. Dias, S.N. Saud, F. Yaghoubidoust, Z. Hadisi, Fabrication and characterisation of novel ZnO/MWCNT duplex coating deposited on Mg alloy by PVD coupled with dip-coating techniques, *J. Alloys Compd.* 728 (2017) 159–168, <https://doi.org/10.1016/j.jallcom.2017.08.161>.
- [34] A. Agrawal, J. Charleston, R. Mirzaifar, Experimental investigation of mechanical behavior at the microstructure of copper-graphene thin films, *Mater. Sci. Eng., A* 862 (2023) 144492, <https://doi.org/10.1016/j.msea.2022.144492>.
- [35] X. Ji, X. Li, H. Yu, W. Zhang, H. Dong, Study on the carbon nanotubes reinforced nanocomposite coatings, *Diam. Relat. Mater.* 91 (2019) 247–254, <https://doi.org/10.1016/j.diamond.2018.11.027>.
- [36] Z. Li, C. Cui, X. Zhou, S. Bian, O. Arteaga, X. Xu, Characterization of amorphous carbon films from 5 nm to 200 nm on single-side polished a-plane sapphire substrates by spectroscopic ellipsometry, *Front. Physiol.* 10 (2022) 968101, <https://doi.org/10.3389/fphys.2022.968101>.
- [37] L.M.M. Barreto, D.M. Da Silva, A.D. Santos, K. Araki, C.B. De Araújo, L.R. P. Kassab, Optical limiting in multilayer graphene films on a cobalt buffer-layer produced by the sputtering technique, *Appl. Opt.* 62 (2023) C122, <https://doi.org/10.1364/AO.477209>.
- [38] I. Mrkvica, T. Szotkowski, A. Slaninkova, T. Jurga, High-efficiency of PVD coating process by applying an additional rotation, *Coatings* 12 (2022) 834, <https://doi.org/10.3390/coatings12060834>.
- [39] M.A. Capano, N.T. McDevitt, R.K. Singh, F. Qian, Characterization of amorphous carbon thin films, *J. Vac. Sci. Technol. A: Vacuum, Surfaces, and Films* 14 (1996) 431–435, <https://doi.org/10.1116/1.580101>.
- [40] Y. Lu, G. Huang, S. Wang, C. Mi, S. Wei, F. Tian, et al., A review on diamond-like carbon films grown by pulsed laser deposition, *Appl. Surf. Sci.* 541 (2021) 148573, <https://doi.org/10.1016/j.apsusc.2020.148573>.
- [41] M. Shakerzadeh, E.H.T. Teo, A. Sorkin, M. Bosman, B.K. Tay, H. Su, Plasma density induced formation of nanocrystals in physical vapor deposited carbon films, *Carbon* 49 (2011) 1733–1744, <https://doi.org/10.1016/j.carbon.2010.12.059>.
- [42] C. Yuen, S.F. Yu, S.P. Lau, G.C.K. Chen, Design and fabrication of ZnO light-emitting devices using filtered cathodic vacuum arc technique, *J. Cryst. Growth* 287 (2006) 204–212, <https://doi.org/10.1016/j.jcrysgro.2005.10.068>.
- [43] L. Sun, G. Yuan, L. Gao, J. Yang, M. Chhowalla, M.H. Gharahcheshmeh, et al., Chemical vapour deposition, *Nat Rev Methods Primers* 1 (2021) 5, <https://doi.org/10.1038/s43586-020-00005-y>.
- [44] M. Li, D. Liu, D. Wei, X. Song, D. Wei, A.T.S. Wee, Controllable synthesis of graphene by plasma-enhanced chemical vapor deposition and its related applications, *Adv. Sci.* 3 (2016) 1600003, <https://doi.org/10.1002/advs.201600003>.
- [45] S.M. George, Atomic layer deposition: an overview, *Chem. Rev.* 110 (2010) 111–131, <https://doi.org/10.1021/cr900056b>.
- [46] L. Qiu, S. He, Y. Jiang, Y. Qi, Metal halide perovskite solar cells by modified chemical vapor deposition, *J. Mater. Chem. A* 9 (2021) 22759–22780, <https://doi.org/10.1039/DITA06459B>.
- [47] D. Lin, Z. Zhan, X. Huang, P. Liu, W. Xie, Advances in components engineering in vapor deposited perovskite thin film for photovoltaic application, *Materials Today Advances* 16 (2022) 100277, <https://doi.org/10.1016/j.mtadv.2022.100277>.
- [48] D. Li, D. Zhang, K. Lim, Y. Hu, Y. Rong, A. Mei, et al., A review on scaling up perovskite solar cells, *Adv. Funct. Mater.* 31 (2021) 2008621, <https://doi.org/10.1002/adfm.202008621>.
- [49] Z. Liu, L. Lin, H. Ren, X. Sun, CVD synthesis of graphene, *Thermal Transport in Carbon-Based Nanomaterials*, Elsevier (2017) 19–56, <https://doi.org/10.1016/B978-0-32-346240-2.00002-9>.
- [50] A.W. Robertson, J.H. Warner, Hexagonal single crystal domains of few-layer graphene on copper foils, *Nano Lett.* 11 (2011) 1182–1189, <https://doi.org/10.1021/nl104142k>.
- [51] D. Geng, K.P. Loh, Controlled growth of graphene crystals by chemical vapor deposition: from solid metals to liquid metals, in: P. Avouris, T.F. Heinz, T. Low (Eds.), *2D Materials*, first ed., Cambridge University Press, 2017, pp. 238–256, <https://doi.org/10.1017/9781316681619.014>.
- [52] H. Sung, N. Ahn, M.S. Jang, J. Lee, H. Yoon, N. Park, et al., Transparent conductive oxide-free graphene-based perovskite solar cells with over 17% efficiency, *Adv. Energy Mater.* 6 (2016) 1501873, <https://doi.org/10.1002/aenm.201501873>.
- [53] J.A. Raiford, S.T. Oyakhire, S.F. Bent, Applications of atomic layer deposition and chemical vapor deposition for perovskite solar cells, *Energy Environ. Sci.* 13 (2020) 1997–2023, <https://doi.org/10.1039/D0EE00385A>.
- [54] I. Jeon, S. Seo, Y. Sato, C. Delacou, A. Anisimov, K. Suenaga, et al., Perovskite solar cells using carbon nanotubes both as cathode and as anode, *J. Phys. Chem. C* 121 (2017) 25743–25749, <https://doi.org/10.1021/acs.jpcc.7b10334>.
- [55] Y. Wu, X. Yang, H. Chen, K. Zhang, C. Qin, J. Liu, et al., Highly compact TiO₂ layer for efficient hole-blocking in perovskite solar cells, *Appl. Phys. Express* 7 (2014) 052301, <https://doi.org/10.7567/APEX.7.052301>.
- [56] Q. Yu, L.A. Jauregui, W. Wu, R. Colby, J. Tian, Z. Su, et al., Control and characterization of individual grains and grain boundaries in graphene grown by chemical vapour deposition, *Nat. Mater.* 10 (2011) 443–449, <https://doi.org/10.1038/nmat3010>.
- [57] T. Wu, X. Zhang, Q. Yuan, J. Xue, G. Lu, Z. Liu, et al., Fast growth of inch-sized single-crystalline graphene from a controlled single nucleus on Cu–Ni alloys, *Nat. Mater.* 15 (2016) 43–47, <https://doi.org/10.1038/nmat4477>.
- [58] J. Zhang, L. Lin, K. Jia, L. Sun, H. Peng, Z. Liu, Controlled growth of single-crystal graphene films, *Adv. Mater.* 32 (2020) 1903266, <https://doi.org/10.1002/adma.201903266>.
- [59] A. Reina, X. Jia, J. Ho, D. Nezich, H. Son, V. Bulovic, et al., Large area, few-layer graphene films on arbitrary substrates by chemical vapor deposition, *Nano Lett.* 9 (2009) 30–35, <https://doi.org/10.1021/nl801827v>.
- [60] X. Li, W. Cai, J. An, S. Kim, J. Nah, D. Yang, et al., Large-area synthesis of high-quality and uniform graphene films on copper foils, *Science* 324 (2009) 1312–1314, <https://doi.org/10.1126/science.1171245>.
- [61] J. Yu, J. Li, W. Zhang, H. Chang, Synthesis of high quality two-dimensional materials via chemical vapor deposition, *Chem. Sci.* 6 (2015) 6705–6716, <https://doi.org/10.1039/C5SC01941A>.
- [62] L. Gomez De Arco, Y. Zhang, C.W. Schlenker, K. Ryu, M.E. Thompson, C. Zhou, Continuous, highly flexible, and transparent graphene films by chemical vapor deposition for organic photovoltaics, *ACS Nano* 4 (2010) 2865–2873, <https://doi.org/10.1021/nm901587x>.
- [63] I. Vlassiouk, M. Regmi, P. Fulvio, S. Dai, P. Datskos, G. Eres, et al., Role of hydrogen in chemical vapor deposition growth of large single-crystal graphene, *ACS Nano* 5 (2011) 6069–6076, <https://doi.org/10.1021/nm201978y>.
- [64] Z. Zhai, H. Shen, J. Chen, X. Li, Y. Jiang, Evolution of structural and electrical properties of carbon films from amorphous carbon to nanocrystalline graphene on quartz glass by HFCVD, *ACS Appl. Mater. Interfaces* 10 (2018) 17427–17436, <https://doi.org/10.1021/acsami.8b01588>.
- [65] O.M. Slobodian, A.V. Rusavsky, A.V. Vasin, Khzhun Oyu, O.I. Gudymenko, V. P. Kladko, et al., Highly porous carbon films fabricated by magnetron plasma enhanced chemical vapor deposition: structure, properties and implementation, *Appl. Surf. Sci.* 496 (2019) 143735, <https://doi.org/10.1016/j.apsusc.2019.143735>.
- [66] J. Liu, C. Wöll, Surface-supported metal–organic framework thin films: fabrication methods, applications, and challenges, *Chem. Soc. Rev.* 46 (2017) 5730–5770, <https://doi.org/10.1039/C7CS00315C>.
- [67] Y. Kim, N. Baule, M. Shrestha, Q.H. Fan, Growth of highly transparent amorphous carbon films using beam plasma source, *Coatings* 12 (2022) 1159, <https://doi.org/10.3390/coatings12081159>.
- [68] K. Liu, K.-P. Du, E.-Z. Ren, G.-Y. Ye, X.-S. Wang, W.-Y. Ming, et al., Preparation and tribological properties of graphene-based coatings on tungsten carbide, *Coatings* 12 (2022) 1385, <https://doi.org/10.3390/coatings12101385>.
- [69] Z. Zhang, L. Wei, X. Qin, Y. Li, Carbon nanomaterials for photovoltaic process, *Nano Energy* 15 (2015) 490–522, <https://doi.org/10.1016/j.nanoen.2015.04.003>.
- [70] J. Jean, P.R. Brown, R.L. Jaffe, T. Buonassisi, V. Bulović, Pathways for solar photovoltaics, *Energy Environ. Sci.* 8 (2015) 1200–1219, <https://doi.org/10.1039/C4EE04073B>.
- [71] B. Kippelen, J.-L. Brédas, Organic photovoltaics, *Energy Environ. Sci.* 2 (2009) 251, <https://doi.org/10.1039/b812502n>.
- [72] X. Fu, L. Xu, J. Li, X. Sun, H. Peng, Flexible solar cells based on carbon nanomaterials, *Carbon* 139 (2018) 1063–1073, <https://doi.org/10.1016/j.carbon.2018.08.017>.
- [73] M. Hadadian, J.-H. Smått, J.-P. Correa-Baena, The role of carbon-based materials in enhancing the stability of perovskite solar cells, *Energy Environ. Sci.* 13 (2020) 1377–1407, <https://doi.org/10.1039/C9EE04030G>.
- [74] L. Wieland, H. Li, C. Rust, J. Chen, B.S. Flavel, Carbon nanotubes for photovoltaics: from lab to industry, *Adv. Energy Mater.* 11 (2021) 2002880, <https://doi.org/10.1002/aenm.202002880>.
- [75] H. Zhu, J. Wei, K. Wang, D. Wu, Applications of carbon materials in photovoltaic solar cells, *Sol. Energy Mater. Sol. Cell.* 93 (2009) 1461–1470, <https://doi.org/10.1016/j.solmat.2009.04.006>.
- [76] M. Morales-Masis, S. De Wolf, R. Woods-Robinson, J.W. Ager, C. Ballif, Transparent electrodes for efficient optoelectronics, *Adv. Elect. Materials* 3 (2017) 1600529, <https://doi.org/10.1002/aem.201600529>.
- [77] F. Bonaccorso, Z. Sun, T. Hasan, A.C. Ferrari, Graphene photonics and optoelectronics, *Nat. Photonics* 4 (2010) 611–622, <https://doi.org/10.1038/nphoton.2010.186>.
- [78] Y. Ma, L. Zhi, Graphene-based transparent conductive films: material systems, preparation and applications, *Small Methods* 3 (2019) 1800199, <https://doi.org/10.1002/smtd.201800199>.
- [79] R.R. Nair, P. Blake, A.N. Grigorenko, K.S. Novoselov, T.J. Booth, T. Stauber, et al., Fine structure constant defines visual transparency of graphene, *Science* 320 (2008), <https://doi.org/10.1126/science.1156965>, 1308–1308.
- [80] D.S. Hecht, L. Hu, G. Irvin, Emerging transparent electrodes based on thin films of carbon nanotubes, graphene, and metallic nanostructures, *Adv. Mater.* 23 (2011) 1482–1513, <https://doi.org/10.1002/adma.201003188>.
- [81] V. Ferguson, S.R.P. Silva, W. Zhang, Carbon materials in perovskite solar cells: prospects and future challenges, *Energy & Environ. Materials* 2 (2019) 107–118, <https://doi.org/10.1002/eem.212035>.
- [82] F. Wang, Y. Han, D. Duan, C. Ge, H. Hu, G. Li, Recent progress of scalable perovskite solar cells and modules, *Energy Rev.* 1 (2022) 100010, <https://doi.org/10.1016/j.enrev.2022.100010>.
- [83] R. He, X. Huang, M. Chee, F. Hao, P. Dong, Carbon-based perovskite solar cells: from single-junction to modules, *Carbon Energy* 1 (2019) 109–123, <https://doi.org/10.1002/cey.211>.

- [84] Z. Ku, Y. Rong, M. Xu, T. Liu, H. Han, Full printable processed mesoscopic CH₃NH₃PbI₃/TiO₂ heterojunction solar cells with carbon counter electrode, *Sci. Rep.* 3 (2013) 3132, <https://doi.org/10.1038/srep03132>.
- [85] D. Sun, C. Liu, W. Ren, H. Cheng, A review of carbon nanotube- and graphene-based flexible thin-film transistors, *Small* 9 (2013) 1188–1205, <https://doi.org/10.1002/smll.201203154>.
- [86] R.M. Jain, R. Howden, K. Tvrdy, S. Shimizu, A.J. Hilmer, T.P. McNicholas, et al., Polymer-free near-infrared photovoltaics with single chirality (6,5) semiconducting carbon nanotube active layers, *Adv. Mater.* 24 (2012) 4436–4439, <https://doi.org/10.1002/adma.201202088>.
- [87] D.J. Bindl, M.-Y. Wu, F.C. Prehn, M.S. Arnold, Efficiently harvesting excitons from electronic type-controlled semiconducting carbon nanotube films, *Nano Lett.* 11 (2011) 455–460, <https://doi.org/10.1021/nl1031343>.
- [88] S. Berson, R. De Bettignies, S. Bailly, S. Guillerez, Poly(3-hexylthiophene) fibers for photovoltaic applications, *Adv. Funct. Mater.* 17 (2007) 1377–1384, <https://doi.org/10.1002/adfm.200600922>.
- [89] D. Jariwala, V.K. Sangwan, L.J. Lauhon, T.J. Marks, M.C. Hersam, Carbon nanomaterials for electronics, optoelectronics, photovoltaics, and sensing, *Chem. Soc. Rev.* 42 (2013) 2824–2860, <https://doi.org/10.1039/C2CS35335K>.
- [90] M.A. Deshmukh, S.-J. Park, B.S. Hedau, T.-J. Ha, Recent progress in solar cells based on carbon nanomaterials, *Sol. Energy* 220 (2021) 953–990, <https://doi.org/10.1016/j.solener.2021.04.001>.
- [91] T.A. Shastry, M.C. Hersam, Carbon nanotubes in thin-film solar cells, *Adv. Energy Mater.* 7 (2017) 1601205, <https://doi.org/10.1002/aenm.201601205>.
- [92] K. Jiao, X. Wang, Y. Wang, Y. Chen, Graphene oxide as an effective interfacial layer for enhanced graphene/silicon solar cell performance, *J. Mater. Chem. C* 2 (2014) 7715–7721, <https://doi.org/10.1039/C4TC00705K>.
- [93] L. Yang, X. Yu, M. Xu, H. Chen, D. Yang, Interface engineering for efficient and stable chemical-doping-free graphene-on-silicon solar cells by introducing a graphene oxide interlayer, *J. Mater. Chem. A* 2 (2014) 16877–16883, <https://doi.org/10.1039/C4TA02216E>.
- [94] P. Fallahzad, Rational and key strategies toward enhancing the performance of graphene/silicon solar cells, *Mater Adv* 4 (2023) 1876–1899, <https://doi.org/10.1039/D2MA00955B>.
- [95] J.L. Blackburn, T.M. Barnes, M.C. Beard, Y.-H. Kim, R.C. Tenent, T.J. McDonald, et al., Transparent conductive single-walled carbon nanotube networks with precisely tunable ratios of semiconducting and metallic nanotubes, *ACS Nano* 2 (2008) 1266–1274, <https://doi.org/10.1021/nn800200d>.
- [96] T.P. Tyler, R.E. Brock, H.J. Karmel, T.J. Marks, M.C. Hersam, Electronically monodisperse single-walled carbon nanotube thin films as transparent conducting anodes in organic photovoltaic devices, *Adv. Energy Mater.* 1 (2011) 785–791, <https://doi.org/10.1002/aenm.201100274>.
- [97] B. Guo, Q. Liu, E. Chen, H. Zhu, L. Fang, J.R. Gong, Controllable N-doping of graphene, *Nano Lett.* 10 (2010) 4975–4980, <https://doi.org/10.1021/nl103079j>.
- [98] W.H. Lee, J.W. Suk, J. Lee, Y. Hao, J. Park, J.W. Yang, et al., Simultaneous transfer and doping of CVD-grown graphene by fluoropolymer for transparent conductive films on plastic, *ACS Nano* 6 (2012) 1284–1290, <https://doi.org/10.1021/nn203998j>.
- [99] J.-H. Huang, J.-H. Fang, C.-C. Liu, C.-W. Chu, Effective work function modulation of graphene/carbon nanotube composite films as transparent cathodes for organic optoelectronics, *ACS Nano* 5 (2011) 6262–6271, <https://doi.org/10.1021/nn201253w>.
- [100] Z. Liu, S.P. Lau, F. Yan, Functionalized graphene and other two-dimensional materials for photovoltaic devices: device design and processing, *Chem. Soc. Rev.* 44 (2015) 5638–5679, <https://doi.org/10.1039/C4CS00455H>.
- [101] P. Fooladvand, M. Eskandari, D. Fathi, N. Das, Single-walled carbon nanotube as hole transport layer in perovskite solar cell: efficiency enhancement, *Energy Rep.* 10 (2023) 3652–3664, <https://doi.org/10.1016/j.egyr.2023.10.020>.
- [102] N. Ahn, I. Jeon, J. Yoon, E.I. Kauppinen, Y. Matsuo, S. Maruyama, et al., Carbon-sandwiched perovskite solar cell, *J. Mater. Chem. A* 6 (2018) 1382–1389, <https://doi.org/10.1039/C7TA09174E>.
- [103] M. Bernardi, J. Lohrman, P.V. Kumar, A. Kirkeminde, N. Ferralis, J.C. Grossman, et al., Nanocarbon-based photovoltaics, *ACS Nano* 6 (2012) 8896–8903, <https://doi.org/10.1021/nn302893p>.
- [104] D.D. Tunc, B.S. Flavel, Advances in carbon nanotube–silicon heterojunction solar cells, *Adv. Energy Mater.* 8 (2018) 1703241, <https://doi.org/10.1002/aenm.201703241>.
- [105] F. Wang, D. Kozawa, Y. Miyauchi, K. Hiraoka, S. Mouri, Y. Ohno, et al., Considerably improved photovoltaic performance of carbon nanotube-based solar cells using metal oxide layers, *Nat. Commun.* 6 (2015) 6305, <https://doi.org/10.1038/ncomms7305>.
- [106] D. Tunc, J. Shapter, Effect of nanotube film thickness on the performance of nanotube–silicon hybrid solar cells, *Nanomaterials* 3 (2013) 655–673, <https://doi.org/10.3390/nano3040655>.
- [107] S.N. Habisreutinger, T. Leijtens, G.E. Eperon, S.D. Stranks, R.J. Nicholas, H. J. Snaith, Carbon nanotube/polymer composites as a highly stable hole collection layer in perovskite solar cells, *Nano Lett.* 14 (2014) 5561–5568, <https://doi.org/10.1021/nl501982b>.
- [108] S. Yoon, S.R. Ha, T. Moon, S.M. Jeong, T.-J. Ha, H. Choi, et al., Carbon nanotubes embedded poly(3,4-ethylenedioxythiophene):poly(styrenesulfonate) hybrid hole collector for inverted planar perovskite solar cells, *J. Power Sources* 435 (2019) 226765, <https://doi.org/10.1016/j.jpowsour.2019.226765>.
- [109] A. Kim, J.K. Dash, P. Kumar, R. Patel, Carbon-based quantum dots for photovoltaic devices: a review, *ACS Appl. Electron. Mater.* 4 (2022) 27–58, <https://doi.org/10.1021/acsaem.1c00783>.
- [110] O.E. Semonin, J.M. Luther, M.C. Beard, Quantum dots for next-generation photovoltaics, *Mater. Today* 15 (2012) 508–515, [https://doi.org/10.1016/S1369-7021\(12\)70220-1](https://doi.org/10.1016/S1369-7021(12)70220-1).
- [111] O. Fernandez-Delgado, P.S. Chandrasekhar, N. Cano-Sampaio, Z.C. Simon, A. R. Puente-Santiago, F. Liu, et al., The role of fullerene derivatives in perovskite solar cells: electron transporting or electron extraction layers? *J. Mater. Chem. C* 9 (2021) 10759–10767, <https://doi.org/10.1039/D0TC05903J>.
- [112] S. Collavini, J.L. Delgado, Fullerenes: the stars of photovoltaics, *Sustain. Energy Fuels* 2 (2018) 2480–2493, <https://doi.org/10.1039/C8SE00254A>.
- [113] R. Zahran, Z. Hawash, Fullerene-based inverted perovskite solar cell: a key to achieve promising, stable, and efficient photovoltaics, *Adv. Mater. Interfac.* 9 (2022) 2201438, <https://doi.org/10.1021/admi.202201438>.
- [114] P. Kumar, S. Dua, R. Kaur, M. Kumar, G. Bhatt, A review on advancements in carbon quantum dots and their application in photovoltaics, *RSC Adv.* 12 (2022) 4714–4759, <https://doi.org/10.1039/D1RA08452F>.
- [115] M.J. Molaei, The optical properties and solar energy conversion applications of carbon quantum dots: a review, *Sol. Energy* 196 (2020) 549–566, <https://doi.org/10.1016/j.solener.2019.12.036>.
- [116] G. Shilpa, P.M. Kumar, D.K. Kumar, P.R. Deepthi, V. Sadhu, A. Sukhdev, et al., Recent advances in the development of high efficiency quantum dot sensitized solar cells (QDSSCs): a review, *Materials Science for Energy Technologies* 6 (2023) 533–546, <https://doi.org/10.1016/j.mset.2023.05.001>.
- [117] H.W. Kroto, J.R. Heath, S.C. O'Brien, R.F. Curl, R.E. Smalley, C₆₀: buckminsterfullerene, *Nature* 318 (1985) 162–163, <https://doi.org/10.1038/318162a0>.
- [118] W. Krätschmer, L.D. Lamb, K. Fostiropoulos, D.R. Huffman, Solid C₆₀: a new form of carbon, *Nature* 347 (1990) 354–358, <https://doi.org/10.1038/347354a0>.
- [119] S. Iijima, Helical microtubules of graphitic carbon, *Nature* 354 (1991) 56–58, <https://doi.org/10.1038/354056a0>.
- [120] S. Iijima, T. Ichihashi, Single-shell carbon nanotubes of 1-nm diameter, *Nature* 363 (1993) 603–605, <https://doi.org/10.1038/363603a0>.
- [121] T. Guo, P. Nikolaev, A. Thess, D.T. Colbert, R.E. Smalley, Catalytic growth of single-walled nanotubes by laser vaporization, *Chem. Phys. Lett.* 243 (1995) 49–54, [https://doi.org/10.1016/0009-2610\(95\)00825-O](https://doi.org/10.1016/0009-2610(95)00825-O).
- [122] M. Terrones, Science and technology of the twenty-first century: synthesis, properties, and applications of carbon nanotubes, *Annu. Rev. Mater. Res.* 33 (2003) 419–501, <https://doi.org/10.1146/annurev.matsci.33.012802.100255>.
- [123] T. Umeyama, D. Matano, S. Shibata, J. Baek, S. Ito, H. Imahori, Thermal precursor approach to pristine fullerene film as electron selective layer in perovskite solar cells, *ECS J Solid State Sci Technol* 6 (2017) M3078–M3083, <https://doi.org/10.1149/2.0161706jss>.
- [124] C. Tian, S. Zhang, S. Li, A. Mei, D. Li, S. Liu, et al., A C₆₀ modification layer using a scalable deposition technology for efficient printable mesoscopic perovskite solar cells, *Sol. RRL* 2 (2018) 1800174, <https://doi.org/10.1002/solr.201800174>.
- [125] K. Wojciechowski, T. Leijtens, S. Siprová, C. Schlueter, M.T. Hörtner, J.T.-W. Wang, et al., C₆₀ as an efficient n-type compact layer in perovskite solar cells, *J. Phys. Chem. Lett.* 6 (2015) 2399–2405, <https://doi.org/10.1021/jacslett.5b00902>.
- [126] J. Jeng, Y. Chiang, M. Lee, S. Peng, T. Guo, P. Chen, et al., CH₃NH₃PbI₃ perovskite/fullerene planar-heterojunction hybrid solar cells, *Adv. Mater.* 25 (2013) 3727–3732, <https://doi.org/10.1002/adma.201301327>.
- [127] J. Zhang, R. Xue, G. Xu, W. Chen, G. Bian, C. Wei, et al., Self-doping fullerene electrolyte-based electron transport layer for all-room-temperature-processed high-performance flexible polymer solar cells, *Adv. Funct. Mater.* 28 (2018) 1705847, <https://doi.org/10.1002/adfm.201705847>.
- [128] Y.-Q. Zhou, B.-S. Wu, G.-H. Lin, Y. Li, D.-C. Chen, P. Zhang, et al., Enhancing performance and uniformity of perovskite solar cells via a solution-processed C₇₀ interlayer for interface engineering, *ACS Appl. Mater. Interfaces* 9 (2017) 33810–33818, <https://doi.org/10.1021/acsami.7b08429>.
- [129] Z. Yang, J. Xie, V. Arivazhagan, K. Xiao, Y. Qiang, K. Huang, et al., Efficient and highly light stable planar perovskite solar cells with graphene quantum dots doped PCBM electron transport layer, *Nano Energy* 40 (2017) 345–351, <https://doi.org/10.1016/j.nanoen.2017.08.008>.
- [130] V.T. Tiong, N.D. Pham, T. Wang, T. Zhu, X. Zhao, Y. Zhang, et al., Octadecylamine-functionalized single-walled carbon nanotubes for facilitating the formation of a monolithic perovskite layer and stable solar cells, *Adv. Funct. Mater.* 28 (2018) 1705545, <https://doi.org/10.1002/adfm.201705545>.
- [131] X. Zheng, H. Chen, Q. Li, Y. Yang, Z. Wei, Y. Bai, et al., Boron doping of multiwalled carbon nanotubes significantly enhances hole extraction in carbon-based perovskite solar cells, *Nano Lett.* 17 (2017) 2496–2505, <https://doi.org/10.1021/acs.nanolett.7b00200>.
- [132] J. Xie, K. Huang, X. Yu, Z. Yang, K. Xiao, Y. Qiang, et al., Enhanced electronic properties of SnO₂ via electron transfer from graphene quantum dots for efficient perovskite solar cells, *ACS Nano* 11 (2017) 9176–9182, <https://doi.org/10.1021/acsnano.7b04070>.
- [133] C. Geng, Y. Shang, J. Qiu, Q. Wang, X. Chen, S. Li, et al., Carbon quantum dots interfacial modified graphene/silicon Schottky barrier solar cell, *J. Alloys Compd.* 835 (2020) 155268, <https://doi.org/10.1016/j.jallcom.2020.155268>.
- [134] C. Geng, X. Chen, S. Li, Z. Ding, W. Ma, J. Qiu, et al., Graphene quantum dots open up new prospects for interfacial modifying in graphene/silicon Schottky barrier solar cell, *Energy Mater Adv* 2021 (2021) 8481915, <https://doi.org/10.13413/2021/8481915>.
- [135] T. Ohta, A. Bostwick, T. Seyller, K. Horn, E. Rotenberg, Controlling the electronic structure of bilayer graphene, *Science* 313 (2006) 951–954, <https://doi.org/10.1126/science.1130681>.

- [136] X. Wang, L. Zhi, K. Müllen, Transparent, conductive graphene electrodes for dye-sensitized solar cells, *Nano Lett.* 8 (2008) 323–327, <https://doi.org/10.1021/nl072838r>.
- [137] H. Bi, F. Huang, J. Liang, X. Xie, M. Jiang, Transparent conductive graphene films synthesized by ambient pressure chemical vapor deposition used as the front electrode of CdTe solar cells, *Adv. Mater.* 23 (2011) 3202–3206, <https://doi.org/10.1002/adma.201100645>.
- [138] J. Liang, H. Bi, D. Wan, F. Huang, Novel Cu nanowires/graphene as the back contact for CdTe solar cells, *Adv. Funct. Mater.* 22 (2012) 1267–1271, <https://doi.org/10.1002/adfm.201102809>.
- [139] Z. Shi, A. Jayatissa, The impact of graphene on the fabrication of thin film solar cells: current status and future prospects, *Materials* 11 (2017) 36, <https://doi.org/10.3390/ma11010036>.
- [140] L. Duan, A. Uddin, Progress in stability of organic solar cells, *Adv. Sci.* 7 (2020) 1903259, <https://doi.org/10.1002/advs.201903259>.
- [141] R. Yu, H. Yao, J. Hou, Recent progress in ternary organic solar cells based on nonfullerene acceptors, *Adv. Energy Mater.* 8 (2018) 1702814, <https://doi.org/10.1002/aenm.201702814>.
- [142] Q. An, F. Zhang, J. Zhang, W. Tang, Z. Deng, B. Hu, Versatile ternary organic solar cells: a critical review, *Energy Environ. Sci.* 9 (2016) 281–322, <https://doi.org/10.1039/C5EE02641E>.
- [143] Q. An, F. Zhang, W. Gao, Q. Sun, M. Zhang, C. Yang, et al., High-efficiency and air stable fullerene-free ternary organic solar cells, *Nano Energy* 45 (2018) 177–183, <https://doi.org/10.1016/j.nanoen.2017.12.050>.
- [144] M. Hilal, J.I. Han, Significant improvement in the photovoltaic stability of bulk heterojunction organic solar cells by the molecular level interaction of graphene oxide with a PEDOT: PSS composite hole transport layer, *Sol. Energy* 167 (2018) 24–34, <https://doi.org/10.1016/j.solener.2018.03.083>.
- [145] Z. Liu, P. You, C. Xie, G. Tang, F. Yan, Ultrathin and flexible perovskite solar cells with graphene transparent electrodes, *Nano Energy* 28 (2016) 151–157, <https://doi.org/10.1016/j.nanoen.2016.08.038>.
- [146] Y. Wang, S.W. Tong, X.F. Xu, B. Özylmaz, K.P. Loh, Interface engineering of layer-by-layer stacked graphene anodes for high-performance organic solar cells, *Adv. Mater.* 23 (2011) 1514–1518, <https://doi.org/10.1002/adma.201003673>.
- [147] S.S. Bagade, S. Patel, M.M. Malik, P.K. Patel, Recent Advancements in Applications of Graphene to Attain Next-Level Solar Cells, 9, 2023, p. 70, <https://doi.org/10.3390/c9030070>.
- [148] Z. Liu, J. Li, Z.-H. Sun, G. Tai, S.-P. Lau, F. Yan, The application of highly doped single-layer graphene as the top electrodes of semitransparent organic solar cells, *ACS Nano* 6 (2012) 810–818, <https://doi.org/10.1021/nn204675r>.
- [149] K. Ihm, J.T. Lim, K.-J. Lee, J.W. Kwon, T.-H. Kang, S. Chung, et al., Number of graphene layers as a modulator of the open-circuit voltage of graphene-based solar cell, *Appl. Phys. Lett.* 97 (2010) 032113, <https://doi.org/10.1063/1.3464319>.
- [150] T.H. Nguyen, D. Yang, B. Zhu, H. Lin, T. Ma, B. Jia, Doping mechanism directed graphene applications for energy conversion and storage, *J. Mater. Chem. A* 9 (2021) 7366–7395, <https://doi.org/10.1039/D0TA11939C>.
- [151] Y.-Y. Lee, K.-H. Tu, C.-C. Yu, S.-S. Li, J.-Y. Hwang, C.-C. Lin, et al., Top laminated graphene electrode in a semitransparent polymer solar cell by simultaneous thermal annealing/releasing method, *ACS Nano* 5 (2011) 6564–6570, <https://doi.org/10.1021/nn201940j>.
- [152] X. Li, H. Zhu, K. Wang, A. Cao, J. Wei, C. Li, et al., Graphene-on-silicon Schottky junction solar cells, *Adv. Mater.* 22 (2010) 2743–2748, <https://doi.org/10.1002/adma.200904383>.
- [153] C. Tan, X. Cao, X.-J. Wu, Q. He, J. Yang, X. Zhang, et al., Recent advances in ultrathin two-dimensional nanomaterials, *Chem. Rev.* 117 (2017) 6225–6331, <https://doi.org/10.1021/acs.chemrev.6b00558>.
- [154] D. Dodoor-Arhin, M. Fabiane, A. Bello, N. Manyala, Graphene: synthesis, transfer, and characterization for dye-sensitized solar cells applications, *Ind. Eng. Chem. Res.* 52 (2013) 14160–14168, <https://doi.org/10.1021/ie4017489>.
- [155] B. Wu, D. Geng, Y. Guo, L. Huang, Y. Xue, J. Zheng, W. Hu, Equiangular Hexagon-Shape-Controlled Synthesis of Graphene on Copper Surface, *Advanced Materials* 31 (23) (2011) 3522–3525, <https://doi.org/10.1002/adma.201101746>.
- [156] A.W. Robertson, J.H. Warner, Hexagonal single crystal domains of few-layer graphene on copper foils, *Nano letters* 11 (3) (2011) 1182–1189, <https://doi.org/10.1021/nl104142k>.
- [157] Q. Yu, L.A. Jauregui, W. Wu, R. Colby, J. Tian, Z. Su, Y.P. Chen, Control and characterization of individual grains and grain boundaries in graphene grown by chemical vapour deposition, *Nature materials* 10 (6) (2011) 443–449, <https://doi.org/10.1038/nmat3010>.
- [158] K. Shaikh, W.A. Khan, S.N. Kazi, M. N.M. Zubir, B. Ahmed, B.A. Razak, J. K. Palaniapan, Environmental and economic benefits due to mitigation of calcium carbonate (CaCO_3) fouling on Brass heat exchanger surface with titanium oxide (TiO_x) coating, *Powder Technology* 120268 (2024), <https://doi.org/10.1016/j.powtec.2024.120268>.